

Characterization of the human aldehyde oxidase: studies on the FAD active site and ROS generation

Alessandro Foti

Dissertation

**zur Erlangung des akademischen Grades
"doctor rerum naturalium"
(Dr. rer. nat.)
in der Wissenschaftsdisziplin "Biochemie"**

**eingereicht an der
Mathematisch-Naturwissenschaftlichen Fakultät
Institut für Biochemie und Biologie
der Universität Potsdam**

Published online at the
Institutional Repository of the University of Potsdam:
URN urn:nbn:de:kobv:517-opus4-410107
<http://nbn-resolving.de/urn:nbn:de:kobv:517-opus4-410107>

LIST OF PUBLICATIONS

Coelho C, **Foti A**, Hartmann T, Santos-Silva T, Leimkühler S, Romão MJ. (Achiron *et al.*, 2015) “Structural insights into xenobiotic and inhibitor binding to human aldehyde oxidase” *Nature Chemical Biology* Oct;11(10):779-83.

Foti A, Hartmann T, Coelho C, Santos-Silva T, Romao MJ, Leimkuhler S. (2016) “Optimization of the expression of Human Aldehyde Oxidase for Investigations of Single Nucleotide Polymorphisms.” *Drug Metab Dispos.* Feb 3. pii: dmd.115.068395.

Romão MJ, Coelho C, Santos-Silva T, **Foti A**, Terao M, Garattini E, Leimkühler S. (2017) “Structural basis for the role of mammalian aldehyde oxidases in the metabolism of drugs and xenobiotics” *Current Opinion In Chemical Biology.* Jan 23;37:39-47. doi: 10.1016.

Foti A, Dorendorf F and Leimkuhler S. (2017) “Single nucleotide polymorphisms cause enhanced radical oxygen species production by human aldehyde oxidase” (manuscript submitted).

CONTRIBUTION TO CONFERENCES

“Structural insights into xenobiotic and inhibitor binding to human aldehyde oxidase” PhD symposium in Luckenwalde, Germany. Nov 2013 oral presentation

“Investigation of single nucleotide polymorphisms (SNP) in the active site of human Aldehyde Oxidase”. IX. Molybdenum & Tungsten Enzymes Conference. Balatonfüred, Hungary. Sep 2015 poster and oral presentation.

“Human aldehyde Oxidase and radical oxygen species (ROS) formation” PhD symposium in Luckenwalde, Germany. Nov 2016 oral presentation.

TABLE OF CONTENTS

1. Introduction	14
1.1 Molybdoenzymes	14
1.2 Sulfuration of the molybdenum cofactor	16
1.3 Characteristics of the Aldehyde oxidases	17
1.3.1 Structure of Aldehyde oxidases	17
1.3.2 An evolutionary perspective: phylogeny of AOXs.....	19
1.3.3 Expression and regulation of hAOX1	20
1.3.4 Substrate specificity and reaction mechanism	21
1.3.5 The human aldehyde oxidase and its intraspecific variability	24
1.4 Reactive oxygen species (ROS) and Flavin cofactors	26
1.4.1 Reactive oxygen species in cell physiology.....	26
1.4.2 Flavin cofactors and reactivity toward oxygen.....	29
1.4.3 Reactive oxygen species and molybdo-flavo enzymes.....	32
2. Aim of this work	37
3. Materials and Methods	38
3.1 Materials	38
3.1.1 Chemicals.....	38
3.1.2 Media, buffer and solutions	38
3.1.3 Plasmids and primers	38
3.1.4 Cell strains	39
3.2 Methods	39
3.2.1 Molecular biological methods.....	39
3.2.1.1 Cultivation of E. coli strains	39
3.2.1.2 Competent E. coli cells	40
3.2.1.3 Transformation of plasmid DNA	40
3.2.1.4 Isolation of plasmid DNA	40
3.2.1.5 Polymerase chain reaction (PCR) and Site Direct Mutagenesis.....	41
3.2.1.6 Determination of DNA concentration and DNA sequencing	43
3.2.2 Biochemical methods.....	44
3.2.2.1 Overexpression of human Aldehyde Oxidase in E. coli TP1000 strain	44
3.2.2.2 Cell lysis	44
3.2.2.3 Affinity purification by Ni-NTA chromatography	44
3.2.2.4 Buffer exchange and desalting.....	45
3.2.2.5 In vitro chemical sulfuration.....	45
3.2.2.6 Size exclusion chromatography	46
3.2.2.7 Ultrafiltration	46
3.2.3 Analytical methods and enzymatic assays.....	46

3.2.3.1 Agarose gel electrophoresis	46
3.2.3.2 Sodium dodecyl sulfate-polyacrylamide gel electrophoresis (SDS-PAGE)....	47
3.2.3.3 Coomassie-Blue staining	48
3.2.3.4 Separation of proteins in native polyacrylamide gels	48
3.2.3.5 Activity-stain for hAOX1	48
3.2.3.6 Characterization of hAOX1 by UV/VIS Spectroscopy	48
3.2.3.7 Photometric determination of the specific activity	49
3.2.3.8 Reduction spectra	50
3.2.3.9 Analysis of the Moco content by HPLC	50
3.2.3.10 Metal content	51
3.2.3.11 Quantitation of the FAD cofactor	51
3.2.3.12 Redox titration of hAOX1	52
3.2.3.13 Kinetics parameters of hAOX1	52
3.2.3.14 Inhibition studies.....	55
3.2.3.15 Electrochemical measurements of H ₂ O ₂ formation	55
3.2.3.16 Cytochrome c reduction assay and determination of O ₂ ^{•-} production	56
3.3 Computational methods	57
3.3.1 Protein modelling.....	57
3.3.2 Determination of Single nucleotide Polymorphisms	57
4. Results	58
4.1. Expression and characterization of hAOX1: comparison of a codon optimized and not codon optimized expression system.....	58
4.1.1 Heterologous expression of a <i>hAOX1</i> codon optimized gene construct	58
4.1.2 Purification of hAOX1	59
4.1.2.1 Ni-NTA affinity chromatography	59
4.1.2.2 In vitro chemical sulfuration.....	60
4.1.2.3 Size exclusion chromatography	63
4.1.3. Characterization of codono optimized hAOX1 (hAOX1).....	65
4.1.3.1 Activity staining of hAOX1	65
4.1.3.2 Metal content	66
4.1.3.3 UV/Vis spectroscopy	67
4.1.4 Enzymatic activity	68
4.1.4.1 State-steady kinetics and substrate specificity.....	68
4.1.4.2 Other electron acceptors	71
4.1.5 Comparison with bXO	72
4.1.5.1 Reactivity of hAOX1 FAD active site	72
4.1.5.2 NADH reduction of hAOX1 and bXO	74
4.1.6 Structural studies on hAOX1.....	75
4.1.7 Inhibition studies.....	77
4.1.7.2 Other inhibitors	80
4.2 hAOX1 mutagenesis and Flavin adenine dinucleotide active site	82
4.2.1 Mutagenesis, expression and purification of the hAOX1 variants	82
4.2.1.1 SNPs identification in hAOX1 and additional mutagenesis.....	82
4.2.1.2 Expression and purification of the hAOX1 variants.....	87
4.2.2 Characterization of the hAOX1 SNP variants	90
4.2.2.1 Cofactor of hAOX1 SNP variants.....	91
4.2.2.2 Catalytic activity of hAOX1 SNP variants	93

4.2.2.3 UV-VIS monitored redox titrations of hAOX1 G46E and L438V.....	95
4.2.3 Characterization of FAD loop hAOX1 variants	97
4.2.3.1. Kinetics constants for FAD loop hAOX1 variants	98
4.2.4 Characterization of additional variants of the FAD site of hAOX1	99
4.3 Reactive oxygen species (ROS) production by hAOX1	101
4.3.1 hAOX1 and O ₂ reactivity.....	101
4.3.2 Hydrogen peroxide production by hAOX1 WT	102
4.3.3 Superoxide production by hAOX1 WT and variants.....	103
4.3.4 Superoxide and hAOX1 variants	104
5. Discussion	107
5.1 Optimization of the expression of hAOX1.....	107
5.2 Characterization of the enzymatic activity of the hAOX1	109
5.3 Structural insights of hAOX1 free and complexed with substrate-inhibitor	110
5.4 Inhibition studies.....	112
5.5 Interaction of hAOX1 with nicotinamide adenine dinucleotide	114
5.6 Studies at the FAD active site of hAOX1	116
5.6.1 Single nucleotide polyphormisms and studies on the flavin adenine dinucleotide of hAOX1	118
5.6.2 Insertion of the bXOR FAD flexible loop I in hAOX1 FAD active site	120
5.7 Reactive Oxygen Species (ROS) and hAOX1	121
5.7.1 Mutagenesis of Leu438 and ROS overproduction.....	124
6. Outlook	127
7. Conclusion	130
8. Summery.....	132
9. References.....	134
10. Appendix.....	148

List of figures

Figure 1.1. Molybdenum-containing enzymes families.....	15
Figure 1.2. Sulfuration of mono-oxo Moco in mammalian cells.....	16
Figure 1.3. General structure of the aldehyde oxidase monomer..	18
Figure 1.4. Scheme of the phylogeny human, monkey and dog aldehyde oxidases.....	20
Figure 1.5. Overall structure of the hAOX1 dimer and location of the SNP-based amino acid exchanges.....	25
Figure 1.6. Reduction of oxygen to water.....	29
Figure 1.7. Structure of Flavin adenine dinucleotide.....	30
Figure 1.8. Close-up and superposition of the crystal structures of the FAD binding sites of hAOX1 bXO and bXDH.....	33
Figure 1.9. FAD binding site of the bovine xanthine oxidase (bXO).....	35
Figure 3. 1. The standard and the site direct mutagenesis PCR.....	42
Figure 3. 2. Site Direct Mutagenesis by PCR	43
Figure 3. 3. Sodium Dodecyl Sulfate (SDS) structure.....	47
Figure 3. 4. Scheme of the Pt-electron H ₂ O ₂ measurements and the Cyt c assay for detection of superoxide anion.....	55
Figure 4. 1. 10% SDS-polyacrylamide gels fractions after Ni-NTA affinity chromatography purification of hAOX1 and native hAOX.....	59
Figure 4. 2. <i>In vitro</i> chemical sulfuration experiments: pH optimum and time range of incubation using hAOX1 and native hAOX1	62
Figure 4. 3. Size exclusion chromatography (Superdex 200 column) purification of hAOX1 and native hAOX1.	63
Figure 4. 4. Specific activity for the eluted fractions.....	64
Figure 4. 5. 10% coomassie stained SDS-PAGE 7% Native PAGE, activity staining gel of native hAOX1 and hAOX1.....	65
Figure 4.6. UV/Vis spectrum of the native hAOX1 and the hAOX1	67
Figure 4. 7. UV/Vis reduction spectrum of hAOX.....	69

Figure 4. 9. Structure of phenanthridine (A), phthalazine and benzaldehyde	69
Figure 4. 10. Reactivity of hAOX1 toward phenanthridine as substrates and several electron acceptors	72
Figure 4. 11. Structure of diphenyliodonium chloride.....	73
Figure 4. 12. The effect of diphenyliodonium on hAOX1 activity.....	73
Figure 4. 13. UV/Vis spectra of hAOX1 in comparison to bXO reduced with NADH under anaerobic conditions.....	75
Figure 4. 14. Crystal of hAOX1 in the presence of phthalazine.....	76
Figure 4. 15. Overlay of the active site residues of hAOX1-free and hAOX1-phthalazine complex.....	77
Figure 4. 16. Structures of thioridazine, loxapine, DCPIP and raloxifene.....	78
Figure 4. 17. Kinetics of phthalazine-thioridazine inhibition of hAOX1, mAOX3, xanthine-thioridazine inhibition of bXO and phenanthridine-thioridazine inhibition of hAOX1..	79
Figure 4. 18. Lineweaver-Burk plots of hAOX1 inhibition by DCPIP.....	81
Figure 4. 19. Lineweaver-Burk plots of hAOX1 inhibition by raloxifene and loxapine.....	81
Figure 4. 20. Amino acidic sequence of hAOX1 with some of the selected single nucleotide polymorphisms selected on the hAOX1 gene.....	82
Figure 4. 21. Amino acid sequence alignment of hAOX1, mAOX3, hXO and bXO.....	83
Figure 4. 22. The location of the SNP exchanged residues in the surrounding of the FAD cofactor of the hAOX1.....	84
Figure 4. 23. Amino acid alignment of hAOX1 wild type and the SNP FAD variants.....	86
Figure 4. 25. Amino acid alignment of hAOX1 wild type and the FAD loop variants.....	86
Figure 4. 26. Elution profiles after size exclusion chromatography.....	88
Figure 4. 27. Characterization of the hAOX1 SNP-based variants.....	91
Figure 4. 28. The effect of diphenyliodonium on the activity of hAOX1 variants.....	95
Figure 4. 29. Redox titration using sodium dithionite of hAOX1 WT and the SNP variants L438V and G46E.....	96
Figure 4. 30. UV/Vis spectra of the indicated proteins isolated from <i>E. coli</i>	98
Figure 4. 31. UV/Vis spectra of the indicated proteins isolated from <i>E. coli</i>	100
Figure 4. 32. Electrochemical measurements of hydrogen peroxide.....	102
Figure 4. 33. Superoxide production by hAOX1 wild-type.....	103
Figure 5. 1. Structure of the hAOX1 homodimer highlighting the inhibitor thioridazine binding pocket.....	112
Figure 5. 2. Structure of bXDH-NADH complex.....	115

Figure 5. 3. Surface superimposition of the FAD binding site of hAOX1-mAOX3 and hAOX1-bXDH.....	115
Figure 5. 4. Shown are the FAD active site of the hAOX1 wild type and a model of the structure of hAOX1 R1231H SNP variant.....	119
Figure 5. 5. Model of the FAD enviroment sourrounding the residue Val in position 438 in comparison to the wild type.....	122
Figure 5. 6. Location of the FAD cofactor between Leu438 and Leu344	124
Figure 5. 7. Location of the residue Leu438 in hAOX1 and distances to the N5-C4a locus.....	126
Figure 6. 1. Cofactor reduction potential of AOXs, XOs and XDHS (adapted from PhD thesis of Dr. M.Mahro, 2013).....	128
Figure A. 1. Sequence alignment of the DNA sequence of the native hAOX1 and a synthetic codon optimized sequence hAOX1.	155
Figure A. 2. Amino acid sequence alignment of hAOX1, mAOX3, hXO and bXO.....	156

List of tables

Table 1: <i>E. coli</i> strains used in this work.	39
Table 2: Standard PCR reaction components.....	41
Table 3: Site directed mutagenesis PCR reaction components.....	42
Table 4: Components for preparation of the SDS-gel.....	47
Table 5: Electron acceptors used in this work.....	54
Table 6: The extinction coefficients used to evaluate the enzymatic activity for hAOX1	55
Table 7: Specific activity of native hAOX1 and hAOX1 before and after <i>in vitro</i> chemical sulfuration.	61
Table 8: Yield of protein of native hAOX1 and hAOX1a.....	64
Table 9: Metal content for of native hAOX1 and hAOX1a.....	66
Table 10: Steady-state kinetics parameters for hAOX1 and native hAOX1a.....	71
Table 11: Kinetic parameters of the phthalazine-thioridazine inhibition of hAOX1 and mAOX3, and of the xanthine- thioridazine inhibition of bXO.....	78
Table 12: Protein yield of hAOX1 wild-type and variantsa.	89
Table 13: Molybdenum, Iron, FAD and FormA content of hAOX1 wild type and SNP-based variants.....	92
Table 14: Steady state kinetic parameters of hAOX1 wild-type and variantsa.	94
Table 15: Steady state kinetic parameters of hAOX1 wild-type and variants and data for saturation with molybdenum and irona.....	99
Table 16: Steady state kinetic parameters of hAOX1 wild-type and variants and data for saturation with molybdenum and irona.....	101
Table 17: Rates of superoxide production from hAOX1 wild type and SNP variantsa	105
Table 18: Rates of superoxide production from hAOX1 wild type and XOR-FAD single and multiple variantsa.....	106
Table A 1. List of buffer and solutions used in this work.....	150
Table A 2. List of chemicals used in this work.....	148
Table A 3. Oligonucleotides used in this study.....	151
Table A 4. Plasmids used in this study.....	153

Abbreviations

List of abbreviations

Å	Ångström = 10^{-10} m
°C	degree celsius = $x + 273.15$ k
λ	wavelength
μ	micro- = 10^{-6}
<i>a. thaliana</i>	arabidopsis thaliana
A_{xxx}	absorbance with indicated wavelength
AGE	agarose gel electrophoresis
AMP	adenosine 5'-monophosphate, [(2R,3S,4R,5R)-5-(6-amino-9H-purin-9-yl)-3,4-dihydroxyoxolan-2-yl] methyl phosphate
Amp	ampicilin, (2s,5r,6r)-6-([(2r)-2-amino-2-phenylacetyl]amino)-3,3-dimethyl-7-oxo-4-thia-1-azabicyclo [3.2.0] heptane-2-carboxylic acid
AOX	aldehyde oxidase gene
AOX/ AOXs	aldehyde oxidase(s)
APS	ammonium persulfate
b	bovine-
bar	kilo-bar = 10^8 kg/m s ²
bp	base pair(s)
c	centi-
cal	kilo-calorie = $4.184 \cdot 10^3$ kg*m ² / s ²
Cm	chloramphenicol, 2,2-dichloro-n-[1,3-dihydroxy-1-(4-nitrophenyl)propan-2-yl] acetamide
CMP	cytidine 5'-monophosphate
cPMP	cyclic pyranopterin-monophosphate
cv	column volume(s)
CYP	cytochrome p450
d	day/ pathlength
<i>D. gigas</i>	Desulfovibrias Gigas
Da	Dalton=1 g/mol
DCPIP	2,6-dichlorophenolindophenol
DDI	drug-drug-interaction

deg	degree
DFT	density functional theory
DMSO	dimethyl sulfoxide, methanesulfinylmethane
DNA	deoxyribonucleic acid
ds	double-stranded
DTT	1,4-dithio-D-threitol, 1,4-disulfanylbutane-2,3-diol
E	energy
E^0	midpoint reduction potential measured
<i>E. coli</i>	escherichia coli
e.g.	exempli gratia, for example
EDTA	ethylenediaminetetraacetate, 2-(2-[bis(carboxylatomethyl)amino]ethyl)(carboxylatomethyl) amino) acetate
EPR	electron paramagnetic resonance
ES	enzyme-substrate complex
ESI	enzyme-substrate-inhibitor complex
EtBr	ethidium bromide, 3,8-diamino-5-ethyl-6-phenylphenanthridin-5-ium bromide
EtOH	ethanol
EXAFS	extended x-ray absorption fine structure
FAD/ FAD ⁺ / FADH ₂	flavin-adenine-dinucleotide (oxidized, semiquinone and reduced form)
FeS	iron-sulfur center
Fig.	figure
FPLC	fast protein liquid chromatography
g	centripetal acceleration = 9.80665 m/s ²
G	giga- = 10 ⁹
GmbH	gesellschaft mit beschränkter haftung
GMP	guanosine 5'-phosphate
GTP	guanosine 5'-triphosphate
h	hour = 3.6 * 10 ³ s, human-
HPLC	high pressure liquid chromatography
HTPS	high throughput screening
Hz	hertz = s ⁻¹
ICP-MS/ ICP-OES	inductively coupled plasma-mass spectrometry/-optical emission spectroscopy

IMP	inosine 5'-phosphate
Inc.	incorporation
IPTG	isopropyl- β -d-thiogalactopyranoside
K	kilo- = 10^3
LB	lysogenic broth
LU	light units = artificial unit
m	meter, milli- = 10^{-3} , murine-
M_{app}	apparent mass
MCS	multiple cloning site
MeOH	methanol
MES	4-morpholineethanesulfonate, 2-(morpholin-4-yl) ethane-1-sulfonate
MFE/ MFEs	molybdo-flavo-enzyme(s)
MGD	molybdopterin guanosine dinucleotide
min	minute = 60 s
mMCSF/hMCSF	murine-/ human molybdenum cofactor sulfurase
mMCSF/hMCSF	murine-/ human molybdenum cofactor sulfurase gene
Moco	molybdenum cofactor
MOCS	molybdenum cofactor synthesis
ModE	molybdate-dependent transcriptional regulator
MPT	molybdopterin
MTP	micro-titer plate
n	nano- = 10^{-9}
NAD ⁺ /NADH	nicotinamide dinucleotide (oxidized, reduced form)
NBT	nitro blue tetrazolium chloride
NHE	normal hydrogen electrode
NMR	nuclear magnetic resonance
NTA	nitrioloacetate, 2-[bis(carboxylatomethyl)amino]acetate
ON	over-night
<i>P. pastoris</i>	<i>pichia pastoris</i>
<i>P. furiosus</i>	<i>pyrococcus furiosus</i>
PAGE	polyacrylamide-gel electrophoresis
PCR	polymerase chain reaction

PDB	protein data bank file
Pfu	pyrococcus furiosus dna directed dna polymerase
pH	decimal cologarithm of proton concentration
pKa	decimal cologarithm of acid dissociation constant
PLP	pyridoxal 5'-phosphate, (4-formyl-5-hydroxy-6-methylpyridin-3-yl) methyl phosphate
PMSF	phenylmethylsulfonyl fluoride
PTLE	protein thin-layer chromatography
<i>R. capsulatus</i>	rhodobacter capsulatus
RNA	ribonucleic acid
ROS	reactive oxygen species
rpm	revolutions per minute
RT	room temperature
SDS	sodium dodecyl sulfate
<i>SF9</i>	<i>spodoptera frugiperda</i> isolate 9
T	temperature
t_{ret}	retention time
Tab.	table
TEMED	tetramethylethylenediamine, [2-(dimethylamino) ethyl] dimethylamine thin layer chromatography
Tris	tris-(hydroxymethyl) aminomethane, 2-amino-2-(hydroxymethyl) propane-1,3-diol
U	unit = 1 $\mu\text{mol}/\text{min}$
UV/Vis	ultra violet-visible
V	volt = 1 $\text{kg}\cdot\text{m}^2/\text{a}\cdot\text{s}^3$
V_{ret}	retention volume
W	watt, $\text{kg}\cdot\text{m}^2/\text{s}^3$
XDH/ XDHs	xanthine dehydrogenase(s)
XO/ XOs	xanthine oxidase(s)
XOR/ XORs	xanthine oxidoreductase(s)

1. Introduction

1.1 Molybdoenzymes

Molybdenum is a transition metal in the fifth period and sixth row of the periodic system. The name is derived from Ancient Greek Μόλυβδος molybdos, meaning lead, derived from its similarity to lead. Molybdenum is essential for most living organisms, primarily for its chemical unique versatility and high bioavailability (Hille, 2002). It was discovered for the first time by the Swedish chemist Carl W. Scheele in 1887.

Due to the solubility of its high valent oxides in water, the molybdenum is largely spread in the biological systems and it is present in the active sites of enzymes that, in general, catalytically transfer an oxygen atom either to or from a physiological acceptor/donor molecule (Hille, 1996). The biologically usable form in nature is the molybdate (MoO_4^{2-}).

In humans, the last step in the metabolism of sulfur-containing compounds requires the molybdo-enzyme sulfite oxidase, which oxidizes sulfite to sulfate and, by cytochrome c, transfers the electrons produced to the electron transport chain, allowing the generation of ATP in oxidative phosphorylation with subsequent sulfate excretion (Johnson *et al.*, 1984; Rajagopalan & Johnson, 1992; Hille, 1999). In most organisms, a crucial stage in the catabolism of purines is the oxidation of xanthine to uric acid, a reaction catalyzed by the molybdo-enzyme xanthine oxidase.

Molybdenum is biologically inactive unless it is complexed by a cofactor and it is bound to a pterin forming the molybdenum cofactor (Moco), the active compound present in the catalytic site of molybdo-enzymes. Within the active site, the metal is found in three different oxidation states (IV, V and VI). In the majority of molybdo-enzymes, the reduction of the molybdenum (VI) is associated with the protonation of ligands to the metal and typically, from Mo=O or Mo=S groups to Mo-OH or Mo-SH, respectively (Hille, 1999). With the exception of the bacterial nitrogenase (Rubio & Ludden, 2008) and the molybdenum-copper carbon monoxide dehydrogenase (Dobbek *et al.*, 2002), all molybdenum containing enzymes possess a single metal in their active site and are termed as mononuclear molybdoenzymes (Hille, 1996). The molybdenum atom is coordinated by a dithiolene group to the molybdopterin (MPT) moiety of the molybdenum cofactor.

The structure of the molybdopterin (MPT) was identified by the analysis of its oxidative products Form A and Form B obtained from chicken sulfite oxidase (Johnson & Rajagopalan, 1982). The proposed structure of MPT was later modified to the ring-closed form, following x-ray crystallographic characterization structures of the aldehyde:ferredoxin oxidoreductase from *Pyrococcus furiosus* (PfaOR) (Chan *et al.*, 1995) and *Desulfovibrio gigas* (DgAOR) (Romão *et al.*, 1995).

The Moco biosynthesis is characterized by the attachment of nucleotides as AMP, CMP, GMP or IMP (present only in prokaryotic molybdoenzymes) to the cofactor (Krüger & Meyer, 1986; Krüger *et al.*, 1987; Satoh & Kurihara, 1987; Karrasch *et al.*, 1990; Schindelin *et al.*, 1996; Boyington *et al.*, 1997; Kisker *et al.*, 1997).

All molybdenum-containing enzymes (with the exception of nitrogenase) are grouped into three large families: DMSO reductase, sulfite oxidase and xanthine oxidase family (Fig. 1.1).

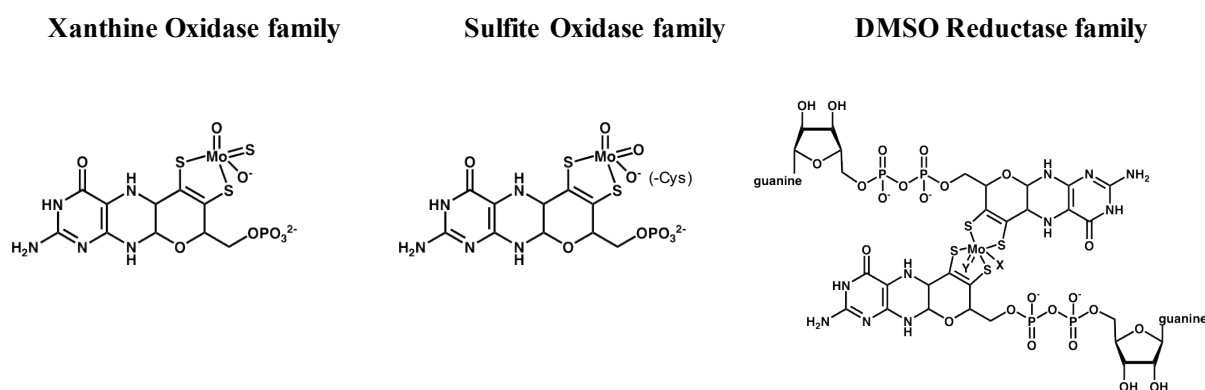


Figure 1.1. Molybdenum-containing enzymes are grouped into three families: xanthine oxidase, sulfite oxidase and DMSO reductase family. The xanthine oxidase family is characterized by a sulfurated Moco where sulfur occupies the equatorial position. In the sulfite oxidase family the molybdenum coordinates two oxygens and a cysteine ligand. The molybdenum cofactor of enzymes of the DMSO reductase family is coordinated by two pyranopterin molecules, which are modified by an attachment of each GMP molecule. The two ligands (-X; -Y) at the molybdenum can be either a sulfur or oxygen atom together with either a hydroxyl group or a cysteine, selenocysteine, aspartate, or serine residue, derived from the protein backbone.

Enzymes of the DMSO reductase family are characterized by two MPT moieties, an oxo-sulfido- or seleno- ligand as well as a cysteine-, selenocysteine- aspartate or serine- ligand provided by the protein or a hydroxo ligand.

Enzymes of the sulfite oxidase family possess a Moco with two additional oxo-ligands and one cysteine-ligand from the protein. The molybdenum in enzymes of the xanthine oxidase family is penta-coordinated in a distorted square- pyramidal geometry (Romão *et al.*, 1995; Kisker *et al.*, 1997). In eukaryotic enzymes of the xanthine oxidases family, one MPT-ligand, an axial

oxo-, an equatorial sulfido- and an hydroxo-ligand make up the coordination sphere of the molybdenum. Notably, in humans only molybdoenzymes of the xanthine oxidase and sulfite oxidase family are present. Aldehyde oxidases (AOXs) are categorized into the xanthine oxidase family.

1.2 Sulfuration of the molybdenum cofactor

In order to generate the active form of Moco in eukaryotic enzymes of the xanthine oxidase family, an equatorial oxo-ligand is exchanged by a sulfido ligand by means of a Moco sulfurase enzyme in the last step of the Moco biosynthesis (Wahl & Rajagopalan, 1982; Amrani *et al.*, 2000; Heidenreich *et al.*, 2005) (Fig.1-2). So far, no mammalian Moco sulfurase has been characterized on the protein level and knowledge is mostly based on studies on the homologs in *Arabidopsis thaliana*, *Drosophila melanogaster* and *Solanum lycopersicum* (Wahl *et al.*, 1982; Watanabe *et al.*, 2000; Bittner *et al.*, 2001; Sagi *et al.*, 2002). Genetic studies on the bovine and human cases indicate that deficiencies in predicted Moco sulfurases are the cause for xanthinuria type II, a disease affecting only proteins dependent on the mono-oxo-Moco (Watanabe *et al.*, 2000; Ichida *et al.*, 2001; Yamamoto *et al.*, 2003). Eukaryotic Moco sulfurases belong to the NifS protein superfamily which are PLP-dependent proteins and carry the sulfur as an cysteine-persulfide (Ichida *et al.*, 2001; Heidenreich *et al.*, 2005; Wollers *et al.*, 2008).

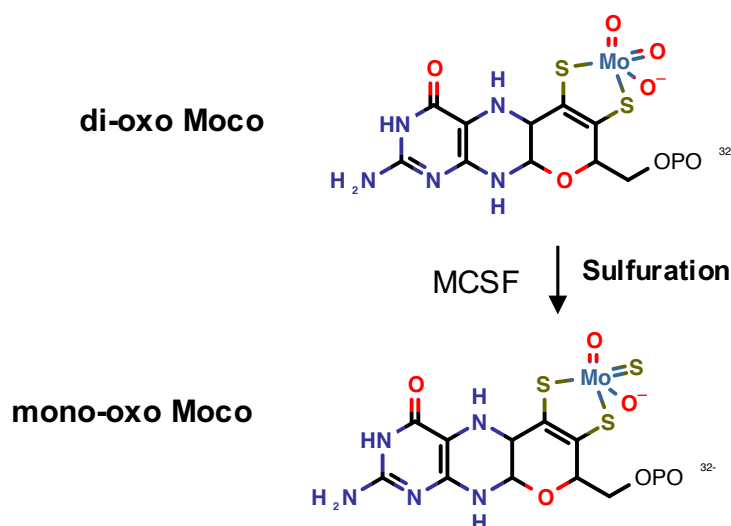


Figure 1.2. Sulfuration of Moco is carried out by a molybdenum cofactor sulfurase (MCSF) in eukaryotes. The figure was created by MarvinSketch Ver. 6.0.0.

1.3 Characteristics of the Aldehyde oxidases

Aldehyde oxidases (AOXs) are a small group of structurally conserved cytosolic enzymes that belong to the molybdenum hydroxylase family, together with xanthine dehydrogenase (XDH) or xanthine oxidase (XO). In their catalytically active forms AOX, XDH and XO exist as a homodimer with a molecular weight of around 300 kDa. Although aldehyde oxidase, xanthine dehydrogenase and xanthine oxidase share a common genetic origin and have a high similarity in the amino acid sequence, primary and secondary structure, cofactor composition and molecular mass, they show a different substrate and inhibitor specificity (Vila *et al.*, 2004). This homology between mouse AOX and XOR is approximately 49% (Vila *et al.*, 2004). AOXs catalyze the oxidative hydroxylation of a large variety of substrates, like aliphatic and aromatic aldehydes, heterocyclic nitrogen compounds and other different drugs. By contrast, XDH and XO are involved in the catabolism of purines, as xanthine and hypoxanthine, and pyrimidines (Garattini *et al.*, 2008). For these characteristics, AOX possess a relatively large substrate binding pocket with increased flexibility to accommodate a wider range of substrates than XDH and XO (Coelho *et al.*, 2015). In the FAD domain, the xanthine oxidoreductases (XOR) present a conserved tyrosine in the central domain, which is responsible for the binding of NAD^+ . This amino acid is replaced by a cysteine in the mammalian AOXs, while in the other AOXs is present a leucine or serine (Garattini *et al.*, 2008). All AOXs use instead of NAD^+ oxygen as electron acceptor and therefore, by the reduction of oxygen, reactive oxygen species (ROS) as hydrogen peroxide and superoxide are formed. Indeed, the role of AOXs in the oxidative stress in the cell is emerging.

1.3.1 Structure of Aldehyde oxidases

AOXs are enzymes that are active as homodimers composed of two identical subunits of about 150 kDa (Coelho *et al.*, 2012; Coelho *et al.*, 2015). The overall dimensions of the hAOX1 homodimer are approximately $150 \text{ \AA} \times 90 \text{ \AA} \times 65 \text{ \AA}$. Each monomer includes 1,336 residues and consists of three domains (Fig. 1.3): an N-terminal domain (20 kDa) containing two spectroscopically distinct [2Fe-2S] clusters, a 40 kDa intermediate domain containing a flavin adenine dinucleotide (FAD) binding site, and a C-terminal domain (85 kDa) containing the substrate binding pocket as well as the molybdenum cofactor binding site (Coelho *et al.*, 2015). The recently solved crystal structures of hAOX1 (Coelho *et al.*, 2015) and mAOX3 (Coelho *et*

al., 2012) revealed new structural insights about these molybdo-enzymes, regarding catalytic differences between AOX and xanthine oxidoreductase (XOR) and regarding the FAD binding site. Generally, the hAOX1 and mAOX3 overall structures confirmed to have high similarity to XORs (Coelho *et al.*, 2012; Coelho *et al.*, 2015). The small N-terminal domain I contains two spectroscopically distinct iron-sulfur centers and can be subdivided into two smaller domains, each containing one [2Fe-2S] center. Domain I is connected to domain II by the linker 1 region (residues 166–231).

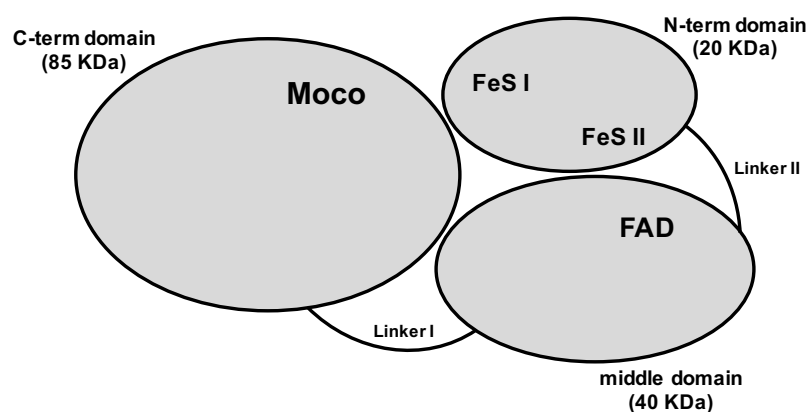


Figure 1.3. General structure of the aldehyde oxidase monomer. The scheme shows the general structure of the aldehyde oxidase monomer, consisting of three conserved domains separated by linker regions. Protein subunits consist of an amino-terminal 20-kDa domain containing two [2Fe-2S] redox centers, a 40-kDa intermediate FAD-binding domain, and the 85-kDa carboxy-terminal domain characterized by the presence of the molybdenum cofactor (MoCo) binding site.

Domain II accommodates the FAD cofactor, with the FAD isoalloxazine ring stacked between two leucine residues (Leu344 and Leu438). In close proximity of the flavin isoalloxazine ring moiety two flexible loops are present and coordinate the environment surrounding the FAD cofactor. The so-called FAD flexible loop I of hAOX1 (Q₄₃₀AQRQENALAI₄₄₀) is superimposable with the one present in the bovine xanthine dehydrogenase (XDH). In bXOR, such flexible loop is involved in the XO-XDH interconversion (Ishikita *et al.*, 2012). At the entrance of the FAD pocket, the flexible loop II (T₁₂₃₀RGPDQ₁₂₃₅) is flipped almost 180° when compared to the corresponding loop in mAOX3, bovine XO and bovine XDH. This loop adopts a conformation so far only found in hAOX1 and sits approximately at the same position as the nicotinamide ring in the bXDH–NADH complex structure (PDB: 3UNI), blocking access of the electron acceptor to the isoalloxazine ring.

The catalytic domain III is connected to domain II through linker 2 (residues 516–555). It harbors the active site, with the Mo=O=S(-OH) catalytic center (Moco) being coordinated by the dithiolene group of a pyranopterin molecule (MPT).

The substrate access to the Moco in AOXs is enabled by a wide and deep funnel that leads into the active site pocket (Coelho *et al.*, 2015). Several residues composing the entrance of the funnel are mobile and they are located in two loop regions within the domain III. These loops are located at the protein surface and form two gates (Gate 1 and Gate 2) which modulate the access of substrates and inhibitors to the active site. The gate 1 (S₆₅₂FCFFTEAEK₆₆₁ in hAOX1) is mostly composed of bulky hydrophobic residues. In the mouse AOX3, the corresponding loop is four residues shorter and lacks the hydrophobic patch (G₆₅₂REEES₆₅₇). The residues present within the gate 1 are not conserved among xanthine oxidoreductases (XO and XDH), with the exception of glutamate in position 660 (hAOX1). The gate 2 (L₈₈₀DESL₈₈₄ in hAOX1) consists of a shorter loop. Instead, in mAOX3 this same loop is highly ordered.

1.3.2 An evolutionary perspective: phylogeny of AOXs.

AOX and XOR, in humans, are the products of distinct genes present on the p and q arms of the chromosome 2 (Xu *et al.*, 1994; Rytönen *et al.*, 1995; Terao *et al.*, 1998). Such organization seems to be similar also for most of the vertebrates (Fig. 1.4). Subsequently, it was shown that its genomic organization is more complex and the identification of novel murine genes showed several forms of aldehyde oxidases (Minoshima *et al.*, 1995; Terao *et al.*, 2001; Kurosaki *et al.*, 2004). Aldehyde oxidase genes present in plants, insects and vertebrates are the result of different evolutionary modifications, such as separated gene duplication and suppression events (Terao *et al.*, 2000).

It is generally believed that the XDH coding gene is the ancestor of all aldehyde oxidase genes, consequently resulting in at least two independent duplication events from the ancestral XDH genes. This idea is also substantiated by the conserved exon organization (Garattini *et al.*, 2003). The most ancient gene of the vertebrate aldehyde oxidase family is the *Aox1* gene, differentiated from an orthologue gene present in an ancestral marine species. The AOX1 gene underwent a further process of duplication in avians forming the AOX presents in the chicken genome (Garattini & Terao, 2006).

Within the human genome, homologous genes to mouse AOX3 (Dupl. 1) and AOX2 (Dupl. 2) were identified in the same genomic region but are not expressed in humans. The human AOX1 gene size approximately 80 kb of DNA and contains 35 exons. Dupl1 and Dupl2 are

transcribed into mRNAs that do not seem to code for protein products, given the presence of in-frame stop codons (Kurosaki *et al.*, 2004).

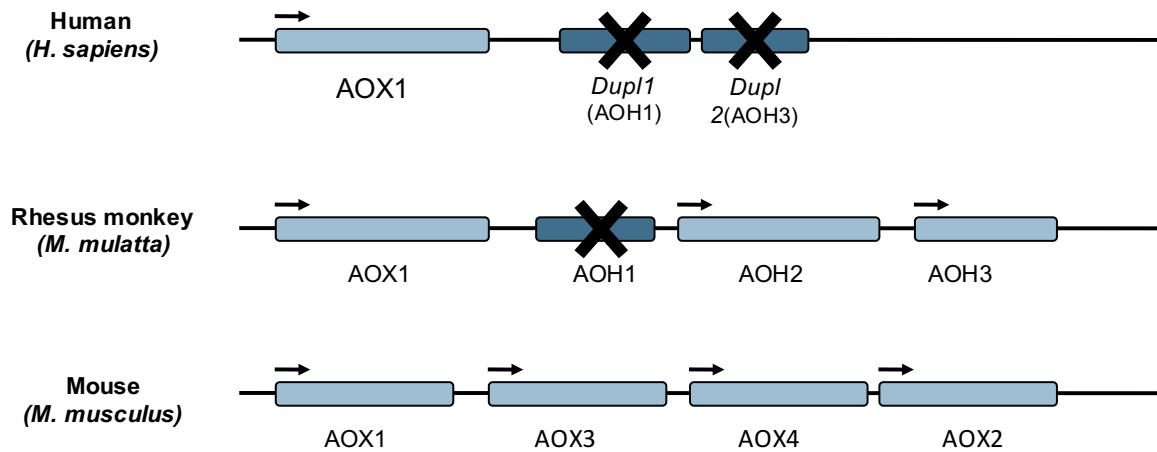


Figure 1.4. Scheme of the phylogeny of human, monkey and mouse aldehyde oxidases. Genetic map of aldehyde oxidase gene with pseudo-genes Dupl1 Dupl2. Direction of transcription is indicated by arrows; pseudogenes are crossed.

1.3.3 Expression and regulation of hAOX1

Aldehyde oxidases are widely expressed in diverse mammalian tissues and organs. In humans, the highest expression of this enzymes is found in liver (Rodriguez-Trelles *et al.*, 2003) but the enzyme is also present in lung, heart, kidney, central nervous system and olfactory tissue. AOX is located in these several organs in different quantities and activities. The expression of AOX1 in the human central nervous system (Berger *et al.*, 1995) was associated with the product of the disease gene resulting in recessive familiar form of amyotrophic lateral sclerosis (ALS). In this study, Berger *et al.* showed the presence of the AOX1 transcript affected glial cell population in the spinal cord. This diversity in distribution and activity depends mostly on the tissues where AOX are expressed as well as on post-translational regulation (Holmes, 1979).

Garattini *et al.* showed a possible post-translational regulation of AOX1 from testosterone, in male and female mice with the same level of AOX1 mRNA (Kurosaki *et al.*, 1999). Additionally, sex hormones were shown to have an influence on the expression of the aldehyde oxidase (Kurosaki *et al.*, 1999). Of these, adiponectin, which is involved in the regulation of fatty acid cycle and glucose metabolism and produced only in fat cells and bloodstream, likely

has a role in the regulation of AOX. Adeponectin induces the activation of peroxisome proliferator-activated receptor alpha (PPAR-alpha) to protect the liver against the fatty acids degeneration. The level of liver hAOX1 activation is reduced by the PPAR-alpha, which may be a connection between an increased level of hAOX1 and fatty liver diseases (Neumeier *et al.*, 2006). Endogenous as well as exogenous stimuli is thought to have a role in the expression of AOX. An oral increment of phthalazine or 1-hydroxyphthalazin in female mice showed an increased specific activity of AOX and XOR in this tissue (Yoshihara & Tatsumi, 1997). It is known that dioxin induces hAOX1, by induction of the mRNA levels, with involvement of the aryl hydrocarbon receptor (AHR) and participation of the Nrf2 transcription factor (Rivera *et al.*, 2005). Maeda *et al.* in 2012, confirmed that the AOX1 gene is regulated by the Nrf2 pathway. Two Nrf2 binding consensus elements (antioxidant responsive element, ARE) were identified, located in the 5' upstream region of the rat AOX1 gene. Molecular analyses showed that Nrf2 binds such regions and strongly activates the rat AOX1 gene (Maeda *et al.*, 2012).

1.3.4 Substrate specificity and reaction mechanism

The substrate specificity of aldehyde oxidases is very broad. The two main reactions catalyzed by aldehyde oxidases are the oxidation of aldehydes into the corresponding carboxylic acids, in presence of oxygen and water, and the hydroxylation of heterocycles (Terao *et al.*, 2001). Although the enzyme uses molecular oxygen as an electron acceptor, the oxygen atom which is incorporated into the carboxylate product is derived from water (Hille, 2002).

The overall reaction mechanism of AOX, and also of the other members of the xanthine oxidase family, is divided in the reductive and oxidative half-reactions of the catalytic cycle. In the reductive half-reaction the molybdenum center becomes reduced from Mo(VI) to Mo(IV) (Hille, 1999). In the oxidative half-reaction, the Flavin hydroquinone is re-oxidized by molecular oxygen and subsequently a new catalytic cycle can start again (Pryde *et al.*, 2010). The multitude of possible physiological substrates is significantly large and the possible involvement of AOX in many metabolisms is shown in several studies (Garattini *et al.*, 2012; Sanoh *et al.*, 2015).

Of high interest is the comparison between AOX and XOR substrates specificities. Diversity in substrate specificity between XOR and AOXs reflects different roles of several residues in substrate recognition and activation (Yamaguchi *et al.*, 2007). Based on the crystal structure of bovine XOR, R881 may form a hydrogen bond with xanthine, but not hypoxanthine. In the

substrate–XOR complex, the side chain of E803 may interact with both xanthine and hypoxanthine by hydrogen bonding. Considering mechanistic and structural similarities between bovine or human XOR and *R. capsulatus* XDH, it appears that residue E1261 of the bovine enzyme, corresponding to E1262 and E730 in humans and *R. capsulatus* enzyme, respectively, is essential for activity. It has been reported that mutation of E730 in *R. capsulatus* XDH resulted in complete loss of catalytic activity (Leimkühler *et al.*, 2004) and it was shown that the mutation of E1262 to alanine in the human enzyme resulted in complete loss of catalytic activity (Yamaguchi *et al.*, 2007). By two mutants of human XOR, E803V and R881M expressed in an *E. coli* expression system, Yamaguchi *et al.*, showed the roles of active site residues in binding and activation of purine substrate (Yamaguchi *et al.*, 2007). The E803V mutation almost completely interrupted the activity towards hypoxanthine as substrate, but very low activity towards xanthine remained. On the other hand, the R881M mutant lacked activity towards xanthine, but retained low activity towards hypoxanthine. Both mutants, however, exhibited significant aldehyde oxidase activity (Yamaguchi *et al.*, 2007).

Garattini *et al.* showed the E1261 of bovine XOR is strictly conserved at the same position as for all the aldehyde oxidase sequences analyzed. This residue is fundamental for the mechanism of the reaction catalyzed by both XOR and aldehyde oxidases. Furthermore, site-directed mutagenesis experiments demonstrated its important role in substrate specificity of E802 and R880 residues (Okamoto *et al.*, 2004).

In the AOXs, a highly conserved glutamate residue (E1265 in mAOX1, E1276 in mAOX2, E1266 in mAOX3, E1267 in mAOX4 and E1270 in hAOX1) favors the extraction of a proton from the Mo–OH group, leading a nucleophilic attack on the substrate. An hydrogen atom is transferred from the aldehyde group of the substrate to the Mo=S, as a hydride. This results in a loss of two electrons at the molybdenum, resulting in an oxidation state change from IV to VI (Alfaro *et al.*, 2009; Schumann *et al.*, 2009; Hartmann *et al.*, 2012; Mahro *et al.*, 2013). A water molecule carries the molybdenum to its original oxidized state.

Aldehyde oxidase is able to catalyze a wide range of substrates and therefore, by this feature, AOX can play an important role in metabolism of drugs and xenobiotic in the human liver cytosol. An *in vitro* study of Obach *et al.* revealed 239 pharmacologically relevant drugs which inhibits AOX (Obach *et al.*, 2004).

By heterologous expression system of mAOX1 in *E. coli*, Schumann *et al.*, have analyzed the role of specific amino acidic residues at the active site. A site-directed mutagenesis exchanged the residues E1265, V806, and M884 to the ones identified in the active site of XORs. The result was a drastic decrease in the oxidation of aldehydes and no increase in the oxidation of

purine substrates (Schumann *et al.*, 2009). The double mutant V806E/M884R and the single mutant E1265Q were catalytically inactive enzymes towards aldehyde or purine substrates (Schumann *et al.*, 2009).

These results showed that for hAOX1 more factors determine the binding and conversion of substrates than was shown for mAOX1, and subsequently the substrate specificity cannot be converted to purine substrates by two amino acid exchanges at the active site (Schumann *et al.*, 2009). Data from Mahro *et al.* showed the fundamental role of the conserved K889 in the molybdenum active-site of mAOX3 in substrate orientation and/or transition state stabilization, similar to the conserved Arginine residue in the molybdenum active-site of XORs (Mahro *et al.*, 2013). Furthermore, in the proposed mechanism for mAOX3, S1085 and G918 coordinate the position of E1266 in proximity to the Mo-OH moiety and increase the basic character of E1266. Thus, E1266 becomes basic and close to the Mo-OH moiety to initiate catalysis. Once the substrate is bound, the highly conserved, charged residue K889 stabilizes the substrate and the transition state by electrostatic interaction. After passing the electrons to the iron-sulfur centers and FAD, the molybdenum in the oxidation state +VI allows the hydrolysis of the enzyme-product complex, releasing the product (Mahro *et al.*, 2013).

Hartmann *et al.* analyzed the impact of SNPs of human AOX1 (Hartmann *et al.*, 2012). They characterized the amino acid exchanges resulting in the AOX1 variants H1297R, N1135S, R802C, and R921H and analyzed for activities and cofactor saturations. The results showed that the SNPs can be classified into three groups in general: fast metabolizers (FMs), poor metabolizers (PMs), and those which have no effect on catalytic efficiency (Hartmann *et al.*, 2012).

Substrate-activity relationship of aldehyde oxidase metabolism were discovered by monitoring the differences between rabbit liver aldehyde oxidase and bovine milk xanthine oxidase (Krenitsky *et al.*, 1972). High metabolic activities of aldehyde oxidase and xanthine oxidase were observed in the cases of 2-hydroxypurine, 4-hydroxypteridine, 4-hydroxypyrido[2,3-d]pyrimidine, 4-hydroxypyrido[3,2-d]pyrimidine, 4-hydroxypyrimidine, 2-mercaptapurine, pteridine, purine, and 6-purinecarboxamide. Whereas aldehyde oxidase mainly metabolizes 6-cyanopurine, 2-hydroxy pyrimidine, 7-hydroxy-(1,2,5)-thiadiazolo[3,4-d]-pyrimidine, and 3-methylhypoxanthine, and xanthine oxidase mainly metabolizes 6,8-dihydroxypurine, hypoxanthine, 1-methylxanthine, pterin, and xanthine (Krenitsky *et al.*, 1972).

Structure and metabolism relationships were evaluated using single substitutions in phthalazine, which is metabolized to 4-hydroxy phthalazine by aldehyde oxidase. In these experiments, a greater lipophilicity of substitutions partially led to higher substrate affinity of

aldehyde oxidase (Beedham *et al.*, 1990). However, Pryde *et al.* reported no strong relationship between aldehyde oxidase activity and lipophilicity (Pryde *et al.*, 2010). Terao *et al.*, 2016, showed data indicating that 5-hydroxyindolacetic acid and tryptophan are novel endogenous mAOX4 substrates (Terao *et al.*, 2016).

The structure-metabolism relationships of aldehyde oxidases may involve other factors in addition to lipophilicity of aromatic heterocyclic compounds. E803 and R881 mutations in the active site of xanthine oxidoreductase decreased metabolic activities towards hypoxanthine and xanthine, but they induced metabolic activities towards the aldehyde oxidase substrates benzaldehyde and p-(dimethylamino)cinnamaldehyde (Yamaguchi *et al.*, 2007). Moreover, both conserved and nonconserved amino acid residues in active sites of aldehyde oxidase and xanthine oxidoreductase are central to their respective metabolic activities (Coelho *et al.*, 2012). These differences are critical for understanding of substrate specificity of aldehyde oxidase and xanthine oxidoreductase, both of which mediate nucleophilic attack using molybdenum cofactors.

1.3.5 The human aldehyde oxidase and its intraspecific variability

The human AOX1 gene is encoded on the chromosome 2q32.3-2q33.1. The human genome therefore keeps a single functional AOX1 gene and three tandem gene duplications with similarity to mouse AOX2, AOX3 and AOX4 (Kurosaki *et al.*, 2004). The most likely hypothesis is that these duplications are pseudo-genes replacing the mouse AOX2, AOX3 and AOX4 loci and that these genomic sequences submitted events of genetic suppression (Kurosaki *et al.*, 2004).

AOX activity was measured in 101 children *in vivo*, at different age range (Tayama *et al.*, 2007). Important connections resulted between AOX activity and several growth parameters as age, body weight, body surface area, and liver volume. The AOX activity of the subjects quickly increased with increasing of the age up to 1 year. These results showed that AOX activity starts to increase soon after birth (Tayama *et al.*, 2007). It has been confirmed that the activity of AOX is increasing depending on the age (Wright *et al.*, 1997).

A reason explaining the intra-population differences in the activity level of hAOX1 could be explained with the presence of single nucleotide polymorphisms (SNPs) within the human genome (Yasuhara *et al.*, 2005).

For its role in the metabolism of xenobiotics, there is interest in gaining information on the factors influencing the activity of AOX1 in humans, considering the importance in predicting individual responses to drugs that are known to be metabolized by this enzyme. An example is the catabolism of methotrexate which is controlled by the inter-individual levels of AOX1 activity in the human population (Garattini *et al.*, 2004).

A major source of inter-individual variability in the human population is represented by the presence of allelic variants of the AOX1 gene coding for proteins with increased or decreased catalytic activity. Missense single nucleotide polymorphisms (SNPs) in the coding region of the AOX1 gene may affect the catalytic function of the enzyme both in a negative and positive fashion (Fig. 1.5).

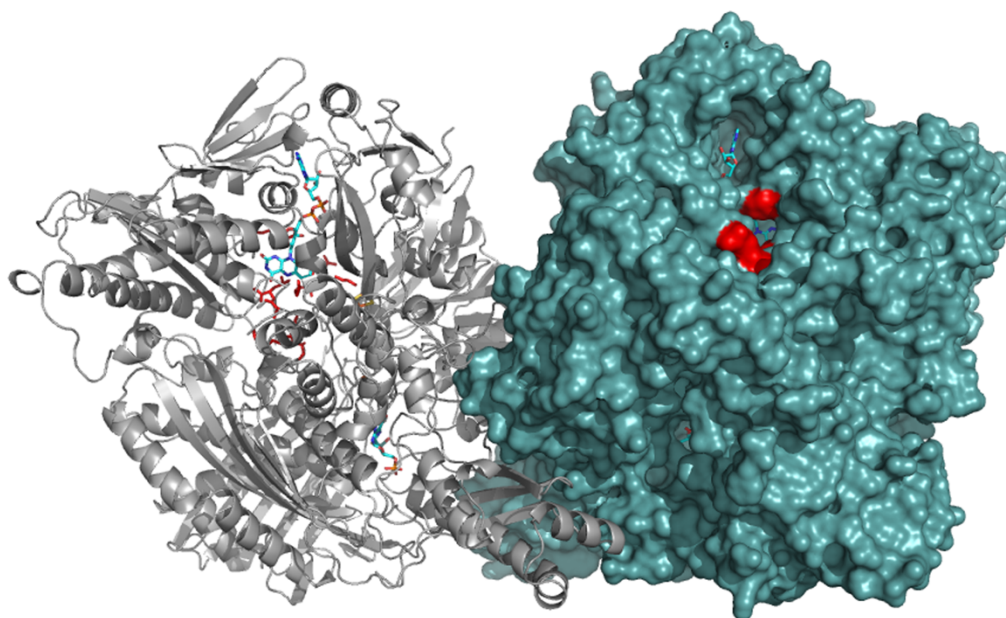


Figure 1.5. Overall structure of the hAOX1 dimer and location of the SNP-based amino acid exchanges. Monomer A is shown as surface representation (right) and the monomer B as cartoon (left) showing the Moco, 2x[2Fe2S] centers and the FAD cofactor. In close proximity to the FAD cofactor the location of the SNP-based amino acid exchanges characterized in this study are shown as red sticks. The Figure was generated using the PDB code 1UHW published by Coelho *et al.*, 2015.

Non-sense nucleotide mutations in the heterozygous state have been shown to decrease AOX1 activity by 50%, whereas, the same mutations in the homozygous state abolish the enzymatic activity. Numerous SNPs of the human AOX1 gene are available in the NCBI dbSNP database, although for the majority of them allelic frequency data are not available. The only results

available on the effects of amino acid exchanges on the catalytic activity of AOX1 were obtained in rats (Zientek *et al.*, 2010). Relatively frequent SNPs in the coding region of the AOX1 gene using a cohort of 180 volunteers were identified, representative of the Italian population (Hartmann *et al.*, 2012) In this population, one non-sense mutation was identified; one SNP was synonymous while five were non-synonymous. The non-sense mutation is located in exon 5 and predicts a short and inactive protein. This mutation has a relatively high incidence (allelic frequency, 2.6%) in the Italian population and is at the basis of a haplo-insufficient phenotype, being observed only as a heterozygous trait (Garattini & Terao, 2011). The most frequent missense mutation identified is a G/A substitution resulting in the presence of an Arginine instead of a Lysine residue at position 1297 (R1297K). Exon 34 is likely to represent a mutational hotspot, as another relatively frequent SNP (T/C) resulting in the substitution of S1271L and a synonymous SNP are located in this exon. A relatively frequent missense SNP corresponding to an A to G transition, resulting in the substitution of Asparagine with a Serine residue at position 1135 is observed in exon 30. By the expression of recombinant AOXs in *E. coli*, Hartmann *et al.*, concluded that individuals characterized by the R802C and the R921H variants may be considered poor metabolizers, since both variants are characterized by reduced catalytic activity. In contrast, individuals with an N1135S and an H1297R genotype can be classified as fast metabolizers, since the two variants show high catalytic activity with all the tested substrates (Hartmann *et al.*, 2012).

1.4 Reactive oxygen species (ROS) and Flavin cofactors

1.4.1 Reactive oxygen species in cell physiology

Although oxygen is considered to be the responsible for the expansion of life on Earth, this molecule represents a source of injuries for living organisms. The oxygen present in the air is a relatively nonreactive chemical (Holland, 2006). However, when oxygen is exposed to high-energy or electron-transferring chemical reactions, it can be converted to various highly reactive chemical forms collectively designated as “reactive oxygen species” (ROS). ROS are toxic to biological organisms because they oxidize lipids, proteins, DNA, and carbohydrates, resulting in the damage to normal cellular, membrane, and reproductive functions.

The term ROS is generally used to refer to the initial species generated by oxygen reduction, mostly superoxide ($O_2^{\cdot-}$) or hydrogen peroxide (H_2O_2), as well as their secondary reactive products (Fig. 1.6).

Although it is called “super-oxide”, this oxygen radical is not a strong oxidizing species. Because of its lower reduction potential (-330 mV for the $O_2/O_2^{\cdot-}$ redox couple), superoxide often acts as a reducing agent rather than an oxidizing species. Indeed, the ferricytochrome c reduction assay, a method for detecting superoxide, is based on the ability of superoxide to reduce this small heme-containing protein (McCord & Fridovich, 1969). The ability of superoxide to directly oxidize biomolecules, including lipids, proteins, and nucleic acids is much limited. However, superoxide is an important ROS that can result in cell and tissue injury (Fridovich, 1997). Superoxide has gradually taken central stage in the research field of ROS in biology and medicine. Indeed, superoxide is considered the primary ROS that gives rise to secondary ROS. This oxygen free radical is generated in a wide variety of biological systems ranging from aerobic microorganisms to human cells, and also formed in the deep ocean and the soils of Earth and possibly the soils of Mars as well. Superoxide is now recognized as an important molecule that is formed via defined mechanisms and involved in diverse physiological and pathophysiological processes (Winterbourn, 2008; Holmstrom & Finkel, 2014).

Other prominent oxygen radical, hydrogen peroxide (H_2O_2) is one of the most extensively studied reactive oxygen species (ROS) in biology and medicine. It is generated constitutively from various cellular processes either directly via two-electron reduction of molecular oxygen or indirectly via dismutation of superoxide. Because of the high activation energy, H_2O_2 reacts poorly with most cellular constituents. However, it may oxidize the thiol groups in certain proteins and enzymes, including these involved in cell signaling transduction. The potential of H_2O_2 to cause oxidative stress and tissue injury primarily results from its reactions with other molecules to form secondary reactive species, including hydroxyl radical and hypochlorous acid. While its tightly controlled production, H_2O_2 plays important roles in various physiological responses and overproduction of this ROS contributes to the pathophysiology of a variety of disease processes and related conditions, including cardiovascular diseases, diabetes, neurodegeneration, cancer, and aging, among many others (Winterbourn, 2008).

Another relevant ROS species is hydroxyl radicals ($\cdot OH$), highly reactive and consequently short-lived molecule. The hydroxyl radical can damage all types of macromolecules: carbohydrates, nucleic acids (mutations), lipids (peroxidation), and amino acids (Reiter *et al.*, 1995). This makes it a very dangerous compound to the organisms (Pablos *et al.*, 1995; Reiter

et al., 1997). The hydroxyl radical has a very short *in vivo* half-life of approximately 10^{-9} seconds and a high reactivity (Sies, 1993).

Unlike superoxide, which can be detoxified by superoxide dismutase, the hydroxyl radical cannot be eliminated by an enzymatic reaction. Mechanisms for scavenging peroxy radicals for the protection of cellular structures includes endogenous antioxidants such as melatonin and glutathione, and dietary antioxidants such as mannitol and vitamin E (Reiter *et al.*, 1995). Of high interest are also the reactive nitrogen species (RNS), reactive species derived from nitric oxide. There is clearly overlap and crosstalk between the production, function and decomposition of the two groups, especially because of the highly favored reaction between superoxide and nitric oxide to give peroxynitrite (Rodriguez & Redman, 2005). Furthermore, nitric oxide is a radical that, although not a good oxidant, forms nitrosothiols that show analogy to thiol oxidation products in cell signaling and regulation.

Reactive oxygen species are produced in a broad range of physiological processes. They are capable of causing biological damage and are implicated in aging and the pathology of many conditions, including cancer and cardiovascular, inflammatory and degenerative diseases.

Before the discovery of superoxide dismutase (SOD), free radicals were considered to be of little biological significance (Ray *et al.*, 2012). However, the realization that an enzyme exists to break down free radicals opened up the field of free radical biology. Nowadays, a greater knowledge is available about the chemistry of physiologically relevant reactive oxidants and how they react with biological molecules (Winterbourn & Hampton, 2008). However, molecular and cell biology studies emphasize the implication of oxidants in increasingly diverse and complex processes, where the underlying chemical mechanisms are often not clear. Identification of specific oxidants involved in a biological process has to be related to their targets and to the reaction mechanisms. Some reactions, although theoretically possible, will not be physiologically relevant.

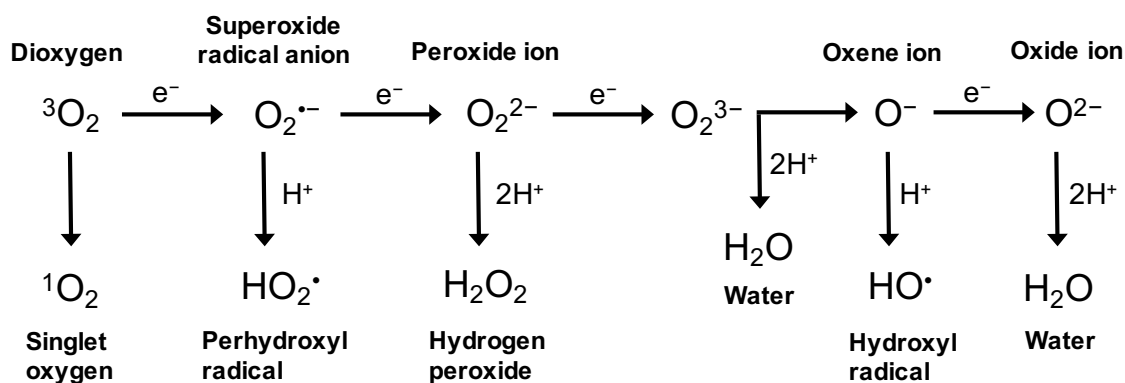


Figure 1.6. Reduction of oxygen to water. Generation of different ROS by energy transfer or sequential univalent reduction of ground state triplet oxygen.

Although this nonspecific, random and damaging aspect of ROS biology persists, there is a growing appreciation that oxidant species, such as superoxide ($\text{O}_2^{\bullet-}$) and hydrogen peroxide (H_2O_2), can also have useful and beneficial effects.

A physiological aspect of those molecules is the redox-dependent signaling mechanism, a well-conserved and presumably ancient feature that is primarily based on the oxidation and reduction of crucial cysteine residues. The concept that oxidants can function as part of signal transduction pathways is a fairly new idea that has gained importance in the last years (Winterbourn, 2016). Both superoxide and hydrogen peroxide have been implicated as potential messengers, although the greater stability of hydrogen peroxide seems to make it to function as a signaling intermediate. Given the chemical simplicity of most ROS, the basis of how redox signaling achieves any measure of specificity has been difficult to understand. Recent evidence that oxidants and their targets might be spatially confined within the cell, could provide at least part of the answer. Although many questions remain, ever growing numbers of observations regarding ROS biology are rapidly shaping the understanding of a range of topics, including metabolic regulation, innate immunity, stem cell biology, the pathogenesis of cancer, and the aging (Holmstrom & Finkel, 2014).

1.4.2 Flavin cofactors and reactivity toward oxygen

The interaction between flavins and oxygen is one of the most fascinating reactions in biochemistry. Flavins (generally FAD or FMN) are redox cofactors, able to receive up to two electrons from reducing substrates and conveying them to electron acceptors (Fig. 1.7) (McDonald *et al.*, 2011). These protein cofactors play a role in networks of redox reactions to

serve the cellular physiological homeostasis. Oxygen is easily available in aerobic organisms, and therefore it is commonly employed as electron acceptor in flavoenzyme catalysis to generate hydrogen peroxide (H_2O_2), which is emerging as a key cell signaling molecule (Forman *et al.*, 2010). Flavoenzyme oxidases are also among the most active generators of ROS, the prime examples of this being the NADPH oxidases (Drummond *et al.*, 2011), mitochondrial Complex I (Pryde & Hirst, 2011), and the monoamine oxidases (Binda *et al.*, 2011). They are important for cellular redox metabolism and homeostasis and many flavin-dependent oxidases are well known drug targets (Makarov *et al.*, 2009). A separate class of flavoenzymes, the flavoprotein monooxygenases, uses oxygen to oxidize reduced flavin, but initially forms a quasi-stable C4a(hydro) peroxyflavin, which can be considered an activated form of oxygen that is capable of incorporating a single oxygen atom into an organic substance (Torres Pazmino *et al.*, 2010).

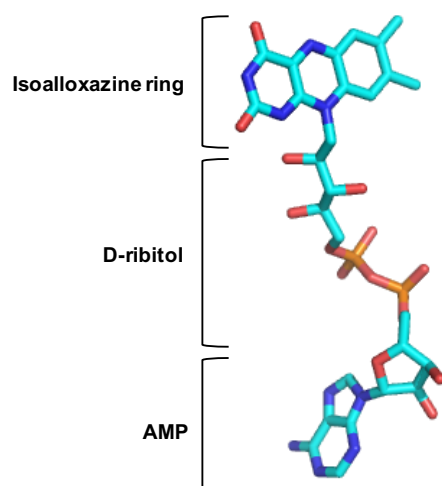


Figure 1.7. Structure of Flavin adenine dinucleotide. FAD consists of three main portions: an adenosine monophosphate (AMP), a D-ribose and the isoalloxazine ring. D-ribose and the isoalloxazine ring form the flavin mononucleotide, named riboflavin. Riboflavin is formed by a carbon-nitrogen (C-N) bond between the isoalloxazine and the D-ribose. Figure obtained using Pymol Mac 6.1.

How the reduced cofactor in flavin-dependent enzyme reacts with oxygen has been one of the most controversial and actively investigated enigmas in enzymology and cofactor biochemistry (Hunt & Massey, 1994). Reaction rates of reduced flavin with oxygen are immensely different among various flavin-dependent enzymes (Mattevi, 2006). No other organic cofactor displays such a range of versatility (Torres Pazmino *et al.*, 2010). During the past several years there have been many significant discoveries related to mechanistic models of how flavin-dependent oxidases and monooxygenases control their reactions with oxygen. This biochemical issue is

gaining further interest because of its direct connection to ROS physiology, and because of its relevance to oxidative stress.

Studies on glucose oxidase has shown that a protonated active site histidine is the crucial positively charged group that contributes to the preorganization energy to facilitate formation of the superoxide radical (Klinman, 2007). Monomeric sarcosine oxidase displayed a conserved lysine residue interacting with the flavin N5 atom via a water-mediated hydrogen bond, a feature conserved in many amine oxidases (Jorns *et al.*, 2010; Kommoju *et al.*, 2011). Site directed mutagenesis to replace the lysine side chain with methionine decreased the rate constant for flavin oxidation by approximately 8000-fold (Zhao *et al.*, 2008). Notably, the enzyme retained the ability to oxidize sarcosine; the mutation effectively led to the conversion of an oxidase into a dehydrogenase, because the enzyme was unable to effectively use oxygen as electron acceptor. Similar mutations with enzymes in the same family such as N-methyltryptophan oxidase and fructosamine oxidase also resulted in large (from 550 to 2500-fold) decreases in the reoxidation rate constants of the enzyme bound reduced flavins (Bruckner & Checchi, 2011; McDonald *et al.*, 2011). A positive charge around the flavin binding site was also shown to be a key feature for enhancing the oxygen reactivity in choline oxidase (Gadda, 2012). Instead of using a positive charge from residues located near the flavin ring, it is the trimethylammonium group of the reaction product that provides the positive charge to generate an electrostatically favorable environment for the reaction of the reduced cofactor with oxygen (Gadda, 2012). However, those evidences are not valid in other cases. Indeed, replacing a positively charged lysine located near the flavin N5 with non charged residues in dihydroorotate dehydrogenase does not result in a significant decrease of the oxidation rates (McDonald *et al.*, 2011). For mouse polyamine oxidase, pH-dependent studies indicate that the neutral (rather than the positively charged) form of an active site lysine is required for more efficient flavin oxidation (Henderson Pozzi & Fitzpatrick, 2010). It was shown from Baron and colleagues that molecular oxygen diffuses through multichannel pathways that guide the gas into a specific site in proximity to the flavin C4a position (Baron *et al.*, 2009). Similar features were also highlighted by computational studies on other oxygen utilizing enzymes such as D-amino acid oxidase (Saam *et al.*, 2010) and Lys-specific histone demethylase 1 (Baron *et al.*, 2011). These findings were confirmed by mutating residues that were shown by the simulations to play a role in gating oxygen access to the flavin. A Phe-to-Trp substitution in p-hydroxyphenylacetate hydroxylase decreased the reactivity of the reduced enzyme with O₂ by 20-fold, and a Gly-to-Val substitution in D-amino acid oxidase decreased

its activity 100-fold (Saam *et al.*, 2010; Baron *et al.*, 2011). Meaningful results were obtained from the research on L-galactono-1,4-lactone dehydrogenase. An Ala-to-Gly substitution targeting a residue adjacent to the flavin N5-C4a locus drastically increased oxygen activity, practically converting the enzyme from being a dehydrogenase to an oxidase capable of efficiently using oxygen as electron acceptor (Leferink *et al.*, 2009a; Leferink *et al.*, 2009b). Another relevant study was performed on aryl-alcohol oxidase. In this case, substitution of a flavin interacting phenylalanine with alanine resulted in a 120- fold decrease in oxidation rate, whereas substitution of the same residue with a bulkier tryptophane yielded a remarkable 2-fold increase in oxidation rate (Hernandez-Ortega *et al.*, 2011). Similar observation was made in choline oxidase, in which substitution of an active site valine with alanine led to a 50-fold decrease in reaction rate of reduced flavin with oxygen (Finnegan *et al.*, 2010). All these previous investigations indicate that oxygen needs to reach the flavin and its access must not be obstructed or hampered by residues that, by being in direct contact with the cofactor, can represent a physical barrier for oxygen. However, an increase in hydrophobicity coupled to a physically more confined environment around the oxygen reacting site can help to guide and locate O₂, facilitating its reaction with reduced flavin.

1.4.3 Reactive oxygen species and molybdo-flavo enzymes

Mitochondria and the NOX family of enzymes are the best characterized intracellular sources of ROS, however, a wide range of enzymes can produce ROS, such as nitric oxide synthase, cyclooxygenases, cytochrome P450 enzymes, lipoxygenases, and the molybdo-flavo-enzyme xanthine oxidase (XO) (Holmstrom & Finkel, 2014).

The ROS species produced by XO are mainly H₂O₂ and O₂^{•-} and a role of XO in reperfusion injury and cardiovascular diseases has been suggested (Saito *et al.*, 1989). Xanthine oxidase is an enzyme that exists in two forms, the oxidase form (XO) taking molecular oxygen as electron acceptor and the dehydrogenase form (XDH) with a high preference towards NAD⁺ as oxidizing substrate at the FAD cofactor of the enzymes. The enzyme is originally expressed as the XDH form and can interchangeably be converted to the XO form either reversibly by formation of disulfide bridges or irreversibly by proteolytic cleavage within the protein backbone (Saito *et al.*, 1989; Nishino *et al.*, 2008). A crucial event during the conversion is the conformational change of the FAD flexible loop I (Gln422- Lys432 in the rat enzyme and Gln423-Lys433 in the bovine enzyme) located near the FAD cofactor (Fig. 1.8). As

consequence, a drastic change in the FAD electrostatic environment hampers the access of the substrate NAD^+ to its binding site (Kuwabara *et al.*, 2003; Asai *et al.*, 2007; Nishino *et al.*, 2008).

Another important difference between XDH and XO is the interaction of four specific amino acid residues, which form a unique amino acid cluster (R334, W335, R426, F549 in the rat enzyme and R335, W336, R427, F549 in the bovine enzyme) at the bottom of the FAD cavity. This four-residues cluster is tightly packed in the XDH form but disrupted in the XO form (Kuwabara *et al.*, 2003; Asai *et al.*, 2007; Okamoto *et al.*, 2008). It was proposed that triggering events, such as the formation of a disulfide bond between C535 and C992 or proteolysis of the linker, relocate F549, resulting in disruption of the four amino acid cluster. Therefore, R426 is then released from the cluster and moves the FAD flexible loop I that blocks the approach of NAD^+ to the flavin ring of the FAD moiety, as well as changing the electrostatic environment (Nishino *et al.*, 2008).

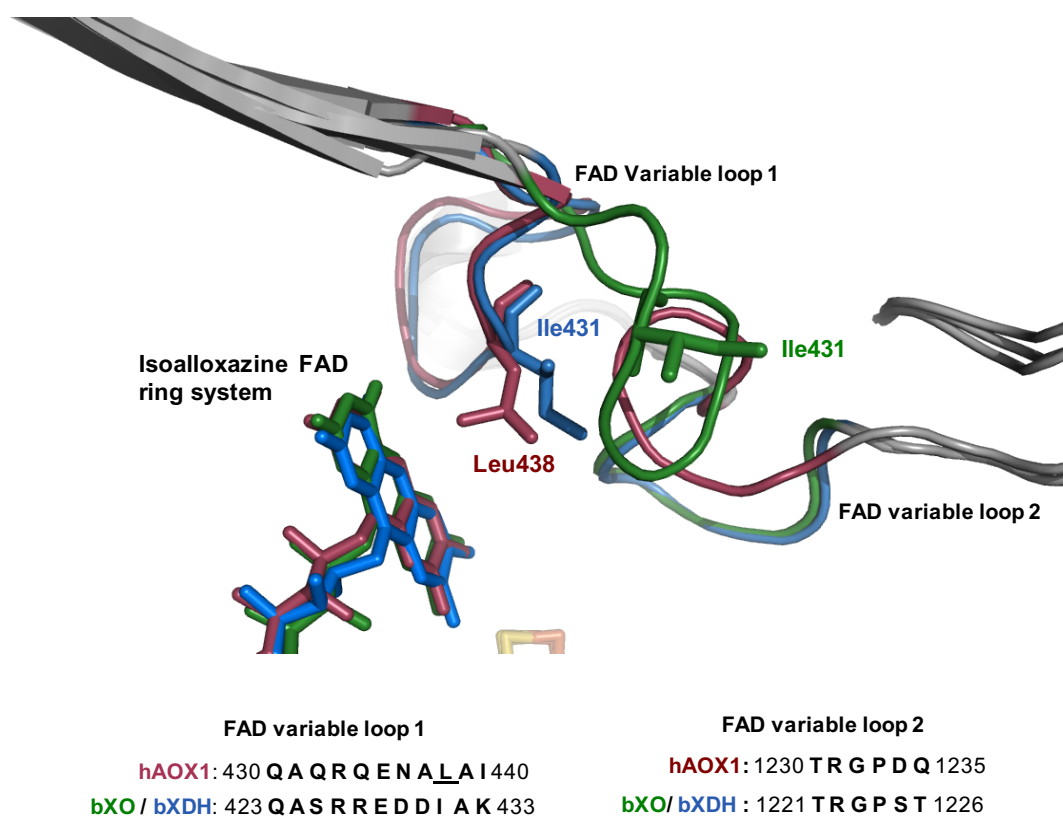


Figure 1.8. Close-up and superposition of the crystal structures of the FAD binding sites of hAOX1 (red, PDB ID: 4UHW), bXO (green, PDB ID: 1FIQ) and bXDH (blue, PDB ID: 1FO4). Shown is the location of the residues Leu438 of hAOX1 (dark red) and Ile431 of bXO/bXDH (green/blue). The FAD variable loops 1 and 2 are located in close proximity to the isoalloxazine ring of the FAD cofactors. The amino acid sequence alignment of the two loops is shown.

The conversion XDH/XO was related with physiological and/or unbalanced oxygen radicals production in the cell (Lee *et al.*, 2014). An important argument, however, against XO as main $O_2^{\bullet-}$ generating source in the cell is that this enzyme is primarily synthesized in the XDH form. The formation of $O_2^{\bullet-}$ by the dehydrogenase form of this enzyme under physiological cellular conditions would be blocked by NAD^+ , due to higher affinity of XDH to NAD^+ instead of O_2 . When the enzyme is converted to the XO form, i.e. under ischaemic conditions, only 15-20% of the total electrons obtained from the substrate oxidation will be used to generate $O_2^{\bullet-}$ by this enzyme form, while the majority of the generated product is H_2O_2 (Nishino *et al.*, 1989a; Nishino *et al.*, 1989b). Thus, it is still unclear whether XO indeed plays a significant role in cellular $O_2^{\bullet-}$ production.

Of great interest but still unclear is the molecular mechanism of ROS production by XO and XDH. It was proposed a crucial role of the FAD semiquinone radical in the formation of superoxide anion in bovine XDH (Kobayashi *et al.*, 1993). The flavin semiquinone is thermodynamically stable in XDH but is unstable in XO (Massey *et al.*, 1989; Nishino & Nishino, 1989). The redox potential of $FADH^{\bullet}/FADH_2$ couple is much lower than that of $FAD/FADH^{\bullet}$ couple in XDH, due to thermodynamic stabilization of the flavin radicals (Hunt *et al.*, 1993). On the other hand, the redox potential of the $FADH^{\bullet}/FADH_2$ couple is always higher than that of the $FAD/FADH^{\bullet}$ couple in XO. Such a stabilization of the semiquinone in XDH seems to be due to flavin-protein interaction and not due to midpotential of flavin (Olson *et al.*, 1974). This property of flavin is maintained also when the flavin has been replaced by artificial flavins having higher redox potentials (Nishino *et al.*, 2005).

Asai *et al.*, generated a bXOR W335A/F336L mutant with the ability to produce a much higher ratio of $O_2^{\bullet-}$, regardless of potential DTT treatment. This mutant produces such amount of superoxide because of its conformation, which is strongly shifted towards the XO form and its FAD redox potential is higher than that of the wild type enzyme. By this mechanism, $O_2^{\bullet-}$ is formed by the reaction of $FADH^{\bullet}$ with molecular oxygen. Thus, $FADH^{\bullet}$ is more thermodynamically stable and accessible during the reaction. In the wild type XOR, the redox potentials of the Fe/S II cluster and of FAD are in thermodynamic equilibrium, so the FAD cofactor exists in both the $FADH_2$ and $FADH^{\bullet}$ forms, producing H_2O_2 and $O_2^{\bullet-}$, respectively, when reacting with oxygen. In the double mutant bXOR W335A/F336L, the FAD redox potential changes to a higher value, and during the catalytic turnover FAD can receive only one electron from Fe/S II to form $FADH^{\bullet}$, which readily with oxygen and $O_2^{\bullet-}$ is produced (Nishino *et al.*, 1989; Harris and Massey, 1997; Asai *et al.*, 2007).

The highly XO-related molybdoenzyme present in most living organisms is aldehyde oxidase, having an amino acid sequence identity of 49.8% to XO and existing only as oxidase form. Both XO and AOX were suggested to be derived from a common ancestor by gene duplication events (Kurosaki *et al.*, 2004). The recently solved crystal structure of human AOX1 (hAOX1) enabled direct comparison of the FAD sites of both enzymes (Coelho *et al.*, 2015). In hAOX1, the FAD cofactor is located in the middle domain of the enzyme, with the isoalloxazine ring stacked between two leucine residues (344 and 438). Notably, hAOX1 and bovine XDH (bXDH) showed a similar conformation of a variable loop at the FAD site (named variable loop I) ranging from amino acids 430-440, which is implicated in the coordination of the FAD cofactor and in the XO/XDH interconversion (Fig. 1.9). In contrast, hAOX1 showed a different conformation of a second loop at the FAD site ranging from amino acids 1230-1235 (named variable loop II). At the entrance of the FAD pocket, loop II T₁₂₃₀RGPDQ₁₂₃₅ is flipped almost 180° in comparison to the corresponding loop in bXO and bXDH. This loop takes a conformation so far only found in hAOX1, and sits approximately at the same position as the nicotinamide ring of the bXDH-NADH complex structure blocking the access to the isoalloxazine ring (Ishikita *et al.*, 2012).

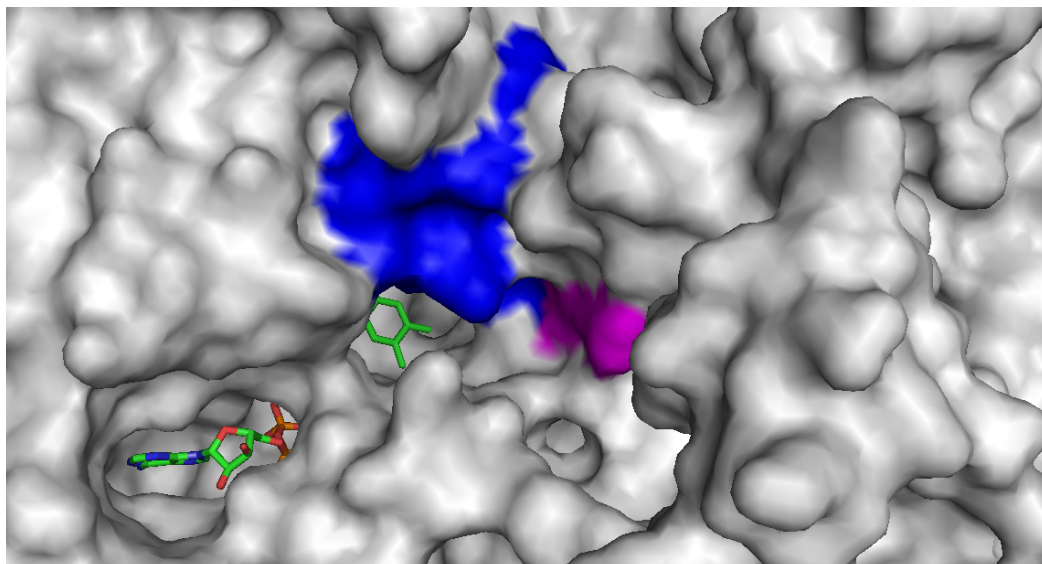


Figure 1.9. FAD binding site of the bovine xanthine oxidase (bXO). Shown as surface the bXO FAD binding site (PDB:1FIQ). The blue region indicates the FAD flexible loop I and the magenta region indicates the FAD flexible loop II. In sticks the FAD structure is represented.

AOX has been suggested to be a source of ROS and further, a role of the generation of nitric oxide (NO) from nitrite reduction during ischemia has also been suggested (Kundu *et al.*, 2012). Thus, in addition to the metabolism of drugs, AOX could serve as an important

biological source of ROS, NO, and reactive nitrogen species (RNS) and might play a crucial role in ROS or RNS mediated signaling and tissue injury (Kundu *et al.*, 2007). While previous investigations on the reactivity of AOX were mainly based on studies using rat or rabbit enzymes, investigations on the ROS production by the human enzyme have not been performed so far.

2. Aim of this work

The human Aldehyde Oxidase (hAOX) is a complex molybdoflavoprotein that belongs to the family of xanthine oxidase enzymes. Like xanthine oxidase (XO), AOX is active as a homodimer composed of two identical subunits of about 150 kDa. The primary difference in the two enzymes, however, is that XO can exist in two interconvertible forms, xanthine oxidase and xanthine dehydrogenase, while AOX exists only in the oxidase form. AOX utilizes only molecular oxygen as an electron acceptor in contrast to XO, which can transfer electrons to both oxygen and NAD^+ . Contrarily to XO, the biochemical and physiological function of AOX is still largely unclear. Notably, the substrate and inhibitor specificities of XO and AOX are different. In general, AOX is able to react toward a broader range of substrates.

The aim of this study was to improve the expression system of hAOX1 by using a codon optimized gene sequence in a *E. coli* heterologous expression system, to increase the yield of protein in order to allow the biochemical characterization of this enzyme. Studies were planned to analyze the kinetic mechanism and to determine the kinetic constants using several substrates and inhibitors. The recently solved crystal structure of hAOX1 (Coelho *et al.*, 2015) provided crucial insights for more kinetics and mechanistic investigations. By site-directed mutagenesis it was planned to study the FAD reactivity with a particular interest in the elucidation of the role of crucial amino acids into the FAD active site of hAOX1. Additionally, it was planned to insert the bXOR FAD flexible loop I (Q₄₂₃ASRREDDIAK₄₃₃) into hAOX1 and study the reactivity toward NAD^+ or NADH. Furthermore, a main goal was to characterize the reactive oxygen species (ROS) produced from the hAOX1 wild type and variants and to determine the residues involved in the mechanism of ROS formation in hAOX1.

3. Materials and Methods

3.1 Materials

3.1.1 Chemicals

Chemicals used in this work are listed in the Appendix Table 1.

3.1.2 Media, buffer and solutions

Solutions and buffers were prepared with deionized Milli-Q water (Merck EMD Millipore Corporation, Billerica, MA,) and listed in Appendix Table 2. The pH value of the solutions were corrected using a glass pH sensor S 100 NE (Knick Elektronische Messgeräte, Berlin) with HCl or NaOH/KOH. Growth media were prepared with deionized water and autoclaved (20 min, 1 bar, 121 °C). Media and media supplements were sterilized by autoclaving (20 min, 1 bar, 121°C) or by sterile filtration.

3.1.3 Plasmids and primers

A synthetic codon-optimized *hAOX1* gene (GeneArt, Thermo Fisher Scientific, Sunnyvale, CA) was used for the heterologous expression of the human Aldehyde Oxidase. The codon optimized *hAOX1* gene contains a DNA sequence that included codons predominantly used in *E. coli* but do not result in a change of the amino acid sequence. The synthetic gene of hAOX1 was amplified using primers designed to permit cloning into the *NdeI* and *Sall* sites of the expression vector pTrcHis (Temple & Rajagopalan, 2000). The resulting plasmid, which was designated pTHco-hAOX1 (Hartmann, 2011), expresses hAOX1 as an N-terminal fusion protein with a His₆-tag. For site-directed mutagenesis and construction of the hAOX1 variants, the expression construct pTHco-hAOX1 was used as a template, and base-pair exchanges were introduced by polymerase chain reaction mutagenesis. Oligonucleotides and primers are listed

in the appendix and were produced from BioTeZ (Berlin Buch GmbH) in purified and desalted quality. All the plasmids and vectors used in this work are listed in the appendix in Table 1.

3.1.4 Cell strains

E. coli strains are listed and characterized in Table 1. Growth conditions are shown in the following sections.

Table 1: *E. coli* strains used in this work.

Cell strain	Genotype	Reference/Source	Cultivation	Usage/Application
DH5α	<i>F</i> -, <i>supE44</i> , Δ <i>lacU169</i> , (ϕ 80 <i>lacZ</i> Δ <i>M15</i>), <i>hsdR17</i> , <i>endA1</i> , <i>gyrA96</i> , <i>thi-1</i> , <i>relA1</i> , <i>recA56</i>	Hanahan, 1983	37°C, LB medium	Host for plasmids and maintenance, cloning
TP1000	<i>araDD(argF-lac)U169</i> <i>rpsLrelA flbB ptsF devC rbsR</i> <i>mobAB:kan</i>	Palmer et al., 1996	30°C, LB medium	Protein expression

3.2 Methods

3.2.1 Molecular biological methods

3.2.1.1 Cultivation of *E. coli* strains

E. coli DH5 α cells (maintenance and cloning strain) were grown in 5 mL LB medium (Bertani, 1951) composed of 5 g/L yeast extract, 10 g /L NaCl, 10 g/L tryptone at 200 rpm for 15 h at 37 °C (Minitron, Infors AG, Switzerland). Subsequently, selective bacterial growth was carried out on agar Petri dishes (LB +2% w/v agar) to obtain individual colonies selected with appropriate antibiotic. *E. coli* TP1000 expression strain was cultivated in LB medium composed of 10 g/L NaCl, 5 g/L yeast extract and 10 g/L peptone per liter of ddH₂O. Initially *E. coli* TP1000 were grown in 50 mL LB pre-cultures overnight (14 h) in 1 mM sodium molybdate (Na₂MoO₄), 20 μ M Isopropyl β -D-1-thiogalactopyranoside (IPTG) and 150 mg/mL of ampicillin at 37°C in anaerobic condition. The main culture was inoculated 1:500 of the pre-

culture with additional supply of the same concentrations of supplements used for the pre-culture and grown for 24 h at 30°C and 130 rpm.

3.2.1.2 Competent *E. coli* cells

E. coli chemo-competent cells (Dagert, 1979) were used for genetic transformation (Hanahan, 1983). For uptake of extrachromosomal plasmid DNA, *E. coli* cells were treated with metal cations to become competent. To obtain competent *E. coli* cells, 100 mL sterile LB containing 20 mM MgSO₄ was inoculated with a single cell colony and incubated while shaking at 250 rpm at 37°C until the cell density reached OD_{600 nm} = 0.9. After cooling the cells on an ice bath for 30 min the cells were harvested by centrifugation at 720 × g (2500 rpm) for 12 min at 0°C. Cell pellets were resuspended in 16 mL MES-buffer and again incubated on ice for 10 min. The cells were harvested afterwards by the same centrifuging process. Finally, the *E. coli* pellets were resuspended in 4 mL MES-buffer and separated in aliquots of 100 µl, frozen immediately in N₂ and stored at -80°C.

3.2.1.3 Transformation of plasmid DNA

For transformation of competent cells strain, a 100 µl aliquot was thawed in ice and plasmid DNA was inserted into competent *E. coli* cells by heat shock transformation. Generally, 50-80 ng of plasmid were added to 100 µl competent *E. coli* cells at 4°C. After incubation for 30 min on ice, the cells were incubated at 42°C for 90 seconds and again incubated on ice for 1 min. 750 µl of LB medium was added to the cells and the mixture was incubated one hour at 37 ° C and 200 rpm. Subsequently, aliquots of 100-200 µl were spread on agar plates containing antibiotics (ampicillin) for selection of transformed cells with plasmid DNA and incubated overnight hypoxically at 37° C.

3.2.1.4 Isolation of plasmid DNA

All the cloned DNA plasmids in this work were purified by the silica-column based NucleoSpin[®] Plasmid kit (Rev.07, MACHEREY-NAGEL GmbH & Co. KG, Germany) in accordance to the manufacturers manual. Plasmid DNA obtained from 5 mL of *E. coli* DH5α

cell culture was eluted with 50 μL of elution buffer AE (5 mM TrisxHCl pH 8.5) following 1 min incubation at room temperature and kept at $-20\text{ }^{\circ}\text{C}$ until usage.

3.2.1.5 Polymerase chain reaction (PCR) and Site Direct Mutagenesis

Amplification of double stranded DNA *hAOXI* gene and site directed mutagenesis were obtained using the polymerase-chain-reaction (PCR) method (Mullis *et al.*, 1992) (Table 2-3). Based on the site direct mutagenesis Quick-change method (Braman *et al.*, 1996), a pair of complementary mutagenic primers were used to amplify the entire plasmid in a thermo-cycling reaction using a Herculase II fusion DNA polymerase. The primers used for the reaction were characterized to be homologous to the cDNA template but containing a mutation within the gene sequence (Fig. 3.1-2). Herculase II polymerase replicates both plasmid strands with high fidelity and without displacing mutant oligonucleotide primers. The proofreading function of the (3'-5')-exo-polymerase activity exhibits a low error rate. As template the vector pTrcHis containing the cDNA of the codon optimized *hAOXI* gene was used. The Herculase II based PCR reaction generated a nicked and circular DNA. Subsequently, the template DNA was eliminated by enzymatic digestion with the restriction site *DpnI*, which is specific for methylated DNA. The template plasmid that is biosynthesized in *E. coli* will be digested, while the mutated plasmid which is generated *in vitro*, and unmethylated, would be left undigested. The *hAOXI* codon optimized wild type gene sequence (Quiagen, Germany) cloned into the pTrcHis expression vector (pTHcoaox) was used as template for all the site direct mutagenesis cloning experiments.

Table 2: Standard PCR reaction components:

Reagents	Concentration	Amount
Sterile H ₂ O		34.5 μl
Template DNA	500 ng/ μl	1 μl
Primer Foward	50 pmol/ μl	1 μl
Primer Reverse	50 pmol/ μl	1 μl
dNTPs	10 mM	1.5 μl
Herculase II Buffer	5x	10 μl
Herculase II Polymerase	1U/ μl	1 μl

Table 3: Site directed mutagenesis PCR reaction components:

Reagents	Concentration	Amount
Sterile H ₂ O		36 μ l
Template DNA	200-400 ng/ μ l	0.5 μ l
Primer Foward	50 pmol/ μ l	0.5 μ l
Primer Reverse	50 pmol/ μ l	0.5 μ l
dNTPs	10 mM	1.5 μ l
Herculase II Buffer	5x	10 μ l
Herculase II Polymerase	1U/ μ l	1 μ l

The standard PCR program contained following steps:

3 min	95°C denaturation	} 35 cycles
30 sec	95°C denaturation	
30 sec	57°C primer annealing	
2:30 min	72°C elongation	
10 min	72°C elongation	

The site direct mutagenesis PCR program contained following steps:

5 min	95°C denaturation	} 18 cycles
30 sec	95°C denaturation	
1 min	65-50°C primer annealing	
5 min	68°C elongation	
7 min	68°C elongation	

Figure 3. 1. The standard (above) and the site direct mutagenesis (below) PCR program used in this work.

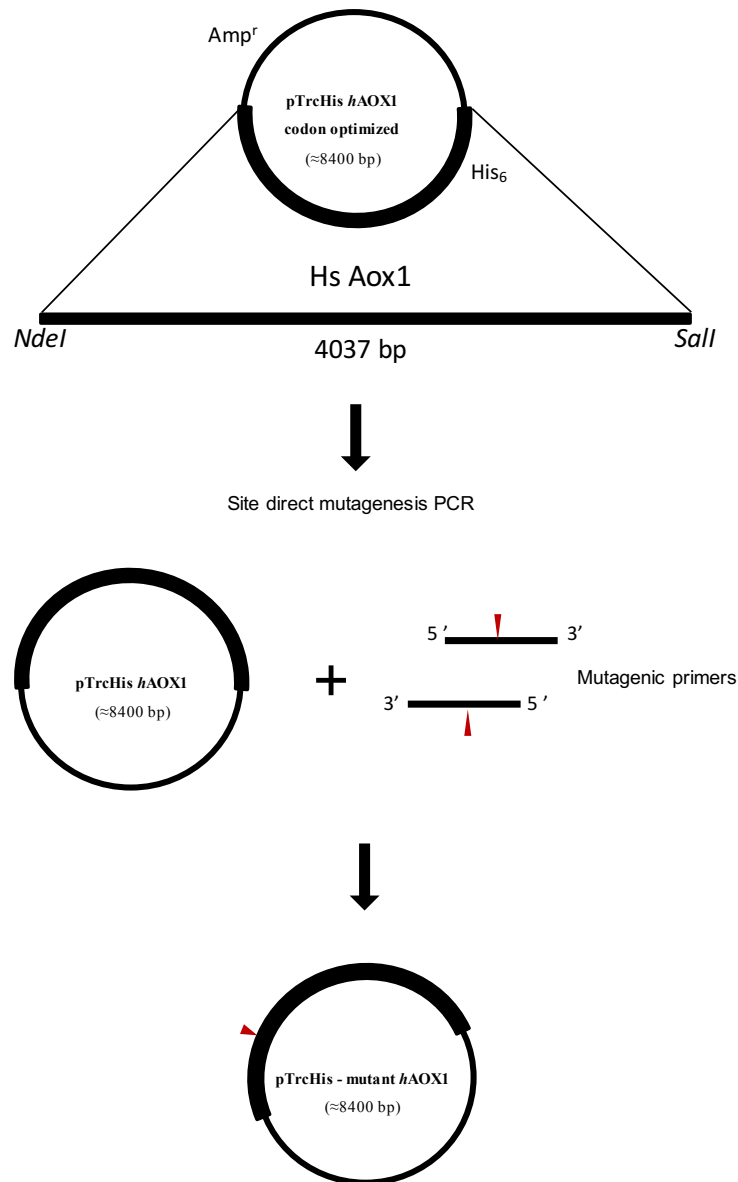


Figure 3. 2. Site Direct Mutagenesis by PCR: mutagenesis of a single base by using mutagenic primers.

3.2.1.6 Determination of DNA concentration and DNA sequencing

The concentration of the PCR products was determined by measuring the absorbance of DNA at the wavelength of 260 nm. The concentration of the cloned DNA samples were determined using a NanoDrop (Shimadzu Scientific). The instrument allows the analysis of 1.5 μ l - 2.0 μ l samples of nucleic acid, without the need for cuvettes or capillaries. Sequencing of plasmid DNA was carried out by GATC Biotech AG, Germany. The required concentration of plasmid DNA were 80 to 120 ng/ μ l within a total volume of 20 μ l sterile H₂O.

3.2.2 Biochemical methods

3.2.2.1 Overexpression of human Aldehyde Oxidase in *E. coli* TP1000 strain

The overexpression of the human AOX1 was performed using *E. coli* TP1000 strain. The genome of *E. coli* TP1000 strain contains a deletion in the *mobA* and *mobB* genes, therefore highly indicated for expressing eukaryotic molybdoenzymes due to lack of guanine dinucleotide (bis-MGD) form of the molybdenum cofactor (Palmer *et al.*, 1996).

The initial step of the expression of hAOX1 was the preparation of a 50 mL pre-cultures, containing 1 mM Na₂MoO₄, 20 μM IPTG and 150 mg/mL of ampicillin, incubated for 14 h in anaerobic condition at 37°C. Subsequently, 2 mL (1:500) per liter of this culture were then transferred to the main culture of supplemented LB medium additionally containing 1 mL of stock solution 1 M Na₂MoO₄, 20 mM IPTG and 150 mg/mL ampicillin. The cultures were then incubated for 24 hours at 30°C and 130 rpm. The bacterial cells were harvested by centrifugation at 11 000 x g for five minutes and the cell pellets resuspended in 10 mL/L of culture of 50 mM sodium phosphate, 300 mM NaCl, pH 8.0 and frozen at -20°C.

3.2.2.2 Cell lysis

As first step of hAOX1 purification, *E. coli* cells were lysed to isolate the overexpressed human enzyme. The frozen cells were thawed on ice and lysed mechanically using a cell disruptor system (TS Benchtop Series 0.75 kW equipped with a 2.72 kbar head; Constant Systems, Northamptonshire, UK). DNase I was added before lysis (1 μg/mL). The cells were disrupted by two passages through the cell disruptor at 1.35 kbar. After cell disruption, the crude extract was centrifuged at 21.000 x g for one hour (in 35 mL SS20 centrifugal tubes). The entire purification procedure was performed at 4 °C to inhibit protease activity.

3.2.2.3 Affinity purification by Ni-NTA chromatography

A Ni-NTA matrix (Ni-NTA superflow) is a complex of Ni²⁺-ions with nitrolo-tri-acetic acid (NTA) functional for affinity protein purification. The six-histidine tag of hAOX1 (at N-terminus) interacts specifically with the complexed Ni²⁺-ions. The elution of the protein can be

achieved by lowering the pH or addition of competitor such as imidazole or histidine. After cell lysis the crude extract containing hAOX was first purified using a Ni-NTA-Superflow-matrix. The cell extract was poured into a column with 0.3 mL of matrix per liter of cell culture. Then the resin mixed to the crude extract was washed with 10 column volumes of 10 mM imidazole, 50 mM sodium phosphate, 300 mM NaCl, pH 8.0, followed by a washing step of 10 column volumes of the same buffer with 20 mM imidazole. His-tagged hAOX was eluted with 250 mM imidazole in 50 mM sodium phosphate, 300 mM NaCl, pH 8.0. Fraction containing hAOX were taken to determine the quality of the protein by SDS-Page on 10% SDS-gel. Since imidazole has a destabilizing effect on the AOX, the eluate was rebuffed, using PD-10 column. The used matrix was regenerated according to the manufacturer's instructions.

3.2.2.4 Buffer exchange and desalting

Long incubation of hAOX1 WT or its variants in the presence of imidazole results in a damage of the enzyme, rendering dialysis unsuitable in most cases. Buffer exchange was therefore performed by means of PD-10 columns (GE Healthcare, Piscataway, NJ). The columns were equilibrated with 25 mL of the target buffer and 2.5 mL of hAOX1 was loaded into the column-matrix. Proteins were eluted by addition of 3.5 mL target buffer 50 mM KH_2PO_4 , 0.1 mM EDTA pH 7.4 (sulfuration buffer).

3.2.2.5 In vitro chemical sulfuration

After Ni-NTA affinity chromatography, 7 mL of hAOX1 25-30 μM was subjected to an in vitro chemical sulfuration, following the methods originally reported from Wahl and Rajagopalan (1982), with slight modifications and optimizations for the specific case of hAOX1. The proteins were incubated under reducing conditions (500 mM dithionite) in an anaerobic chamber (Coy Laboratory Products, Grass Lake, MI) in addition to sodium sulfide (2 mM) as sulfur source. Methyl viologen (25 μM) was used to confirm the absence of oxygen during the reaction. After a 30-minutes incubation at room temperature (RT) the reaction was stopped and the enzyme was exchanged into buffer of 50 mM Tris x HCl, 200 mM NaCl, and 1 mM EDTA, pH 8.0, by using PD-10 gel filtration columns.

3.2.2.6 Size exclusion chromatography

Molecules of different size can be separated by size exclusion chromatography due to the composition of the matrix particles which contain pores with tunnels in which the size can be controlled depending on the size of molecules to be separated. Smaller molecules have a more complex pathway to exit, than larger molecules. Thereby, larger molecules elute first and smaller molecules elute last in size exclusion chromatography. Eluted protein was collected in fractions and analyzed by SDS-PAGE as well as with UV/Vis detection at 280 nm, 450 nm and 550 nm.

The final step of the purification of the human aldehyde oxidase consisted of a size exclusion chromatography using a Superose 6 or Superdex 200 10/300 GL Column (GE Healthcare) on an ÄKTA system. After the in vitro chemical sulfuration the protein was loaded onto the column which was previously equilibrated with 50 mM Tris x HCl, 200 mM NaCl, 1 mM EDTA, pH 8.0 buffer.

3.2.2.7 Ultrafiltration

Proteins were concentrated by ultrafiltration using Centriprep YM-50 concentrators (50 kDa cut-off membrane). The concentrators were used following the manufacturer's instructions.

3.2.3 Analytical methods and enzymatic assays

3.2.3.1 Agarose gel electrophoresis

Agarose gel electrophoresis was used to separate a mixed population of macromolecules of DNA in a matrix of agarose applying an electric field. Agarose gels (1% w/v in 40 mM Tris x Acetate, 1 mM EDTA pH 8.00 containing 0.4 % EtBr (3,8 Diamino-5-ethyl-6-phenylphenanthridinium bromide) were run at 90 V constant field (PowerPac 300, Bio-Rad Laboratories, Inc) for 45 min in 10 cm running chambers (Mini-Sub Cell GT, Bio-Rad). DNA intercalated with EtBr was visualized by UV-light exposure in an Gel Doc Universal Hood II (Bio-Rad) and fragment length was estimated by means of Gene Ruler TM 1kb DNA ladder (Fermentas - Thermo-Fisher-Scientific GmbH, Germany).

3.2.3.2 Sodium dodecyl sulfate-polyacrylamide gel electrophoresis (SDS-PAGE)

hAOX1 WT and variants were qualitatively separated by SDS-PAGE under denaturing and reducing conditions according to their molecular weight in discontinuous Tris/Glycine-SDS-gels (Laemmli, 1970) (Table 4). It is used for the separation of protein mixtures in a containing polyacrylamide gel and applied electric field. The anionic detergent sodium dodecyl sulfate or SDS (Fig. 3.3), is incorporated in a ratio of 1:1.4 into the protein, denatures it and forms a soluble complex. Because of the high negative charge of SDS, the movement of the proteins depends only on their mass. Separation is improved by the discontinuity of the pH between the lower separating and the upper stacking gel.

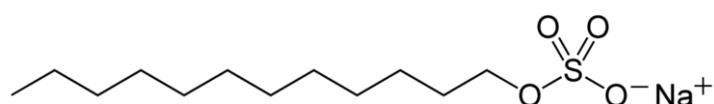


Figure 3. 3. Sodium Dodecyl Sulfate (SDS) structure.

Proteins samples were mixed with SDS-PAGE loading buffer and denatured for 5 min at 95°C. Molecular weight of the separated proteins was determined by comparison with a protein standard (Molecular Weight Marker, MWM, Fermentas). For the separation of proteins, gels were run at constant 15 mA for 90 minutes at room temperature. Cause of the hAOX1 monomer mass of 150 kDa 10% gels were used to obtain an effective separation. The composition of the stacking and separation SDS-gels:

Table 4: Components for preparation of the SDS-gel.

Separation gel		Stacking gel	
H ₂ O	2.1 mL	H ₂ O	1.14 mL
Lower Tris 4 x	1.25 mL	Upper Tris 4 x	500 µL
Acrylamide/ bisacrylamide 33:1	1.67 mL	Acrylamide/ bisacrylamide 33:1	340 µL
TEMED	10 µL	TEMED	2.5 µL
APS	25 µL	APS	10 µL

3.2.3.3 Coomassie-Blue staining

For the staining of the proteins separated by SDS-PAGE Triphenylmethane dye Coomassie Brilliant Blue R250 was used. In an acidic environment, Coomassie-Blue binds to the basic groups of the amino acids lysine, histidine and arginine. After SDS-PAGE the gel was incubated for 30 min - 1 h at room temperature in the Coomassie staining solution. The gel was subsequently destained by a methanol/acetic acid based destaining solution until the protein bands were visible on a colorless background. The sensitivity of Coomassie-Blue staining is about $1\mu\text{g protein}/\text{mm}^2$ (Luo *et al.*, 2006). Subsequently, the gels were documented on a GelDoc (Bio-Rad).

3.2.3.4 Separation of proteins in native polyacrylamide gels

For native polyacrylamide gels, the separation gel contained 7% acrylamide, 0.325 M Tris x HCl pH 8.8; 0,01% (v/v) TEMED and 0.1% (w/v) ammonium persulfate. The stacking gel was prepared using 3% acrylamide, 0.125 M Tris x HCl pH 6.8; 0.01% (v/v) TEMED and 0.1% (w/v) ammonium persulfate. Samples were mixed with loading buffer containing bromophenol blue as a color marker which is visible during electrophoresis to show the running front. For separation of the proteins in a native conformation, gels were run at 15 mA for 3 hours in a cold-room at 4°C.

3.2.3.5 Activity-stain for hAOX1

hAOX1 can be visualized in native polyacrylamide gels with a staining solution containing Nitro Blue Tetrazolium (NBT). Reduced NBT is seen as dark-blue color. The staining solution contains 100-300 μM substrate, 1 mM NBT in 50 mM Tris/HCl, 200 mM NaCl, 1 mM EDTA pH 8.0 buffer. The native gel was incubated in staining solution at 37°C until a specific color change was visible representing hAOX1 enzymatic activity.

3.2.3.6 Characterization of hAOX1 by UV/VIS Spectroscopy

Protein concentrations and photometric measurements were determined by utilization of the equation of Lambert-Beer and the calculated molar extinction coefficient of hAOXs was based on the absorbance of 450 nm wavelength.

Beer-Lambert law:

$$E = \epsilon * c * d$$

E = absorbance at a certain wavelength

ϵ = specific molar extinction coefficient in 1/mol*cm

c = protein concentration

d = path length of the cuvette

Determining the concentration of the hAOX1 was carried out by measurement the absorbance at a wavelength specific for the hAOX1 bound FAD on a Shimadzu UV-2401PC spectrophotometer. The absorption was measured at 450 nm to detect the FAD prosthetic groups of hAOX. The specific molar extinction coefficient of hAOX1 is 21 100 M⁻¹ x cm⁻¹ at 450 nm.

To measure the absorbance in the range of 250-800 nm 500 μ l of protein solution was inserted in an UV cuvette (Sarstedt, AG & Co., Germany) at room temperature. Absorption spectra were recorded in 50 mM Tris x HCl, 200 mM NaCl, 1 mM EDTA, pH 8.0.

The concentration of hAOX was calculated as follows:

$$c_{\text{AOX}} [\text{mol /L}] = E_{450} / \epsilon_{450} [\text{M}^{-1} * \text{cm}^{-1}] * d [\text{cm}]$$

3.2.3.7 Photometric determination of the specific activity

Enzyme activity was assayed spectrophotometrically by detection of product formation (e.g. phenanthridinone at 321 nm) or substrate degradation (e.g. cinnamaldehyde at 420 nm). Several electron acceptors were used for detection of enzymatic activity (e.g. ferricyanide, PMS, DCPIP).

The specific activity can be calculated:

$$\text{Spec. Act. [mU / mg]} = (\Delta \text{Abs} * \epsilon_E * V_{\text{ass}} * d * 1000) / (A_E * \epsilon_S * M_E * V_E * d)$$

ΔAbs = Change in absorbance in mAU / min

ϵ_E = hAOX1 extinction coefficient ($21,100 \text{ M}^{-1} \cdot \text{cm}^{-1}$)

ϵ_S = substrate extinction coefficient ($16,100 \text{ M}^{-1} \cdot \text{cm}^{-1}$)

V_{ass} = assay volume

V_E = volume of enzyme

A_E = adsorption of used hAOX1 at 450nm

M_E = Molar Mass of hAOX1 (150,000 kDa)

d = thickness of the used cell

3.2.3.8 Reduction spectra

Measurement of reduction spectra allows the calculation of the active enzyme portion in protein samples. The hAOX1, with a concentration of $4 \mu\text{M}$ was incubated in the anaerobic chamber, to recreate anaerobic condition. The measurement of the spectrum was carried out on a Varian Cary 50 Bio-photometer connected to an optic fiber cable inside the anaerobic chamber. With addition of $500 \mu\text{M}$ benzaldehyde the hAOX1 was substrate reduced. The recording of the spectrum was in the range between 800 and 250 nm. Complete reduction of the sample was achieved with adding sodium dithionite (20 mM) (Leimkühler *et al.*, 2003).

3.2.3.9 Analysis of the Moco content by HPLC

High-performance liquid chromatography (HPLC) is a chromatographic technique used to separate a mixture of compounds with the purpose of identifying, quantifying and purifying the individual components of the mixture. The separation by means of HPLC is based on the polarity of the compounds. It has a mobile phase and a stationary phase. The mobile phase is continuously pumped at a fixed flow rate through the system and mixed by the pump. By this method the molybdenum cofactor is converted to Form A (Johnson *et al.*, 1984) and used for semiquantitative detection of the molybdenum cofactor from the analyzed sample. For a single measurement, $200 \mu\text{L}$ of $0.5/1 \mu\text{M}$ protein was combined with $25 \mu\text{L}$ of 1% I_2 /2%KI in 1 M HCl and incubated overnight at room temperature. The denatured protein was removed by centrifugation for 10 minutes at 12,000 rpm. The supernatant was added to $27.5 \mu\text{L}$ of freshly prepared ascorbic acid (1% in ddH₂O). The pH was adjusted to 8.3 by addition of $100 \mu\text{L}$ 1 M

Tris. The phosphate monoester of Form A was cleaved by addition of 10 μ l 1 M MgCl_2 and one unit of alkaline phosphatase, and then incubated for 45 minutes at room temperature. Reaction was stopped adding 10 μ l of 50% acetic acid. Dephospho Form A was identified by HPLC analysis. Reactions were analyzed by injection onto a C-18 reversed phase HPLC column on an Agilent 1100 Series HPLC system inject (Thermo Scientific), equilibrated with 5 mM ammonium acetate with 15% methanol. Fluorescence was measured with excitation at 383 nm at emission at 450 nm using a FLD detector (Agilent 1100 Series).

3.2.3.10 Metal content

Inductively coupled plasma optical emission spectrometry with an Optima 2100 DV (PerkinElmer Life and Analytical Sciences, Waltham, MA) was used to measure the metal content of hAOX1 WT and variants. ICP-OES is an analytical technique used for the detection of trace metals. It is a type of emission spectroscopy that uses the inductively coupled plasma to produce excited atoms and ions that emit electromagnetic radiation at wavelengths characteristic of a particular element. The intensity of this emission is indicative of the concentration of the element within the sample (Stefansson *et al.*, 2007).

500 μ l of purified hAOX1 (about 10 μ M) and an equal volume of 65% nitric acid were mixed to denature the protein at 100 °C overnight. Subsequently, the samples were diluted with 4 mL of millipore water. The buffer used as reference was 50 mM Tris HCl, 200 mM NaCl, and 1 mM EDTA, pH 8.0. The detection was performed at wavelengths of 203.845 nm, 202.031 nm, and 204.597 nm for molybdenum and 238.204 nm, 239.562 nm, and 259.939 nm for iron. A standard was used for calibration and quantification of the detected metals (standard solution XVI; MerckMillipore, Darmstadt, Germany). The resulting mass concentrations were calculated and related as percent of protein saturated with molybdenum and iron corresponding to the two [2Fe–2S] clusters.

3.2.3.11 Quantitation of the FAD cofactor

One mL of hAOX1 WT and variants (10 μ M) was incubated with 150 μ M of trichloroacetic acid (50% w/v) for 10 min on ice. The denatured protein was spin down at 14 000 g for 20 min, and the pellet was resuspended in 200 μ l of trichloroacetic acid (5% w/v) and spin down again for 10 min. Both supernatants were combined, and 300 μ l of 2 M K_2HPO_4 was added. The

released FAD was detected photometrically on a Shimadzu UV-2401 PC photometer (Shimadzu Europa, Duisburg, Germany) at 450 nm. The hAOX1 WT and variants FAD saturation was calculated from the specific extinction coefficient of free FAD ($11,300 \text{ M}^{-1} \text{ cm}^{-1}$ at 450 nm) and from a calibration curve obtained from different concentrations of free FAD in solution.

3.2.3.12 Redox titration of hAOX1

UV-VIS monitored redox titrations were performed anaerobically at room temperature (24 ± 3 °C) under argon saturated atmosphere (Nippon Medical School, Tokyo, Japan). The redox titrations were performed by reducing hAOX1 WT and variants with increasing amount of dithionite ($\text{Na}_2\text{S}_2\text{O}_4$) or substrate (phenanthridine or benzaldehyde). Reaction mixtures contained 5–10 μM of protein in 50 mM Tris, 200 mM NaCl, 1 mM EDTA pH 8.0 buffer in a total volume of 1 mL. The reaction was performed into a glass-pipe fused quartz cuvette (T. Nishino) filled with argon gas and tightly attached to a Hamilton syringe to allow a controlled release of the reducing solution ($\text{Na}_2\text{S}_2\text{O}_4$ or substrate). The reaction mixture was titrated by adding a strictly controlled amount of $\text{Na}_2\text{S}_2\text{O}_4$ or substrate injected into the protein solution. Subsequently, UV-Vis spectra of the sample were obtained on a spectrophotometer (Shimadzu Spectrophotometer) were taken over time. After stabilization of the inter-molecular electron transfer, spectra were recorded in the range of 280 – 800 nm. Absorbance at 450 nm, 550 nm (2[2Fe-2S] centers) and 620 nm (flavin semiquinone radical) were plotted as ratio 450/550 nm and 550/620 nm.

3.2.3.13 Kinetics parameters of hAOX1

The determination of kinetic parameters k_{cat} and K_{M} , and the catalytic efficiency $k_{\text{cat}}/K_{\text{M}}$ was performed on a Shimadzu UV-2401PC photometer at 30°C. Steady-state enzyme kinetics were performed with purified hAOXs in 50 mM Tris buffer, pH 8.0, containing 200 mM NaCl and 1 mM EDTA at 25 C in a final volume of 500 μl . The substrates benzaldehyde and phthalazine were used in a range of 1–100 μM using dichlorophenolindophenol (DCPIP; 100 μM) or ferricyanide (1 mM) as electron acceptors. For the substrate phenanthridine, in addition to ferricyanide and DCPIP, molecular oxygen was used as an electron acceptor and the product phenanthridone was detected at 321 nm. The substrate phenanthridine was used in a range of

1– 100 μM . Total enzyme concentration varied between 100–200 nM. Reactions monitored over a range of 30 seconds. Kinetics parameters were calculated using the extinction coefficient of 16,100 $\text{M}^{-1}\text{cm}^{-1}$ at 600 nm for DCPIP, 2080 $\text{M}^{-1}\text{cm}^{-1}$ at 420 nm for ferricyanide, and 6,400 $\text{M}^{-1}\text{cm}^{-1}$ at 321 nm for phenanthridinone. The obtained data from three individual measurements were fitted nonlinear using the equation of Michaelis-Menten (eq. 1) to obtain the kinetic constants K_M and turnover numbers (eq. 2).

$$v = \frac{V_{max} [S]}{K_m + [S]} \quad (1)$$

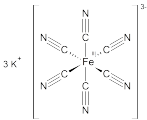
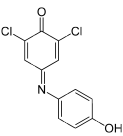
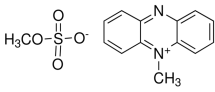
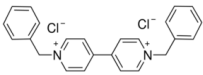
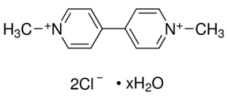
$$k_{cat} = \frac{V_{max}}{E_t} \quad (2)$$

Fitting of the Michaelis-Menten curves was carried out using the software OriginPro 8.1G (Waltham, MA) considering the bi-substrate reaction mechanism (eq.3).

$$k_{cat,app} = \frac{k_{cat} [S][O]}{K_{ms}[O] + K_{mo}[S] + [S][O] + K_{ms} K_{mo}} \quad (3)$$

Bisubstrate kinetics equation (Bisswanger 1st ed., 2002; Alberty, 2011) with $k_{cat,app}$ = observed reaction rate, $[S]$ = concentration of reducing substrate, $[O]$ = concentration of oxidizing substrate, k_{cat} = maximum rate under saturated non-inhibited conditions, K_{m_S} = Michaelis- Menten constant for the reducing substrate, K_{m_O} = Michaelis Menten constant for the oxidizing substrate. Further substrates used were cinnamaldehyde, p-Dimethylaminocinnamaldehyde (DMAC), vanillin and chloroquinazolinone. Furthermore, additional electron acceptor as methyl viologen (MV), benzyl viologen (BV) and phenazine methosulfate (PMS) were used (Table 5). The extinction coefficients used to calculate the kinetics parameters are shown in Table 6.

Table 5: Electron acceptors used in this work.

Electron acceptor	Redox potential	Structure
Molecular oxygen	+ 0.8 V ^a	$\text{O}=\text{O}$
Potassium ferricyanide	+ 0.42 V ^b	
2,6-Dichlorophenolindopheno (DCPIP)	+ 0.22 V ^b	
Phenazine methosulfate (PMS)	+ 0.08 V ^b	
Benzyl viologen	- 0.358 V ^b	
Methyl viologen	- 0.430 V ^b	

^a Concepts and Models of Inorganic Chemistry, Problems Douglas, Bodie E., McDaniel, Darl H., Alexander, John J. Published by Wiley, 1983. ^b Mediator compounds for the electrochemical study of biological redox systems: a compilation. Mary Lou Fultz and Richard A. Durst, 1982.

Table 6: The extinction coefficients used to evaluate the enzymatic activity for hAOX1^a

Detected molecule	Extinction coefficients ϵ ($M^{-1} cm^{-1}$)
Phenanthridinone	6,380
4-(Dimethylamino)cinnamaldehyde (p-DMAC)	30,500
Vanillin	8,850
Cinnamaldehyde	25,100
Ferricynide	2,100
2,6-Dichlorophenolindophenol (DCPIP)	16,100
Phenothiazine methosulfate (PMS)	26,300
Methyl viologen	9,800
Benzyl viologen	8,700

^a measured by spectro-photometric assay

3.2.3.14 Inhibition studies

Inhibition studies on hAOX1 WT and variants were performed using several inhibitors as thioridazine, loxapine, raloxifene and DCPIP (Sigma-Aldrich). Furthermore, inactivation experiments were performed using diphenyleneiodonium chloride (DPI) as irreversible inhibitor of the FAD cofactor of hAOXs and XOR. All the inhibition studies were measured by spectrophotometric assay (Shimadzu spectrophotometer) using phenanthridine, phthalazine or cinnamaldehyde as substrates (1-100 μ M) and molecular oxygen or ferricyanide (1 mM) as electron acceptors. The concentrations of the inhibitors were variable from 0 to 500 μ M. Inhibition experiments were performed also with bXO/bXDH using xanthine/hypoxanthine as substrate and thioridazine or allopurinol as inhibitors.

3.2.3.15 Electrochemical measurements of H₂O₂ formation

Electrochemical measurements were carried out with a PalmSens (Utrecht, Netherlands) electrochemical station. Amperometric biosensors function by the production of a current when a potential is applied between two electrodes. For H₂O₂ detection, a platinum Clark electrode

was used. This consists of a platinum cathode at which H_2O_2 is oxidized and a silver/silver chloride reference electrode. hAOX1 WT and variants were tested in air-saturated 50 mM Tris buffer, 200 mM NaCl and 1 mM EDTA pH 8.0, in the presence of phenanthridine as substrate and H_2O_2 was quantified amperometrically using a Pt-Clark electrode at +0.6 V (H_2O_2) in an electrochemical cell (Fig.3.4 A). The system was calibrated with fixed concentration of H_2O_2 in solution.

3.2.3.16 Cytochrome c reduction assay and determination of $\text{O}_2^{\cdot -}$ production

The production of superoxide was monitored following its reduction of cytochrome c by one electron transfer (Massey, 1959; McCord and Fridovich, 1969). The specificity for reduction of Fe^{3+} to Fe^{2+} of the cytochrome c heme cofactor by $\text{O}_2^{\cdot -}$ was tested by adding superoxide dismutase (10 $\mu\text{g}/\text{mL}$) or raloxifene (10 μM), a potent specific hAOX1 inhibitor, in the assay (Fig.3.4 B). Furthermore, Catalase (100 U/mL) was used as further control. Diphenyleneiodonium (DPI) was used as specific suicide inhibitor to confirm the location of the reaction at the FAD site (Harris *et al.*, 1999; Yesbergenova *et al.*, 2005). The reduction of cytochrome c was spectro-photometrically measured by Δ_{abs} at 550 nm and the extinction coefficient of 21,000 $\text{M}^{-1}\text{cm}^{-1}$ was used to calculate the specific activity.

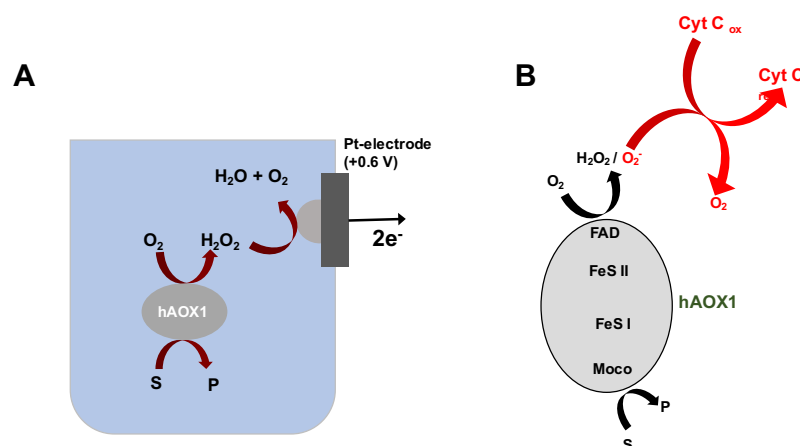


Figure 3. 4. Scheme of the Pt-electron H_2O_2 measurements (A) and the Cyt c assay for detection of superoxide anion (B).

3.3 Computational methods

3.3.1 Protein modelling

Protein crystal structures were obtained by the pdb files of hAOX1 WT pdb: 4UHW (Coelho *et al.*, 2015); hAOX1 in complex with phthalazine and thioridazine pdb: 4UHX (Coelho *et al.*, 2015); hAOX1 S1271L pdb: 5EPG (Foti *et al.*, 2016); mAOX3 pdb: 3ZYV (Coelho *et al.*, 2012); bXDH pdb:1FO4 (Enroth *et al.*, 2000), bXO pdb:1FIQ (Enroth *et al.*, 2000) and were taken from the RCSB protein databank <http://www.rcsb.org/pdb>. All protein structures were visualized by Pymol modelling software (MacPyMol 2006, Delano Scientific LLC).

3.3.2 Determination of Single nucleotide Polymorphisms

The Single Nucleotide Polymorphism Database (dbSNP) is a free public archive for genetic variation within and across different species developed and hosted by the National Center for Biotechnology Information (NCBI) in collaboration with the National Human Genome Research Institute (NHGRI). All the SNPs produced in this work were obtain from dbSNP <https://www.ncbi.nlm.nih.gov/projects/SNP>.

4. Results

4.1. Expression and characterization of hAOX1: comparison of a codon optimized and non codon optimized expression system

4.1.1 Heterologous expression of a *hAOX1* from a codon optimized gene construct

The heterologous expression of human genes in *E. coli* can result in a low yield of protein, due to different codon usage by human and bacterial cells (Alfaro *et al.*, 2009; Barr & Jones, 2011; Hartmann *et al.*, 2012). To overcome this limit, in this work we used a synthetic *hAOX1* gene (*hAOX1*) which was constructed using the genetic code with the most frequently used codons in *E. coli*. In this construct, the codons poorly used by the *E. coli* translation system are replaced with the preferred codons, without changing the amino acids sequence of the synthesized hAOX1 protein (hAOX1). The synthetic gene was cloned into the vector pTrcHis (Temple & Rajagopalan, 2000), using the *NdeI-SalI* restriction sites and the resulting plasmid was named pTHco-*hAOX1* (Hartmann, 2010). Subsequently, one misinserted codon was exchanged to the correct one and the construct was further modified to obtain the correct sequence. Upstream of the starting codon, the construct is fused to a sequence for a tag of six histidines (His₆) for expression of an N-terminal–His₆ tag fusion protein that facilitates the protein purification.

The expression of the optimized gene sequence was conducted in *E. coli* TP1000 ($\Delta mobAB$) cells (Palmer *et al.*, 1996) shown previously to be optimal for the expression of molybdopterin–containing proteins owing to their inability to synthesize the bis-molybdopterin guanine dinucleotide cofactor present in most *E. coli* molybdoenzymes (Palmer *et al.*, 1996). The cell cultures were incubated for 24 hours at 30°C and 130 rpm. The cells were harvested by centrifugation at 11000 x g for five minutes and the cell pellets resuspended in 10 mL/L of culture by 50 mM sodium phosphate, 300 mM NaCl, pH 8.0 buffer and frozen at -20°C upon usage.

The expressed and purified protein obtained from the codon-optimized *hAOX1* gene was compared with the non–codon optimized gene sequence containing a *hAOX1* gene (native *hAOX1*) that was isolated from human cDNA (Hartmann *et al.*, 2012). Both genes were cloned into the same vector for better comparison (Temple & Rajagopalan, 2000) and both constructs were expressed using equal conditions to allow subsequent analytical and comparative studies.

The codon optimized cDNA of hAOX1 was synthesized by GeneArt (Thermo Fisher Scientific, Sunnyvale, CA) and the gene sequence is shown in the appendix (Fig.1 Appendix).

4.1.2 Purification of hAOX1

4.1.2.1 Ni-NTA affinity chromatography

The protein purification started with thawing the *E.coli* cell pellet followed with the cells lysis by means of 2 cycles under 1.35 kBar of a cell disruption system, to obtain the cells crude extract.

The resulting crude extracts of both native hAOX1 and hAOX1 were used for the subsequent protein purification. The first purification step was a nickel-NTA affinity chromatography, allowing purification of His₆ tagged proteins. After cells disruption, the crude extract was incubated with 0.3 mL of Ni-NTA matrix per liter of cell culture. The Ni-NTA matrix was previously inserted into the column before the loading of the cell lysate. After two washing steps, with 10 and 20 mM imidazole-containing buffer, the protein was eluted with a 250 mM imidazole containing buffer, and the eluted fractions were analyzed by SDS-polyacrylamide gel electrophoresis (Fig. 4.1). This first step already shows that the hAOX1 expression is improved in terms of an increased yield of the protein, in comparison to the native hAOX1 expression construct.

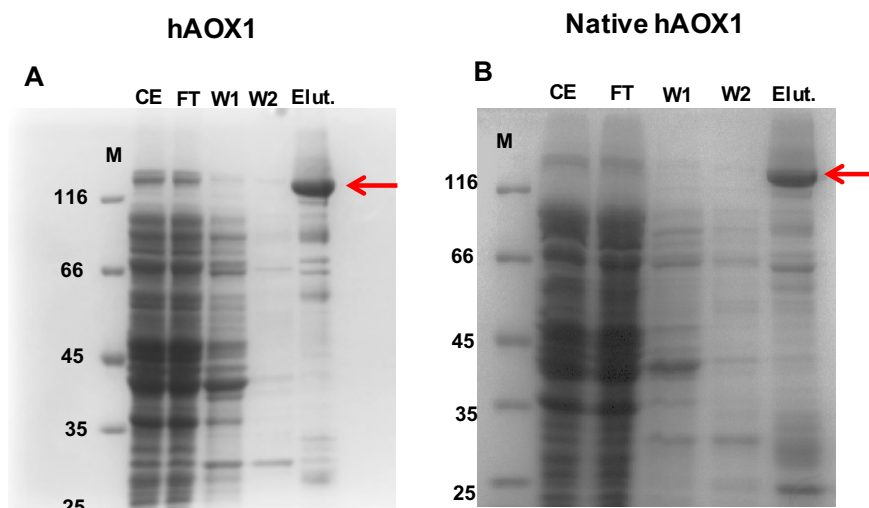


Figure 4. 1. 10% SDS-polyacrylamide gels fractions after Ni-NTA affinity chromatography purification of hAOX1 (A) and native hAOX1 (B). The red arrows indicate the eluted hAOX1s after 250 mM imidazole elution. Shown are the crude extract (CE), the flow through (FT), the first washing step by 10 mM imidazole-containing

buffer (W1), the second washing step with 20 mM imidazole-containing buffer (W2) and the eluted protein (Elut.). 0.3 mL of Ni-NTA matrix was used for the purification of both samples.

However, both enzymes as purified showed poor enzymatic activity of 113.6 ± 34.1 mU/mg and 141.4 ± 29.8 for the native hAOX1 and hAOX1 respectively. The low levels of enzymatic activity are caused due to a low insertion of the equatorial sulfido ligand at the molybdenum atom in the active site. To increase the portion of the active protein, an *in vitro* chemical sulfuration was performed (Wahl & Rajagopalan, 1982).

4.1.4.2 *In vitro* chemical sulfuration

hAOX1 and all the members of the xanthine oxidase family possess a modified Moco with a sulfur ligand complexed to the molybdenum atom in the equatorial position of the Moco. Such sulfur ligand is essential for the catalytic activity of those enzymes (Wahl & Rajagopalan, 1982; Leimkühler *et al.*, 2004).

The specific activity of both proteins, native hAOX1 and hAOX1, after purification was comparable, with 141.4 ± 29.8 mU/mg for the hAOX1 and 113.6 ± 34.1 mU/mg for the native hAOX1 (Table 7). This result suggests that the activity of the purified protein was not affected by the alteration of the codon optimized sequence. However, native hAOX1 and hAOX1 as purified showed poor levels of enzymatic activity caused by the inefficient sulfido ligand incorporation to the Moco. Such low enzymatic activity of hAOX1 as purified is caused by the lack of the specie-specific human moco sulfurase enzyme (hMCSF) in *E. coli* cells, which performs the last step of the Moco biosynthesis in humans (Sakamoto *et al.*, 2001) consisting in the insertion of the sulfido ligand to the molybdenum cofactor.

In this work, an *in vitro* chemical sulfuration was performed between the Ni-NTA affinity chromatography and the size exclusion purification steps to increase the enzymatic activity of hAOX1 (Table 7). The *in vitro* chemical sulfuration reaction was performed as described previously (Wahl & Rajagopalan, 1982) with further modifications to raise the efficiency of the procedure for hAOX1. After the Ni-NTA purification step, the protein was incubated under anaerobic and reducing conditions with 500 μ M sodium dithionate, 2 mM sodium sulfide and 25 μ M methyl viologen. After 30 minutes incubation at room temperature (RT) the protein was further purified by a gel filtration step (PD-10 column) to separate all the reducing compounds present in the chemical reaction from the enzyme. After that, the protein was purified by the size exclusion chromatography on a Superdex 200 column.

Table 7: Specific activity of native hAOX1 and hAOX1 before and after *in vitro* chemical sulfuration.

	native hAOX1	hAOX1
Specific activity ^a (mU/mg) before <i>in vitro</i> chemical sulfuration	113.6 ± 34.1	141.4 ± 29.8
Specific activity ^a (mU/mg) after <i>In vitro</i> chemical sulfuration	1516.7 ± 182.7	1459.1 ± 170.5

^aspecific activity of hAOX1 measured using phenanthridine as substrate and molecular oxygen as electron acceptor. Data are mean values from three independent measurements (± S.D.).

The results in Table 7 show that the *in vitro* chemical sulfuration resulted in a 8-10 fold increase of the specific activity for hAOX1. The protein showed quite high stability during all the procedure. The buffer used for the *in vitro* chemical sulfuration was KH_2PO_4 x KOH 50 mM, 0.1 mM EDTA pH 7.4. Subsequently, several experiments were performed to optimize the *in vitro* chemical sulfuration reaction for hAOX1. Different pH conditions were used to identify the pH optimum for this chemical procedure in order to improve specific activity and stability of the enzyme (Fig.4.2).

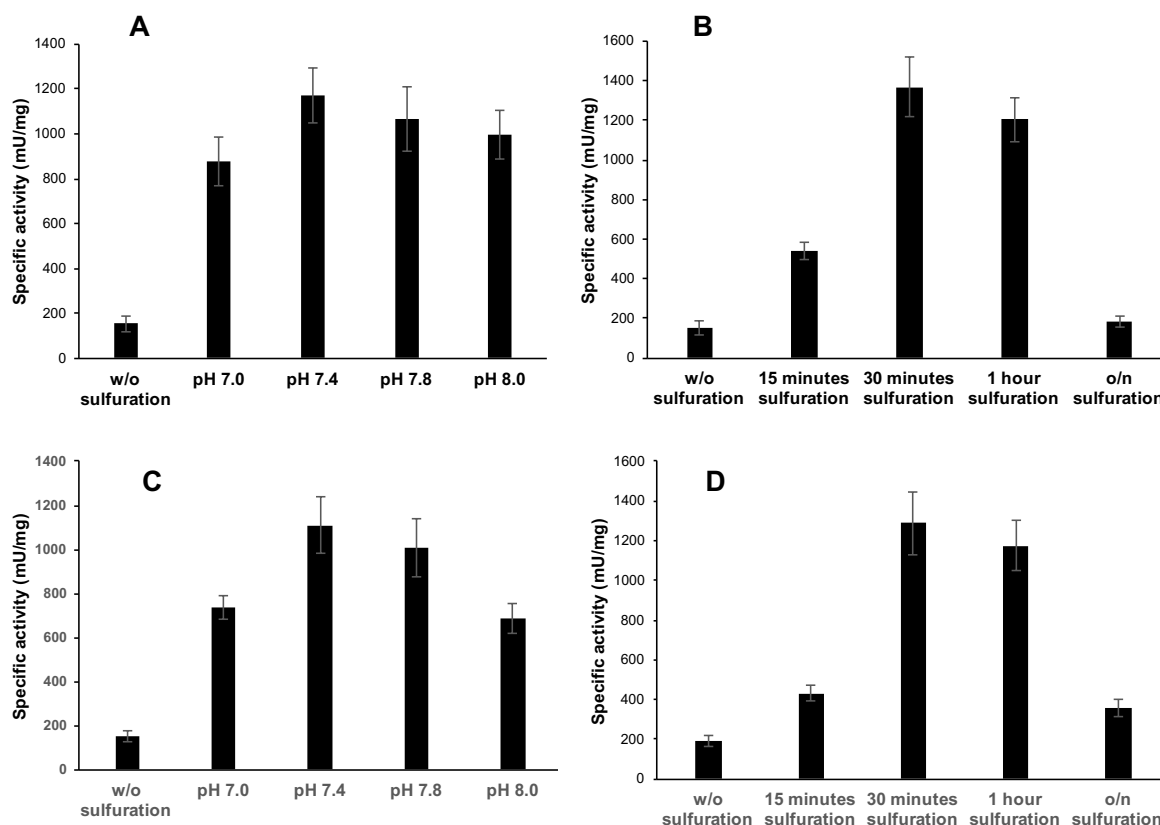


Figure 4. 2. *In vitro* chemical sulfuration experiments: pH optimum and time range of incubation using hAOX1 (A-B) and native hAOX1 (C-D). Specific activity was measured by spectrophotometric assay using phenanthridine as substrate and molecular oxygen as electron acceptor. The measurements were performed in Tris 50, mM NaCl 200 mM, 1 mM EDTA buffer pH 8.0 at 30°C. The protein concentrations used in this experiments ranged 150-250 nM in the assay.

The pH optimum was identified as 7.4, which was the condition where the enzyme showed a highest specific activity toward the phenanthridine:oxygen reaction. Furthermore, a timing experiment was performed to select the right incubation time for the *in vitro* chemical sulfuration of hAOX1. 30 minutes incubation time resulted as the more efficient, leading to the highest specific activity (Fig. 4.2 B-D). Comparable results were obtained for both enzyme expressed using the native *hAOX1* gene sequence and for the *hAOX1* (fig 4.2). After the 30 minutes reaction, the *in vitro* chemical sulfuration was stopped by de-salting the proteins using PD-10 gel filtration columns. Subsequently, the enzymes were concentrated and prepared for the last step of the purification procedure.

4.1.2.3 Size exclusion chromatography

The last step of the purification procedure for hAOX1 was a size exclusion chromatography (SEC) step using a Superdex 200 column on a FPLC system. The eluted fractions were analyzed by 10% SDS-PAGE (Fig.4.3).

All the elution profiles of hAOX1 show a prominent peak after around 11.5 mL of elution volume (Fig. 4.3). By standard curves obtained using known molecular weight proteins, the elution peak at 11.5 mL demonstrates that hAOX1 is expressed mainly as dimer having a size of around 300 KDa (Fig. 4.3 A-B). The profile also shows a minor part of multimeric and monomeric form for both hAOX1 after the elution (Fig. 4.3 A-B). The codon-optimized hAOX1 yielded mainly the dimeric form with an aggregation peak after around 7.5 ml of elution volume, indicating an aggregated form of the enzyme (Fig. 4.3 A). Instead the native hAOX1 showed a significant portion of the monomeric hAOX1 (Fig. 4.3 B). The 10% SDS-gels of both elution profiles shows lower amount of contaminants in the case of the hAOX1 expressed protein as compared to the native hAOX1 (Fig. 4.3 C-D).

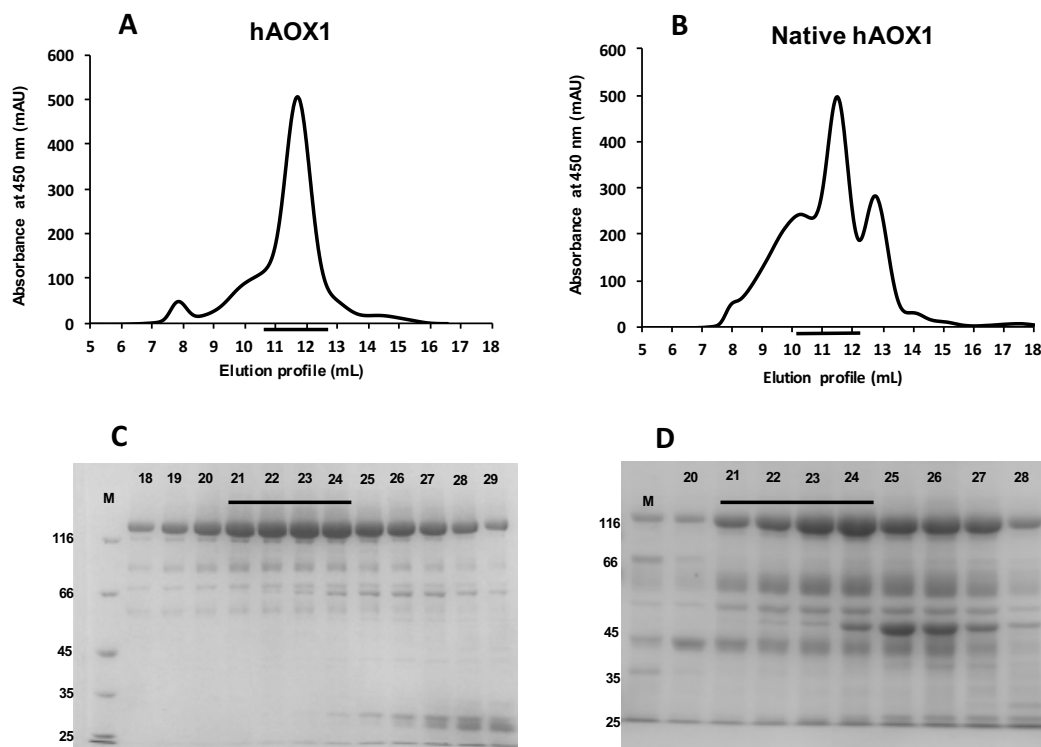


Figure 4. 3. Size exclusion chromatography (Superdex 200 column) purification of hAOX1 and native hAOX1. Shown are (A) the size-exclusion chromatogram (absorbance at 450 nm) of hAOX (B) the size-exclusion chromatogram (absorbance at 450 nm) of native hAOX1, (C) 10% SDS-gel of the eluted fractions of hAOX1 and (D) 10% SDS polyacrylimide gel of the eluted fractions of native hAOX1. The majority of the lower bands

determined by SDS-PAGE were identified as degradation products of hAOX1. The black lines stand for the pooled fractions.

For a better purification, we related the several elution fractions to the functionality of the enzyme. The SEC eluted fractions for the hAOX1 were tested for their specific activity toward phenanthridine as substrate and oxygen as electron acceptor. The result showed the highest enzyme activity from the elution fractions 21-24 corresponding to the main peak for the dimeric form of the enzyme, the only active form of hAOX1 (Fig. 4.4). Therefore, those fractions were collected for further enzymatic studies on the AOX1.

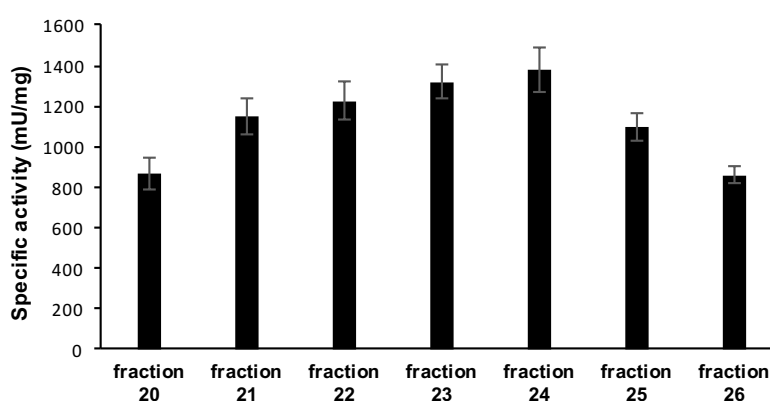


Figure 4. 4. Specific activity for the eluted fractions. Specific activity measured by spectrophotometric assay using phenanthridine as substrate and oxygen as electron acceptor in 50 mM Tris x HCl, 200 mM NaCl, 1 mM EDTA pH 8.0 buffer.

The yield of the proteins expressed from the native hAOX1 construct and codon-optimized hAOX1 (hAOX1) construct was compared (Table 8).

Table 8: Yield of protein of native hAOX1 and hAOX1^a

	native hAOX1	hAOX1
Total yield of protein (mg/L of culture)	0.09 ± 0.02	1.0 ± 0.3

^aProteins concentrations measured by absorbance at 450 nm. Data are mean values from three independent measurements (± S.D.).

The results show that the codon-optimized construct led to a 10-fold higher protein yield than the construct containing the human codon sequence, with an average of 1.0 ± 0.3 mg protein per liter of *E. coli* culture.

4.1.3. Characterization of purified hAOX1 (hAOX1)

4.1.3.1 Activity staining of hAOX1

After purification, the stability of the proteins was tested. hAOX1 obtained from both expression systems, codon optimized and native sequence, showed quite high protein stability, however, both proteins have a tendency to aggregate after several freezing and thawing steps. The theoretical isoelectric point (pI) was estimated of 6.79. The optimal condition to make analytical assays was determined using the fresh purified protein, or directly after thawing on ice. Only the dimeric form of the protein was used for analytical assays (fractions 22-24). Besides hAOX1 protein band (≈ 150 kDa) on the SDS-gel, weak protein bands could be also detected (Fig. 4.5 A). The intensity of these lower bands is related to the intensity of the protein bands of hAOX1 on the gel. Such bands resulted to be degradation products of hAOX1 as reported previously (Hartmann, 2010).

Monkey and mouse but not rat AOX1 have a tendency to degrade in SDS-PAGE (Hoshino *et al.*, 2007; Asakawa *et al.*, 2008; Schumann *et al.*, 2009; Mahro *et al.*, 2013). Native-PAGE and activity gel staining of hAOX1 obtained from both expression systems (Fig. 4.5 B-C) show two major bands that seem to stand for the oligomeric form (upper band) and the dimeric form (lower band). Analysis of the several elution fractions after purification showed that the more catalytically active portion is the dimeric one.

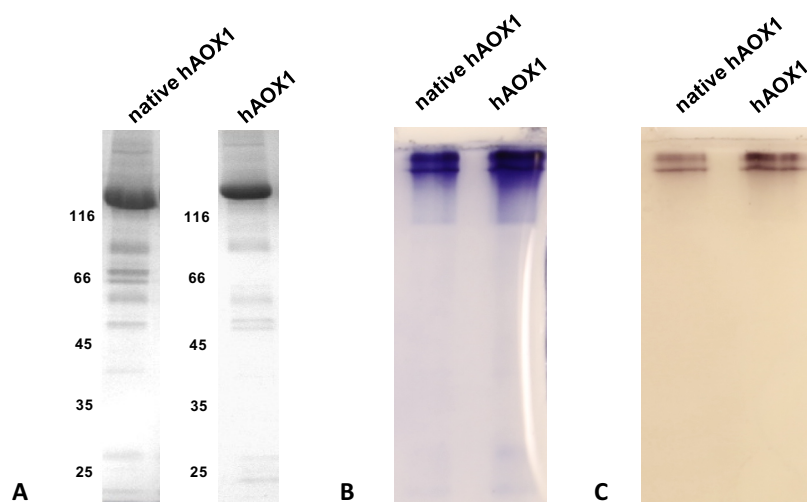


Figure 4. 5. 10% coomassie stained SDS-PAGE (A) 7% Native PAGE (B), activity staining gel (C) of native hAOX1 and hAOX1. Activity with benzaldehyde are shown for 10 μ l of 5 μ M hAOX1 loaded for native polyacrylamide gel (8%) electrophoresis and stained for activity assay . The staining solution contains 500 μ M

benzaldehyde, 1mM Nitro Blue Tetrazolium (NBT) in 50 mM Tris/HCl, 200 mM NaCl, pH 8.0 buffer. The native gel was incubated in staining solution at 37°C until a specific color change was visible representing hAOX1 activity with benzaldehyde.

4.1.3.2 Metal content

Expression on molybdenum containing eukaryotic enzymes often have the disadvantage of low cofactors saturation (Huang *et al.*, 1999; Adachi *et al.*, 2007; Yamaguchi *et al.*, 2007). As a measure for the quality of the recombinant expression system, the metal content of native and codon optimized hAOX1 was performed.

Molybdenum and iron content (based on $2x[2Fe-2S]$ clusters) in the protein was determined by using inductively coupled plasma optical emission spectrometry (ICP-OES). The measurement was performed using a reference standard (Solution XVI, Merck), to exactly quantify both elements. The concentration of the elements was calculated to a percentage scale of saturation values (Table 9). The saturation of molybdenum was around 55% and 65% and iron around 71% and 77% for native hAOX1 and hAOX1 respectively. This fact implies, that 40 – 45 % of recombinant hAOX1 was expressed in the Moco-free form. No major differences were observed between the cofactor insertion in the enzymes obtained from the two expression systems.

Table 9: Metal content for of native hAOX1 and hAOX1^a.

	native hAOX1	hAOX1
Mo content ^a %	55.2 ± 8.41	66.4 ± 6.58
Fe content ^a %	71.2 ± 10.37	76.7 ± 5.63

^adetermined by using inductively coupled plasma optical emission spectrometry (ICP-OES). Data are mean values from three independent measurements (± S.D.).

Furthermore, by trichloroacetic acid extraction assay, the flavin adenine nucleotide content of hAOX1 was measured. The result shows a high FAD saturation of around 93% and 85% for hAOX1 and native hAOX1 respectively. Among all three type of cofactors present in the enzyme, the FAD has the highest insertion level into the mature protein structure.

4.1.3.3 UV/Vis spectroscopy

The ultraviolet–visible (UV/Vis) spectrum of hAOX1 in its oxidized form displayed the typical features of molybdo-flavoenzymes: absorption at 280 nm, typical of the aromatic amino acids, absorption at 450 nm, characteristic for protein-bound FAD and the absorption shoulder at 550 nm, characteristic for protein bound $2\times[2\text{Fe-2S}]$ cluster. Both native hAOX1 and hAOX1 showed comparable UV/Vis absorption spectra features (Fig. 4.6).

Based on previous knowledge on the highly-related enzyme xanthine oxidase (XO), a way to determine the purity of the protein and the saturation of the cofactors are the ratios of the absorbance at 280/450 nm and 450/550 nm. The ratio 280:450 nm absorbance of 5.0 for the recombinant protein indicates a high purity of the enzyme. A ratio of A_{280}/A_{450} higher than 5 indicates impurities in the sample. The 450:550 nm absorbance ratio in the UV/Vis spectrum of 3.0, demonstrates a correct ratio FAD:FeS. Generally, hAOX1 showed a 280:450 nm absorbance ratio of 5.2-5.7 indicating the quite high purity of the enzymes, and the 450:550 nm absorbance ratio of around 3.0-3.3, demonstrating the correct saturation with FAD cofactor ($\epsilon_{\text{hAOX1}, 280 \text{ nm}} = 114.600 \text{ M}^{-1} \text{ cm}^{-1}$) an equal relation of FAD and $2\times[2\text{Fe2S}]$ clusters. Measurement of the hAOX1 concentrations were performed by the absorption at 450 nm with a specific hAOX1 extinction coefficient of $21.100 \text{ M}^{-1} \text{ cm}^{-1}$ (Alfaro *et al.*, 2009; Hartmann *et al.*, 2012).

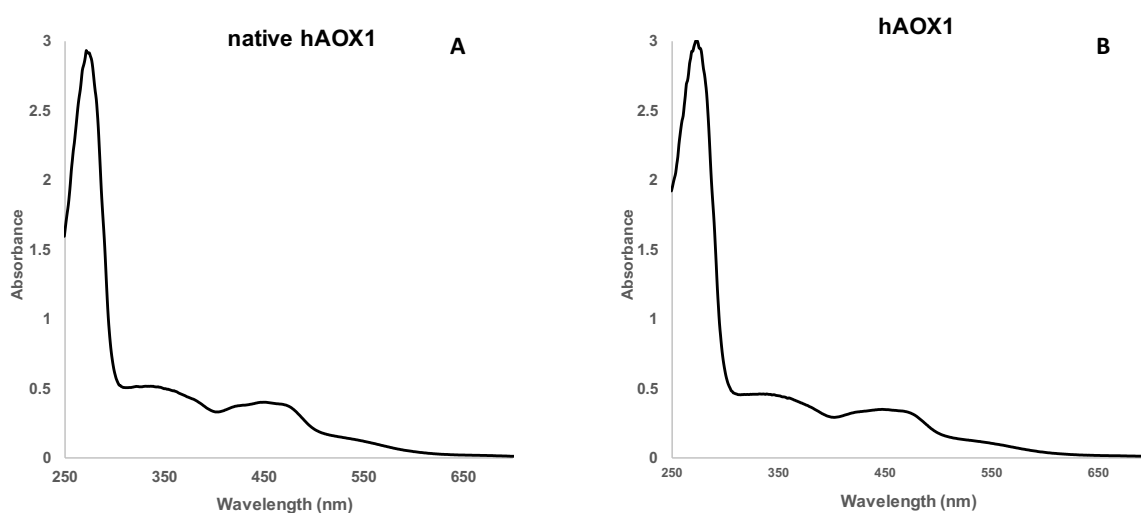


Figure 4.6. UV/Vis spectrum of the native hAOX1 (A) and the hAOX1 (B) in their oxidized form with a concentration of $18 \mu\text{M}$. The UV-Vis spectra were determined using purified air-oxidized hAOX1 proteins in 50 mM Tris (pH 8.0) at RT.

To measure the active portion of hAOX1, a reduction spectrum was taken under anaerobic conditions and using benzaldehyde 1 mM as reducing substrate and with subsequent full reduction by sodium dithionite in a volume of 2 mL (Fig. 4.7).

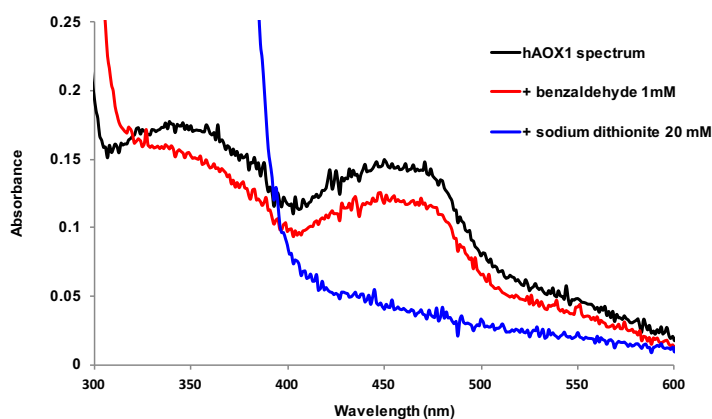


Figure 4. 7. UV/Vis reduction spectrum of hAOX. The reduction spectrum was performed under anaerobic conditions using 1 mM benzaldehyde as reducing substrate after 1 minute. For the fully reduction of hAOX1 20 mM sodium dithionite was used. The hAOX1 concentration used was 7 μ M in the assay.

The result showed a decrease at the absorption spectrum peak of 450 nm, corresponding to the reduced FAD cofactor. The active portion of hAOX1 by reduction spectrum was calculated to be around 30%, revealing that only around the 50% of the Moco was efficiently sulfurated. This experiment was performed using the hAOX1 produced by the codon optimized expression system considering the high amount of enzyme required for the assay.

4.1.4 Enzymatic activity

4.1.4.1 State-steady kinetics and substrate specificity

In this work, we determined enzymatic constants of the enzyme toward several substrates and electron acceptors to elucidate new aspects about the catalytic mechanism of hAOX1.

Firstly, to assay the optimal condition for enzymatic activity measurements, the optimum pH for the hAOX1 catalytic activity was measured (Fig. 4.8). The pH-dependent catalytic profiles were measured within a pH range of 4.0-10.0, using 100 mM acetate buffer (4.0-7.0 pH), 50 mM Tris-HCl buffer (7.0-9.0 pH) and 100 mM phosphate buffer (7.5-10.0 pH). In general, the pH optimum was obtained using 50 mM Tris-HCl buffer of around pH 8.0 for hAOX1 with

phenanthridine as substrate and molecular oxygen as electron acceptor (Fig. 4.8) as well as for the other substrates and electron acceptors. Therefore, all the steady-state kinetics were determined at pH 8.0.

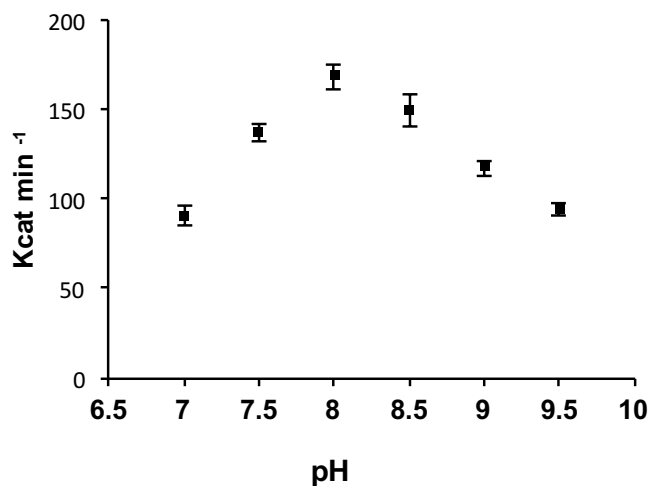


Figure 4. 8. pH optimum for hAOX1 wild-type. Specific activity was measured by spectrophotometric assay using phenanthridine as substrate and molecular oxygen as electron acceptor in air-saturated buffer. The measurements were performed in Tris 50, mM NaCl 200 mM, 1 mM EDTA buffer pH 8.0 at 30°C.

The enzymatic activity of both native hAOX1 and hAOX1 was measured by spectrophotometric assays using several substrates and electron acceptors in combination. To determine the kinetic parameters, hAOX1 was tested with phenanthridine, phthalazine and benzaldehyde as substrates (Fig. 4.9) in combination with ferricyanide, 2,6-dichlorophenolindophenol (DCPIP) and molecular oxygen as electron acceptors. Furthermore p-dimethylaminocinnamaldehyde (p-DMAC), (2*E*)-3-phenylprop-2-enal (cinnamaldehyde), 4-hydroxy-3-methoxybenzaldehyde (vanillin), 2-hydroxybenzaldehyde (salicylaldehyde) were tested as substrates.

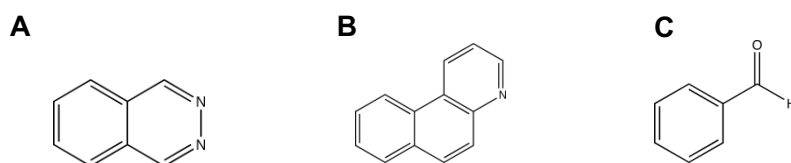


Figure 4. 9. Structure of phenanthridine (A), phthalazine (B) and benzaldehyde (C).

Kinetic experiments were performed by spectrophotometric assay following product formation (phenanthridinone), the substrate decrease (p-DMAC:oxygen, Vanillin:oxygen,

Cinnamaldehyde:oxygen) or the reduction of the electron acceptors (DCPIP, ferricyanide, PMS, methyl viologen and benzyl viologen).

The steady-state kinetics of the hAOX1s showed the highest k_{cat} values with phenanthridine as substrate when molecular oxygen was used as electron acceptor, whereas with electron acceptors like ferricyanide and DCPIP, the k_{cat} values were decreased (Table 5). Generally, molecular oxygen as physiologic electron acceptor resulted in a higher k_{cat} compared with ferricyanide or DCPIP as electron acceptors. However, in all cases DCPIP drastically decreased the k_{cat} and K_M for all three substrates tested. Phenanthridine was the substrate showing the higher reactivity toward hAOX1, followed by phthalazine and benzaldehyde (Table 5). Notably, ferricyanide increased the K_M for all the substrates. Considering the highest catalytic rate, the reaction phenanthridine:oxygen was used as standard activity assay for hAOX1 in this work.

The fact that native hAOX1 and hAOX1 showed comparable kinetic constants indicates that the codon-optimization of the gene and the resulting higher expression levels did not influence the correct folding and cofactor insertion of the protein during expression in *E. coli* cells, showing that the codon-optimized construct is suitable for further studies. Consequently, only the codon optimized hAOX1 (hAOX1) was used for all the following studies.

Table 10: Steady-state kinetics parameters for hAOX1 and native hAOX1^a.

Enzyme	Substrate	Electron acceptor	k_{cat} (min^{-1})	K_M (μM)	$\frac{K_{cat}}{K_M}$ ($\text{min}^{-1}\mu\text{M}^{-1}$)
hAOX1	phenanthridine	molecular oxygen	307 ± 12	16 ± 3	19.3
		ferricyanide	221 ± 6	25 ± 4	8.8
		DCPIP	28 ± 5	2 ± 0.5	15.3
	phthalazine	ferricyanide	272 ± 14	196 ± 11	1.4
		DCPIP	27 ± 4	22 ± 4	1.2
	benzaldehyde	ferricyanide	188 ± 14	80 ± 8	2.3
DCPIP		57 ± 9	12 ± 3	4.7	
native hAOX1	phenanthridine	Molecular oxygen	285 ± 11	27 ± 7	10.7
		ferricyanide	292 ± 16	26 ± 5	11.5
		DCPIP	27 ± 1	0.78 ± 0.1	34.4
	phthalazine	ferricyanide	223 ± 11	126 ± 4	1.8
		DCPIP	32 ± 4	9 ± 1	3.5
	benzaldehyde	ferricyanide	204 ± 12	45 ± 6	4.5
DCPIP		30 ± 1	4 ± 0.3	6.5	

^aKinetics parameters up to 100% molybdenum saturation. Substrates concentrations ranged between 1 and 100 μM . The hAOX1 concentration was ~ 200 nM. Activity measurement performed by spectrophotometrical assay. Data are mean values from three independent measurements (\pm S.D.).

4.1.4.2 Other electron acceptors

The enzymatic activity of the hAOX1 was also tested under anaerobic condition using phenanthridine as substrate and PMS, methyl viologen and benzyl viologen as electron acceptors (Fig. 4.10). As shown in Fig. 4.10, the reaction in presence of oxygen toward phenanthridine with PMS, methyl viologen and benzyl viologen as electron acceptors was not detectable because of the fast re-oxidation of the electron acceptors in presence of oxygen. Instead, the reactions hAOX1:phenanthridine using oxygen, ferricyanide and DCPIP as electron acceptors showed around 1420, 1350 and 230 mU/mg, respectively.

Contrarily, under anaerobic conditions hAOX1 gained a considerable specific activity particularly with PMS (2380 mU/mg of hAOX1) as electron acceptor. The reaction

phenanthridine:methyl viologen gained a specific activity of around 1610 mU/mg of hAOX1, comparable ferricyanide. Instead, benzyl viologen showed slightly lower catalytic activity (1210 mU/mg of hAOX1) (Fig. 4.10).

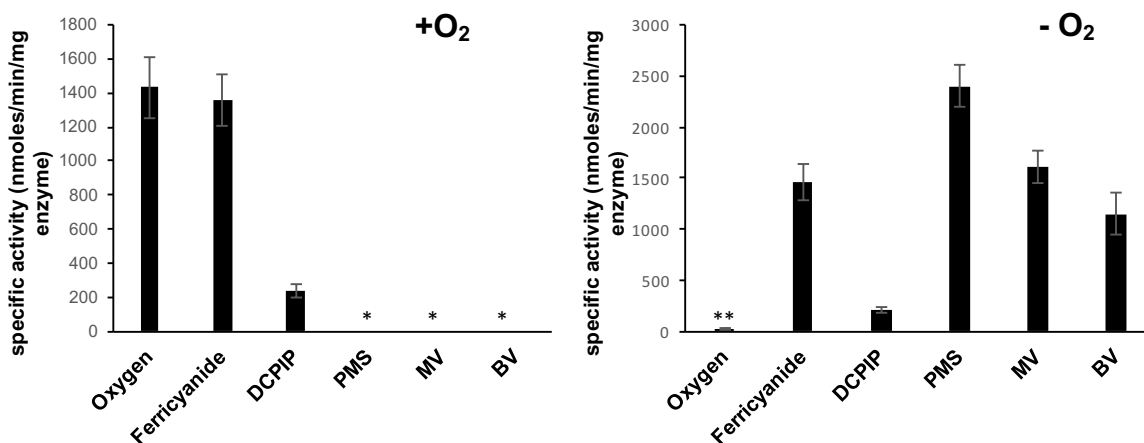


Figure 4. 10. Reactivity of hAOX1 toward phenanthridine as substrates and several electron acceptors, in presence (A) or absence (B) of oxygen. Specific activity was measured by spectrophotometric assay using phenanthridine as substrate and molecular oxygen, ferricyanide, DCPIP, PMS methyl viologen and benzyl viologen as electron acceptors. The measurements were performed in Tris 50, mM NaCl 200 mM, 1 mM EDTA buffer pH 8.0 at 30°C. Substrate concentrations ranged between 1 and 100 μ M. The hAOX1 concentration was \sim 200 nM.

4.1.5 Comparison with bXO

Aldehyde oxidase and xanthine oxidase are related enzymes that share an amino acid homology of around 50 %, showing common and overall structural features (Coelho *et al.*, 2015). However, the diverse substrate specificity indicates a different active site functionality for AOX and XO (Marho *et al.*, 2013). Considering XO as well studied enzyme of this family, a comparison with hAOX1 provides fundamental information regarding enzymatic activity and structural characteristics of this enzyme.

4.1.5.1 Reactivity of the FAD active site of hAOX1

For a better characterization of the catalytic mechanism of hAOX1 and its FAD active site, we compared the functional reactivity of the electron acceptors oxygen, ferricyanide and DCPIP, with hAOX1 and bovine XO in presence of diphenyliodonium (DPI) (Fig. 4.11). DPI is a well-known inhibitor of flavoenzymes, which covalently binds to the reduced FAD/FMN

cofactors and consequently blocks the electron transfer pathway through the flavin cofactors (Chakraborty & Massey, 2002).

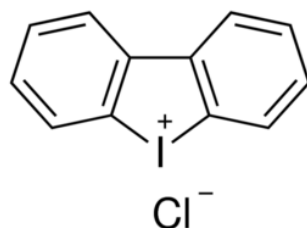


Figure 4. 11. Structure of diphenyliodonium chloride.

The results in Fig. 4.12 show the data obtained for hAOX1 in comparison to the ones obtained for the bXO.

For both hAOX1 and bXO the obtained specific activities show that the xanthine/phenanthridine:O₂ reaction and the xanthine/phenanthridine:ferricyanide reaction were inhibited by DPI, whereas the xanthine/phenanthridine:DCPIP activity was not influenced by the presence of DPI in the assay. This shows that both O₂ and ferricyanide are accepting the electrons at the FAD site of hAOX1 and bXO, whereas DCPIP directly reacts at the Moco active site, as previously suggested (Branzoli & Massey, 1974). In contrast to bXO, hAOX1 showed a significantly reduced specific activity with DCPIP as electron acceptor, confirming that DCPIP is an inhibitor for hAOX1, but not for bXO (Barr & Jones, 2011; Foti *et al.*, 2016). The detected uncompetitive inhibition mode of hAOX1 with DCPIP likely shows that DCPIP reacts with the reduced form of Moco (Foti *et al.*, 2016) (Results section 4.1.7.2.).

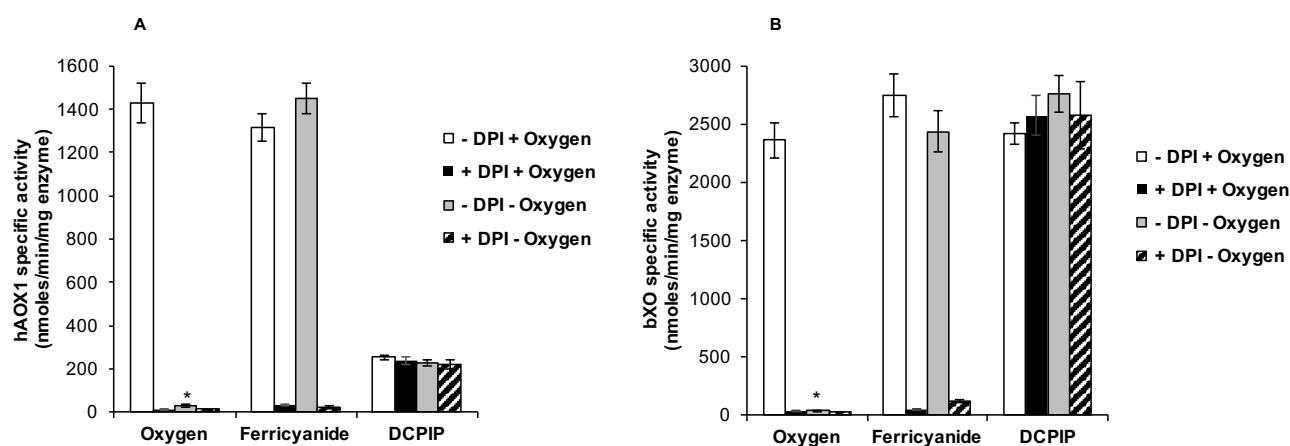


Figure 4. 12. The effect of diphenyliodonium on hAOX1 activity. Specific activities of (A) hAOX wild-type with 80 μ M phenanthrine as substrate and (B) of bXO with 50 μ M xanthine as substrate. Assays were performed

using molecular oxygen (air-saturated buffer) or 500 μM ferricyanide and 100 μM 2,6-dichlorophenolindophenol (DCPIP) as electron acceptors either under aerobic or under anaerobic conditions. The effect of 5 μM diphenyleneiodonium (DPI) on enzyme activity was assayed under these conditions.

4.1.5.2 NADH oxidase activity of hAOX1 and bXO

The human AOX1, as well as other AOXs, is not able to react with NAD^+ but reacts toward molecular oxygen as physiological electron acceptor (Garattini *et al.*, 2008). Contrarily, some AOXs can accept electrons and be reduced by NADH as shown for mouse AOX3 (Mahro *et al.*, 2013). Some previous works proposed for aldehyde oxidases a role as NADH oxidase in the cell (Kundu *et al.*, 2012).

In this work, we tested the hAOX1 for its capacity to oxidase NADH (Fig. 4.13). hAOX1 was pre-incubated under anaerobic conditions to exclude oxygen from the reaction toward NADH. The concentration of the enzyme in the assay was $\sim 10 \mu\text{M}$ and the reaction was performed in Tris x HCl 50 mM, NaCl 200 mM, EDTA 1 mM pH 8.0 buffer, under anaerobic conditions. After 4 h of anaerobic incubation at 4 $^{\circ}\text{C}$, to favor the exclusion of molecular oxygen from the enzyme solution, hAOX1 was incubated with NADH 100 μM and UV/Vis spectra were measured over time from 0 to 20 minutes. Although hAOX1 was mixed with 10-fold larger amount of NADH, no reduction of the FAD cofactor was observed during the assay. The result clearly show the inability of hAOX1 to oxidize NADH (Fig. 4.13 A). As a control bXO was tested under the same experimental conditions. bXO was also incubated with 100 μM NADH under the same condition of hAOX1 and it showed a progressive and constant reduction of the absorbance peak of around 450 nm, indicating the FAD reduction and the passage of the electrons from NADH to bXO (Fig. 4.13 B). After 20 min of anaerobic incubation together with NADH, to both enzymes $\text{Na}_2\text{S}_2\text{O}_2$ was added to a final concentration of 1 mM to show the fully reduction of the enzymes.

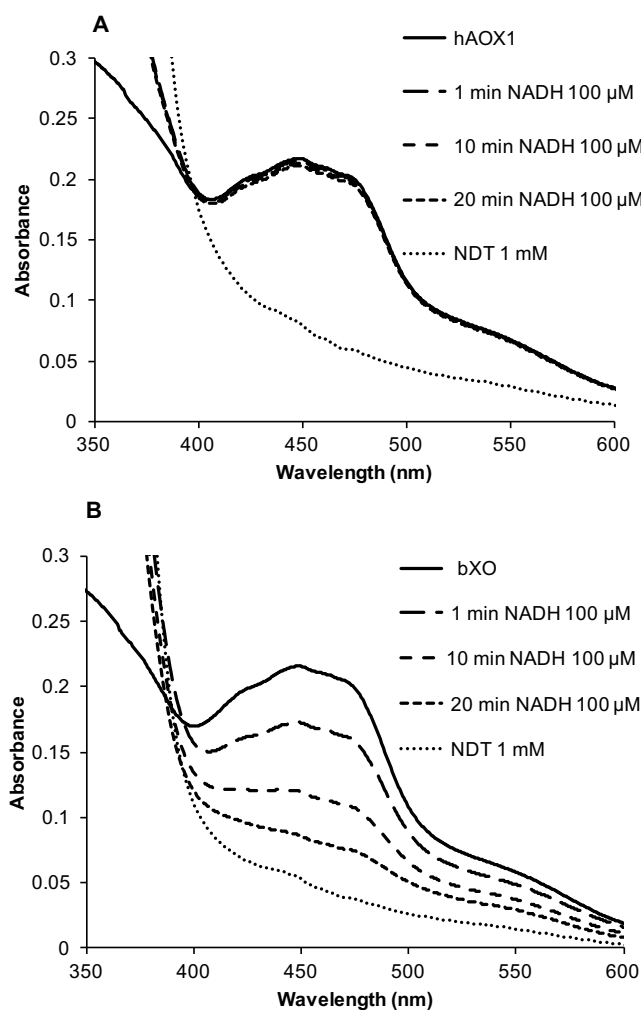


Figure 4. 13. UV/Vis spectra of hAOX1 in comparison to bXO reduced with NADH under anaerobic conditions. The Figure illustrates UV-Vis spectra of 10 μ M hAOX1 (A) and 10 μ M bXO (B) in the oxidized state (solid line) and reduced enzyme with 0.1 mM NADH after 1 min, 10 min and 20 min (dashed lines) and of the enzyme reduced with 1 mM sodium dithionite (NDT) (dotted line). The spectra were recorded in 50 mM Tris, pH 8.0.

4.1.6 Crystallization of hAOX1

It was of interest to solve the crystal structure of hAOX1 in order to obtain new insights regarding the structural-functional features of this enzyme, as well as the relation with the other enzymes belonging to the same family. The number of the AOXs varies from the four isoforms present in rodents to the single active gene present in humans (Kurosaki *et al.*, 1999). Due this important inter-specific diversity, specie-specific AOX information are needful to clarify the functions of those enzymes in different organisms. Therefore, extensive crystallographic studies were performed on the human AOX1.

By the collaboration with the group of Dr. Prof. Maria João Romão (Universidade Nova de Lisboa, Portugal), crystallization experiments were performed on the hAOX1 free enzyme and also in presence of substrates and inhibitors.

Crystals of hAOX1 were obtained with the conditions of 4-6% polyethylene glycol 4000 (PEG 4K), 0.1 sodium malonate, pH 5.0 at 20 °C for the precipitation of the enzyme. Crystals appeared a few hours after setting up the crystallization drops and generally grew to their maximum size within 24 hours (Fig. 4.14). The hAOX1 crystals resulted indeed fragile and therefore were immediately flash-cooled in liquid nitrogen using a cryo-solution containing 15% glycerol. The crystallization experiments were carried out manually or by using an automatized system. hAOX1 crystallized in the presence of polyethylene glycol diffracted to 2.6 Å resolution. The hAOX1 3-D structure was solved by C. Coelho employing crystals obtained under similar conditions (Coelho *et al.*, 2015). The overall dimensions of the hAOX1 homodimer are approximately 150 Å × 90 Å × 65 Å, with the typical butterfly shape that is observed in other dimeric members of the XO family (PDB 4UHW). Each monomer comprises 1,336 residues and can be divided into three distinct domains according to cofactor localization (Coelho *et al.*, 2015).



Figure 4. 14. Crystal of hAOX1 in the presense of phthalazine 20 mM for co-crystallization experiments.

To better understand the structural features of hAOX1, catalytic and inhibition mechanism, crystallization studies using different compounds were performed. Several experiments of co-crystallized hAOX1 with the substrate phthalazine were carried out together with soaking experiments using some of the most potent inhibitors reported (Obach *et al.*, 2004). Furthermore, soaking experiments with the inhibitor thioridazine were performed and a 2.7-Å

resolution crystal structure of hAOX1 in the presence of both substrate and inhibitor (hAOX1-Pht-Thi, PDB 4UHX) was obtained from C.Coelho (Coelho *et al.*, 2015). Analysis of the hAOX1 complex bound with inhibitor-substrate structure showed that the Phthalazine molecule is stacked between F885 and I1085, with one of its nitrogen atoms 3.8 Å away from the labile hydroxyl ligand. The binding of the substrate phthalazine at the active site cavity caused clear changes in the orientations of the L812 side chain and the phenyl rings of F885 and F923 (Fig. 4.15).

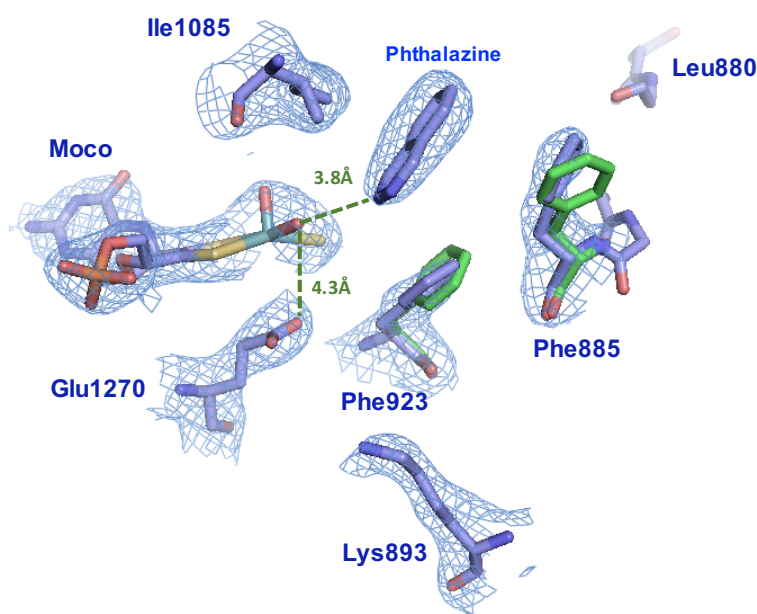


Figure 4. 15. Overlay of the active site residues of hAOX1-free (blue) and hAOX1-phthalazine complex (green). Adapted from Coelho *et al.*, 2015.

The complex hAOX1-phthalazine-thioridazine showed that the substrate and the inhibitor molecules were bound at distinct sites 34 Å apart and the thioridazine molecule stacked within a novel inhibition pocket away from the active site. To confirm these structural observation inhibition studies were performed.

4.1.7 Inhibition studies

To assay the effect of pharmacologically relevant molecules (Fig. 4.16) on hAOX1 enzymatic activity, inhibition studies were performed by spectro-photometric measurements using different substrates and electron acceptors. The condition for the standard inhibition assays was Tris 50 mM, 200 mM NaCl, 1 mM EDTA pH 8.0 buffer at 30 °C. All data were fitted by non-

linear regression to the appropriate model examined by plotting $1/k_{cat-app}$ vs $1/[substrate]$ (Lineweaver-Burk plot).

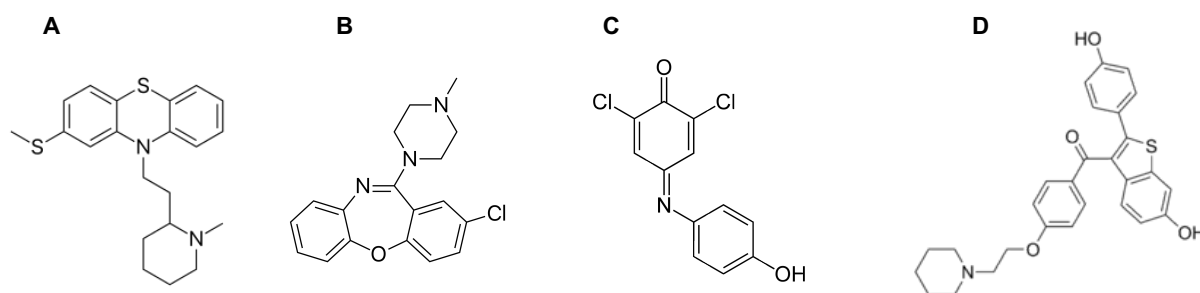


Figure 4. 16. Structures of thioridazine (A), loxapine (B), DCPIP (C) and raloxifene (D).

4.1.7.1 Inhibition studies with thioridazine

Thioridazine (phenothiazine drug family), a widespread antipsychotic drug, was tested for inhibitory effects on the hAOX1 and related enzymes as mAOX3, bXO and bXDH. To test the impact of thioridazine inhibition on these enzymes, we performed steady-state kinetic measurements with hAOX1 and mAOX3, using phthalazine as a substrate, and with bXO, using xanthine as a substrate. The results show a noncompetitive type of inhibition for the phthalazine-thioridazine inhibition of hAOX1 and mAOX3, using ferricyanide as electron acceptor (Table 11). The inhibition constants we obtained were $K_{i \text{ thio}}$ of $1.3 \pm 0.3 \mu\text{M}$ for hAOX1 and $K_{i \text{ thio}}$ of $16.4 \pm 1.4 \mu\text{M}$ for mAOX3. The kinetics of the xanthine-thioridazine inhibition of bXO with molecular oxygen as electron acceptor showed a mixed type of inhibition instead (Fig 4.17, table 11).

Table 11: Kinetic parameters of the phthalazine-thioridazine inhibition of hAOX1 and mAOX3, and of the xanthine- thioridazine inhibition of bXO

	$K_m(\mu\text{M})$	$k_{cat}(\text{min}^{-1})$	$K_i(\mu\text{M})$	$K_{ii}(\mu\text{M})$
hAOX1 ^a	56.7 ± 10.3	13.07 ± 1.9	1.3 ± 0.3	–
mAOX3 ^a	6.45 ± 3.7	17.43 ± 1.2	16.4 ± 1.4	–
bXO ^b	7.9 ± 1.3	55.86 ± 0.7	198 ± 9	590 ± 28

^aInhibition of 0.2–0.5 μM of hAOX1 or mAOX3 using 1–40 μM phthalazine and 0.1–25 μM thioridazine in the presence of 1 mM ferricyanide as an electron acceptor; in buffer at 30 °C, pH 7.5.

^bInhibition of 0.1 μM bXo using 5–200 μM xanthine and 10–50 μM thioridazine in the presence of molecular oxygen as an electron acceptor; in buffer at 30 °C, pH 8.0. Data are mean values \pm s.d. from three independent measurements.

The inhibition was about 10- to 20-fold weaker than the phthalazine-thioridazine inhibition of hAOX1 and mAOX3, with $K_{i\text{thio}} = 440 \pm 31 \mu\text{M}$ and $K_{ii\text{thio}} = 70 \pm 9 \mu\text{M}$. These results suggested a tight binding of the inhibitor to hAOX1 far from the active site and less effective in mAOX3 and in bXO. Although the binding of thioridazine to the inhibitor-binding pocket of hAOX1 and mAOX3 occurs to the same extent in the free and substrate-bound enzymes, in bXO the inhibition constants are different. The mixed-inhibition mode suggested that binding of substrate to the active site influenced the affinity of the inhibitor for the inhibitor-binding site. In the following plot (Fig. 4.17) are shown the measurements using ferricyanide instead of DCPIP as electron acceptor.

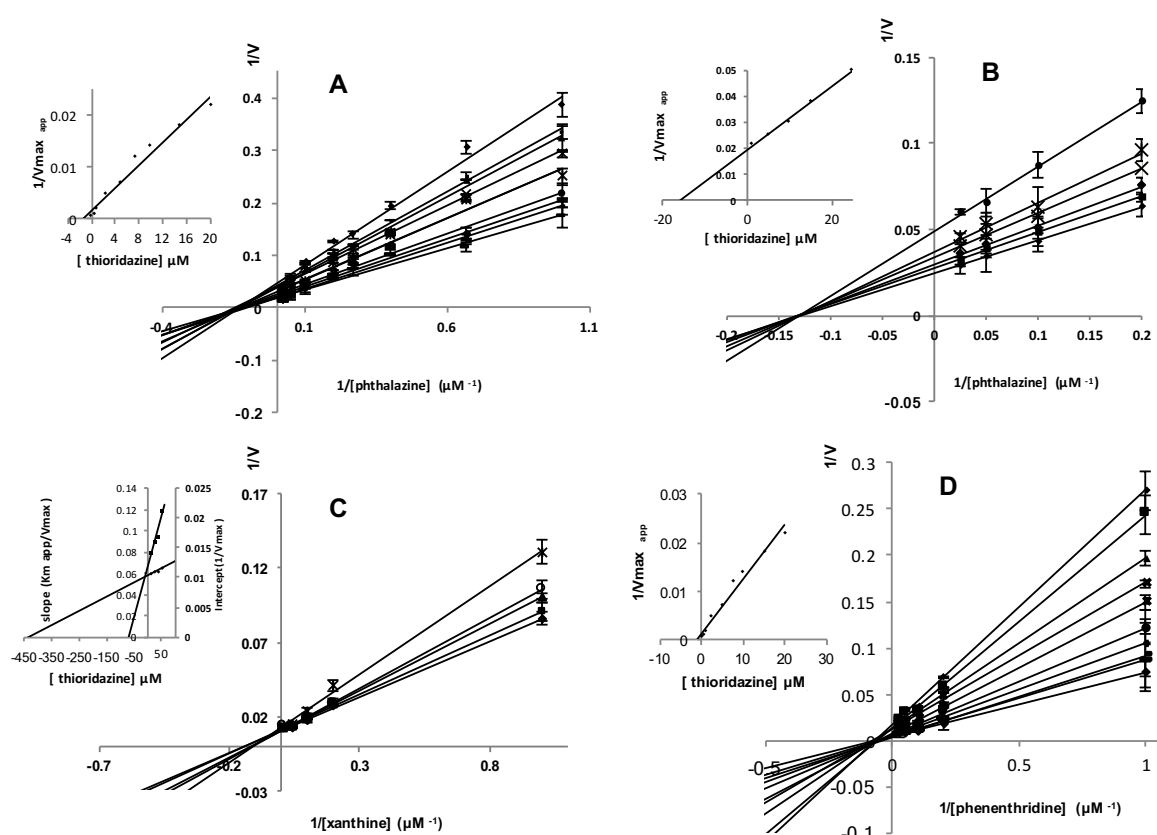


Figure 4. 17. Kinetics of phthalazine-thioridazine inhibition of hAOX1 (A), mAOX3 (B), xanthine-thioridazine inhibition of bXO (C) and phenanthridine-thioridazine inhibition of hAOX1 (D). Lineweaver-burk plots for substrate-electron acceptor reaction of hAOX1, mAOX3 and bXO in the presence of thioridazine. A) inhibition of 0.2–0.5 μM hAOX1 using 1, 1.5, 2.5, 3.75, 5, 10, 20, 40 μM phthalazine and 0.1, 0.5, 1, 2.5, 5, 7.5, 10, 15 μM thioridazine in the presence 1 mM ferricyanide as electron acceptor. Inset: the K_i value was obtained from the secondary plot of the apparent $1/V_{\text{max}}$ of the Lineweaver-Burk plot. B) inhibition of 0.2–0.5 μM mAOX3 using 1, 5, 10, 20, 40 μM phthalazine and 1, 5, 10, 15, 25 μM of thioridazine in the presence 1 mM ferricyanide as electron acceptor. Inset: the K_i value was obtained from the secondary plot of the apparent $1/V_{\text{max}}$ of the Lineweaver-Burk plot. C) inhibition of 0.1 μM bXO using using 5, 10, 25, 10, 200 μM xanthine and 10, 25, 35, 50 μM thioridazine in the presence of molecular oxygen as electron acceptor. Inset: the K_i and K_{ii} values were obtained from the secondary plot of the slope apparent $1/V_{\text{max}}$ of the Lineweaver-Burk plot, respectively. D) A) inhibition of 0.2–0.5 μM hAOX1 using 1, 5, 10, 20, 40 μM phenanthridine and 0.1, 0.5, 1, 2.5, 5, 7.5, 10, 15, 20 μM thioridazine in the presence of molecular oxygen as electron acceptor. Inset: the K_i value was obtained from the secondary plot of the apparent $1/V_{\text{max}}$ of the Lineweaver-Burk plot. Data are mean values from three independent measurements (\pm S.D.).

To further confirm the inhibitory effect of thioridazine against hAOX1, inhibition experiments using phenanthridine as substrate and oxygen as electron acceptor were performed. The results for the phenanthridine-thioridazine inhibition using O_2 as electron acceptor gave similar K_i values of phthalazine-ferricyanide experiments showing that the inhibition is not influenced by the substrate or electron acceptor used. Further inhibition studies on XDH from *Rhodobacter capsulatus* were performed. In these experiments was used xanthine as substrate and NAD^+ as electron acceptor. Those results showed no inhibition of XDH activity due to thioridazine. Those results were consistent the crystal structure of hAOX1-thioridazine-phthalazine showing a new inhibitor binding site far from the Moco active site (Coelho *et al.*, 2015). Other electron acceptors, as DCPIP (2,6-dichlorophenolindophenol), which is an inhibitor of hAOX1 (Barr & Jones, 2011) could not be employed.

4.1.7.2 Other inhibitors

To characterize the influence of DCPIP on the catalytic constants of hAOX1, inhibition studies with varying concentrations of DCPIP were performed. Using hAOX1 and cinnamaldehyde as substrate (substrate consumption detectable by decreased absorbance at 295 nm), inhibition studies showed an uncompetitive inhibition pattern for hAOX1-DCPIP (Fig. 4.18) with a K_i value of $41.7 \mu\text{M}$. These data are consistent with previously reported parameters (Barr & Jones, 2011). Additionally, we determined the inhibitory effect of the potent inhibitor raloxifene. The inhibitor showed an uncompetitive binding mode with a K_i value of $7.25 \pm 6 \mu\text{M}$ for hAOX1 wild type. Since the inhibition mode is uncompetitive, the inhibitor probably binds at a position different from the active site.

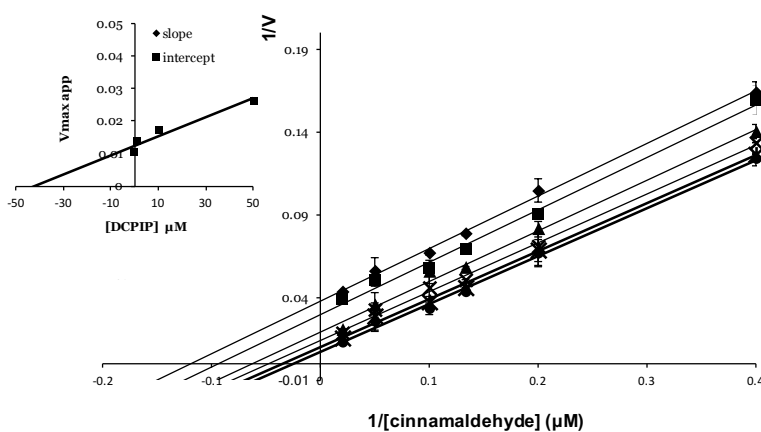


Figure 4. 18. Lineweaver-Burk plots of hAOX1 inhibition by DCPIP. Inhibition of hAOX1 using DCPIP concentrations between 0 and 200 mM were measured: 200 mM (Gatchel *et al.*), 100 mM (filled square), 50 mM (triangle), 10 mM (empty circle), 1 mM (empty square), and 0 mM (filled circle). Inset: secondary plot of $1/V_{max,app}$ and inhibitor concentration to determinate K_i value. The product formation was measured with 5–100 mM cinnamaldehyde as substrate using molecular oxygen as electron acceptor. Data are mean values from three independent measurements (\pm S.D.).

Further inhibition studies were performed using loxapine, an antipsychotic drug belonging to the dibenzoxazepine class, highly related to thioridazine (Fig. 4.19 B). The inhibition pattern hAOX1-phenanthridine-loxapine showed non-competitive inhibition by the loxapine with a K_i of $22 \pm 5 \mu\text{M}$ (fig. 4.19). The same kind of inhibition reported for thioridazine and most likely also the same interaction drug-enzyme. The estrogen raloxifene was already shown to be a potent and selective inhibitor of the human aldehyde oxidase (Obach *et al.*, 2004). Raloxifene revealed an uncompetitive-type inhibition in the reaction with phenanthridine as substrate (fig. 4.19 A).

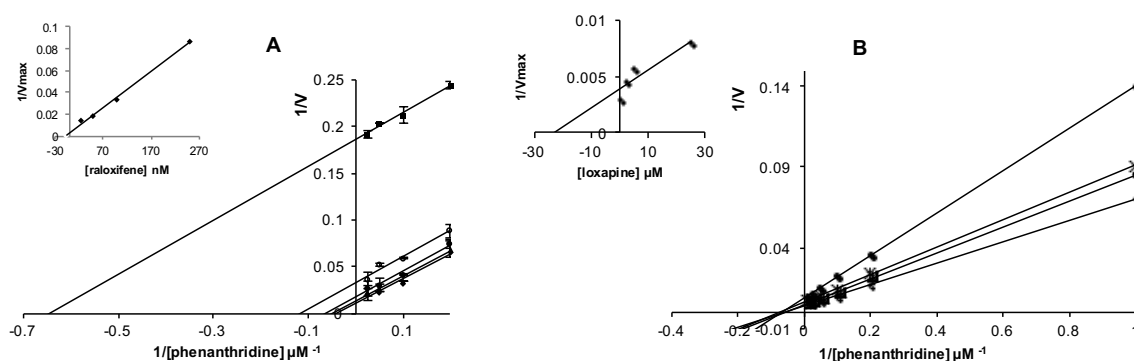


Figure 4. 19. Lineweaver-Burk plots of hAOX1 inhibition by raloxifene (A) and loxapine (B). Inhibition of hAOX1 using raloxifene and loxapine concentrations between respectively 0- 20 μM and 0-50 μM were measured. Inset: secondary plot of $1/V_{max,app}$ and inhibitor concentration to determinate K_i value. The product formation was measured with 1–100 μM phenanthridine as substrate using molecular oxygen as electron acceptor. Protein concentration was around 200 nM in the assay. Data are mean values from three independent measurements (\pm S.D.).

4.2 Site-directed mutagenesis and studies of the effect of SNPs on hAOX1 activity

4.2.1 Mutagenesis, expression and purification of the hAOX1 variants

4.2.1.1 Introduction of SNPs into the hAOX1 gene for heterologous expression

Among the human population an intra-specific diversity effects the expression, the tissue distribution and the enzymatic activity of hAOX1. In humans, a major reason for the differences between individuals are considerably attributed to single nucleotide polymorphisms (SNPs) located in the *AOX1* gene. An increasing number of SNP variations in the *AOX1* genomic sequence are listed in the NCBI SNP gene data bank (<http://www.ncbi.nlm.nih.gov/snp>) (Fig. 4.20) and several of these polymorphisms were identified to be located in the space surrounding the FAD active site (Fig. 4.21).

Previous studies indicated that several of this SNPs can have an important role in the catalytic activity of hAOX1, leading to the replacement of distinct highly conserved amino acids effecting the enzymatic activity (Hartmann *et al.*, 2012).

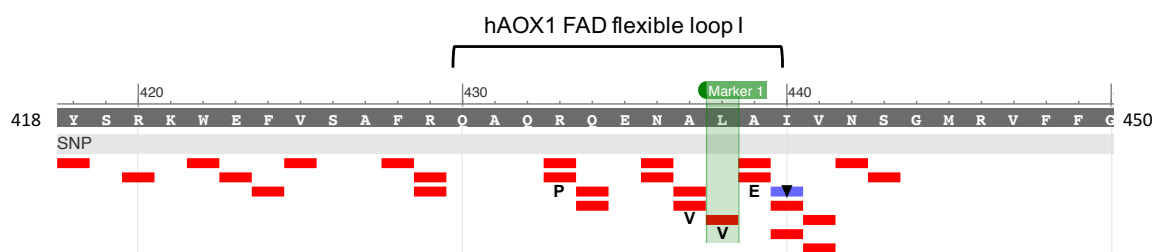


Figure 4. 20. Amino acidic sequence of hAOX1 with some of the selected single nucleotide polymorphisms selected on the hAOX1 gene from the SNPs data bank (<http://www.ncbi.nlm.nih.gov/snp>)

According to the single nucleotide polymorphism data bank, several promising SNPs, all located in the vicinity of the FAD binding site of hAOX1, were chosen for these studies (Fig. 4.21-22-23). Figure 4.21 shows the amino acid sequence of the hAOX1 with the polymorphisms present per each amino acid and particularly the variations present within the FAD flexible loop sequence (Q430-I440) at the FAD binding site (middle domain).

Here we investigated the functionality of the FAD active site, in relation to its structural properties, employing an extensive mutagenesis approach. The hAOX1 variants generated in

this work are grouped in three categories: I) hAOX1 single nucleotide polymorphisms (SNP); II) XOR-FAD loop hAOX1 variants; III) additional single point hAOX1 variants.

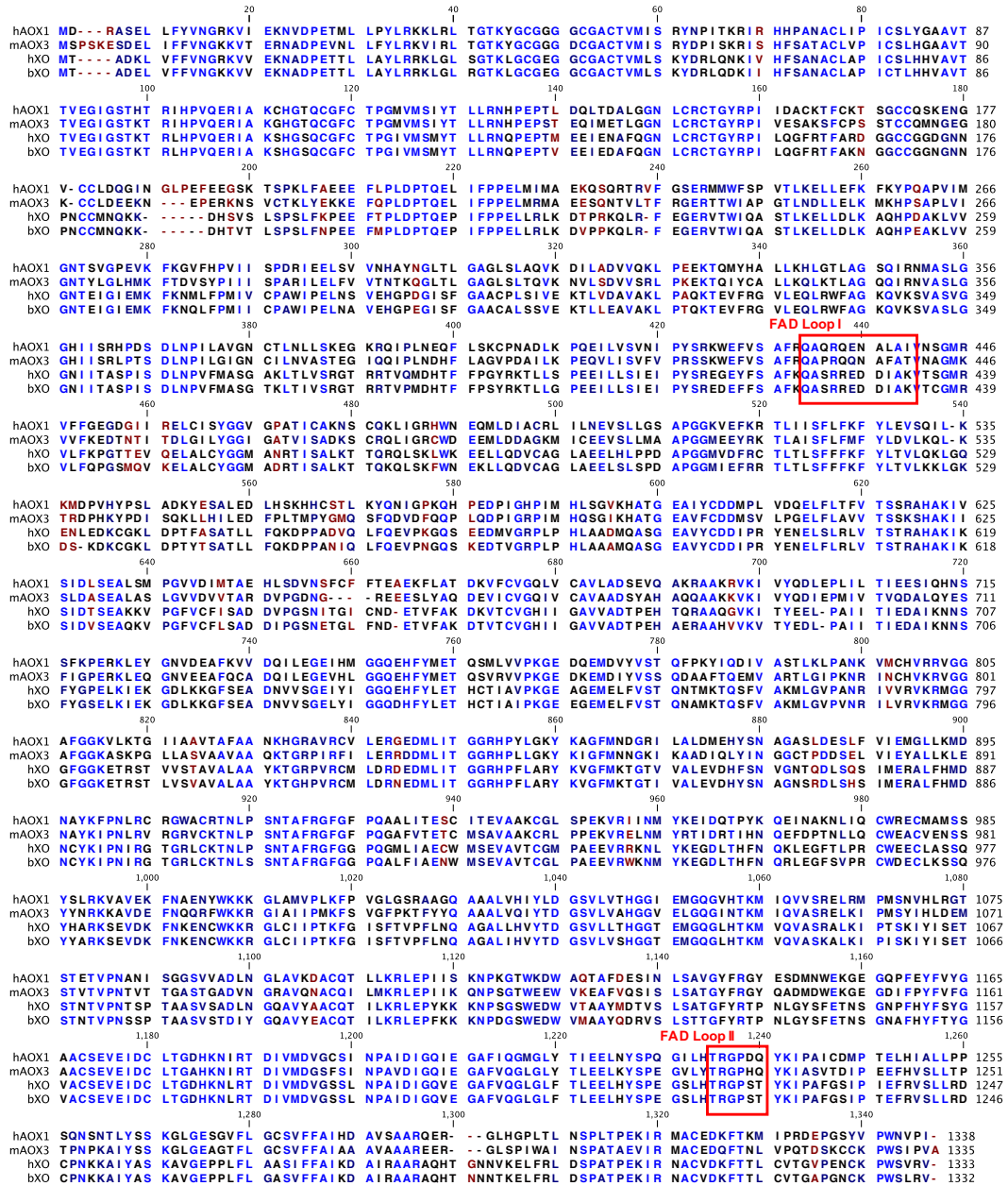


Figure 4. 21. Amino acid sequence alignment of hAOX1, mAOX3, hXO and bXO. Red boxes indicate the FAD flexible loops. Figure created by CLC Sequence Viewer version 6.3.

A number of ten hAOX1 SNP variants were introduced into the hAOX1 gene by site directed mutagenesis and a characterization was carried out. The SNPs variants produced are: hAOX1 G46E, hAOX1 G50T, hAOX1 G346R, hAOX1 H363Q, hAOX1 R433P, hAOX1 A437V,

hAOX1 L438V hAOX1 A439E, hAOX1 R1231H and hAOX1 K1237N (Fig. 4.22). Those variants might be grouped in three sub-categories: 1) mutations located on the variable loop 1 and 2 (hAOX1 R1231H, hAOX1 A439E, hAOX1 R433P, hAOX1 L438V, hAOX1 K1237N and hAOX1 A437V); 2) mutations in closed proximity of the FAD cofactor (hAOX1 G346R, hAOX1 H363Q); 3) mutation among the FeS center II and the FAD center (hAOX1 G46E, hAOX1 G50D).

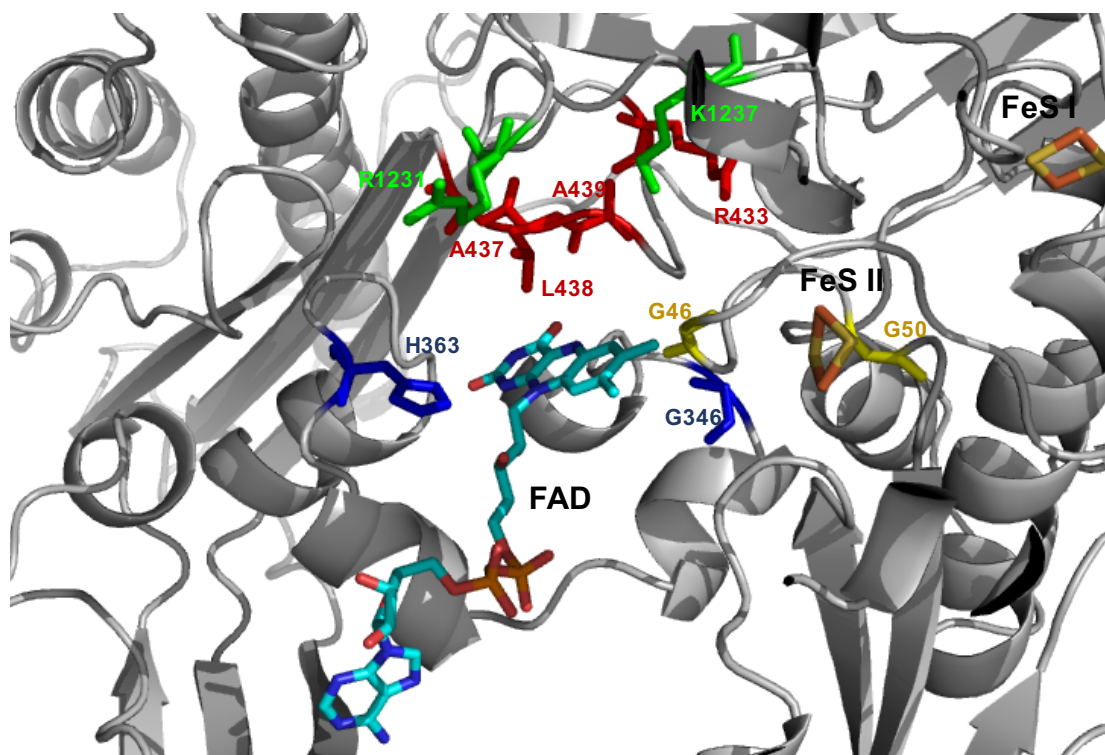


Figure 4. 22. The location of the SNP exchanged residues in the surrounding of the FAD cofactor of the hAOX1. Red and green residues are located within the FAD loop I and II respectively. The yellow residues are located between FAD and FeSII. The blue residue are located in the vicinity of the FAD cofactor. Figure created using MacPymol 6.0.

As previously mentioned, a major structural difference between mammalian XOR and aldehyde oxidases occurs at the FAD binding site (Fig.4.22). The structural differences are functionally related to different properties of those enzymes: catalytic activity (kinetics parameters), electron acceptors (O_2 and NAD^+) and reactive oxygen species (ROS) production.

hXOR	EGEYFSAFK QASRREDDIAK VTSGMRVLFKPGTTEVQEL	452
hAOX1 WT	KWEFVSAFR QAQRQENALAI VNSGMRVFFGEGDGIIREL	460
hAOX1 R433P	KWEFVSAFRQAQ P QENALAIVNSGMRVFFGEGDGIIREL	460
hAOX1 A437V	KWEFVSAFRQAQRQEN V LAIVNSGMRVFFGEGDGIIREL	460
hAOX1 L438V	KWEFVSAFRQAQRQEN A VAIVNSGMRVFFGEGDGIIREL	460
hAOX1 A439E	KWEFVSAFRQAQRQEN A EIVNSGMRVFFGEGDGIIREL	460
hXOR	LFTLEELHYSPEGSLH TRGP STYKIPAFGSIPIEFRVSLLR	1245
hAOX1 WT	GLYTIEELNYSPPQILH TRGPD QYKIPAICDMPTELHIALLP	1244
hAOX1 R1231H	GLYTIEELNYSPPQILH T HGPDQYKIPAICDMPTELHIALLP	1244
hAOX1 K1237N	GLYTIEELNYSPPQILH TRGPD QY N IPAICDMPTELHIALLP	1244
hXOR	DPETLLAYLRRKLGSLGSKLGC EGGCG ACTVMLSRYD	59
hAOX1 WT	DPETMLLPYLRKKLRLTGTYG CGGGCG ACTVMISRYN	60
hAOX1 G46E	DPETMLLPYLRKKLRLTGTYG CGEGGCG ACTVMISRYN	60
hAOX1 G50D	DPETMLLPYLRKKLRLTGTYG CGGGCGD ACTVMISRYN	60

Figure 4. 23. Amino acid alignment of hAOX1 wild type and the SNP FAD variants.

In hAOX1, the reduced FAD cofactor releases the electrons to the di-oxygen (electron acceptor) generating either hydrogen peroxide or superoxide radical, allowing the re-oxidation of the enzyme for a new cycle. A crucial portion within the FAD active site, in all XOR family enzymes consist in the flexible loop I (Q₄₂₃ASRREDDIAK₄₃₃ in bXO/bXDH), essential for conversion from XDH to XO and vice versa, due to its role in determining the redox potential and the structural changes at the FAD site (Ishikita *et al.*, 2012). bXOR contains more charged residues within the loop than the hAOX1.

To better understand the role of this flexible loops in the function of hAOX1, XOR FAD-flexible loop I was partially inserted in hAOX1 and six new variants were produced (XOD-FAD loop hAOX1 variants): hAOX1 A437D, hAOX1 N436D/A437D, hAOX1 N436D/A437D/L438I, hAOX1 N436D/A437D/L438I/I440K, hAOX1 Q434R/N436D/A437D/L438I/I440K (Fig. 4.24-25). The final aim was to obtain the flexible loop I of bXOR in hAOX1 and to study the structural/functional impact.

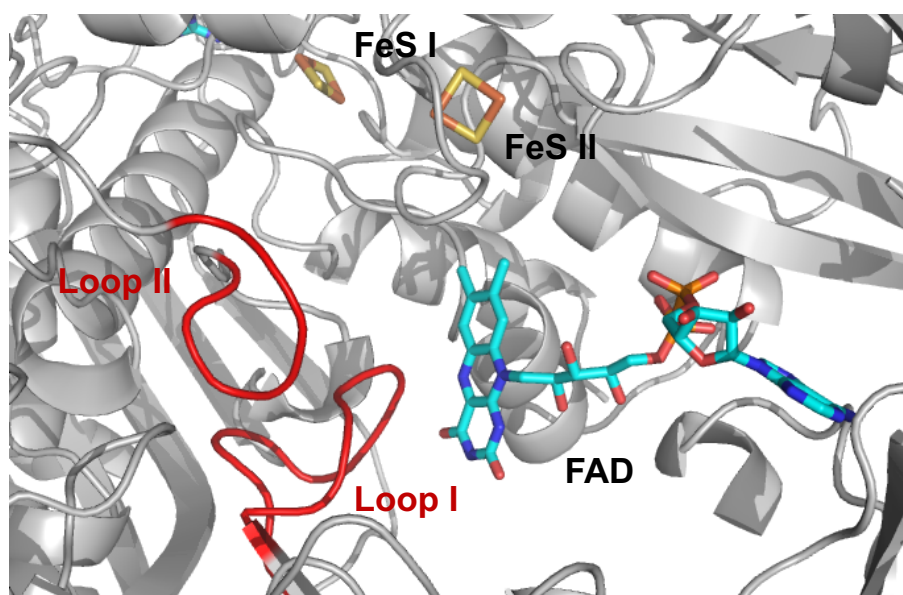


Figure 4. 24. FAD active site of hAOX1. Shown are the FAD flexible loop I and loop II (red cartoon), the FAD structure (sticks) and the FeS I and FeSII (sticks). Figure created using MacPymol 6.0.

For additional detailed studies at the FAD active site of the hAOX1, other five new hAOX1 variants were generated: hAOX L438F, hAOX1 L438K, L438A, hAOX1 L344F and D1234H. The residues F344 and H1234 are derived from the mouse AOX3 amino acidic sequence. The residue Leu438 was exchanged to a Lys considering the fact that for many flavoenzyme the proposed mechanism of superoxide production involves an interaction Lys-N5 of the isoalloxazine ring of the FAD cofactor (Chaiyen *et al.*, 2012).

hXOR	EGEYFSAFK QASRREDDIAK VTSGMRVLFKPGTTEVQEL	452
hAOX1 WT	KWEFVSAFR QAQRQENALAI VNSGMRVFFGEGDGIIREL	460
hAOX1 A437D	KWEFVSAFRQAQRQEN D LAIVNSGMRVFFGEGDGIIREL	460
hAOX1 N436D/A437D	KWEFVSAFRQAQRQ EDD LAIVNSGMRVFFGEGDGIIREL	460
hAOX1 N436D/A437D/L438I	KWEFVSAFRQAQRQ EDDI AIVNSGMRVFFGEGDGIIREL	460
hAOX1 N436D/A437D/L438I/I440K	KWEFVSAFRQAQRQ EDDI A K VNSGMRVFFGEGDGIIREL	460
hAOX1 Q434R/N436D/A437D/L438I/I440K	KWEFVSAFRQAQR REDDI A K VNSGMRVFFGEGDGIIREL	460

Figure 4. 25. Amino acid alignment of hAOX1 wild type and the FAD loop variants.

Site-directed mutagenesis of the hAOX1 variants was performed using the expression vector pTHcoaox (pTrcHis-hAOX1 codon optimized) as a template and base pair exchanges were introduced using the protocol from the site directed mutagenesis kit (Quick Change, Agilent Technologies) but with further modifications for the specific case of hAOX1 as indicated in the material and methods section of this manuscript. Base pair exchanges were introduced into

the hAOX1 gene by PCR mutagenesis. The introduction of the mutation was accomplished using two primers containing the specific mutation of interest. The human codon optimized *Aox1* gene was completely amplified by means of the mutagenic primers together with the vector sequence.

4.2.1.2 Expression and purification of the hAOX1 variants

The first purification step was a NI-NTA affinity chromatography, allowing the purification based on the binding of the His₆-tag fusion proteins to the Nickel beads present into the column. Then, the hAOX1 variants were eluted by a 250 mM imidazole solution and de-salted by using gel-filtration PD-10 columns. After that, an *in vitro* chemical sulfuration was performed for all the expressed variants as well as for the wild type enzyme. As last step of the proteins purification, a size exclusion chromatography was performed. All the procedure was carried out under the same conditions used for the wild type hAOX1.

The general protein yield was about 1 mg of protein per liter of *E. coli* culture for most of the variants (Table 12), apart from the variants hAOX1-G50D, which was purified with a 10-fold lower yield as compared to the wild type protein, and the variants hAOX1 N436D/A437D/L438I and hAOX1N436D/A437D/L438I/I440K which were also poorly expressed (Table 12, Fig. 4.26 C-R-S). The variant hAOX1 L344F was not stable enough to be purified, likely due to the impact of the residues exchange during its maturation.

The size exclusion chromatography elution profiles show all the expressed hAOX1 variants eluted mainly as a dimer with a molecular mass of 300 kDa. The variants G46E, G50D, L438K and N436D/A437D/L438I/I440K showed a higher aggregation peak (Fig. 4.26).

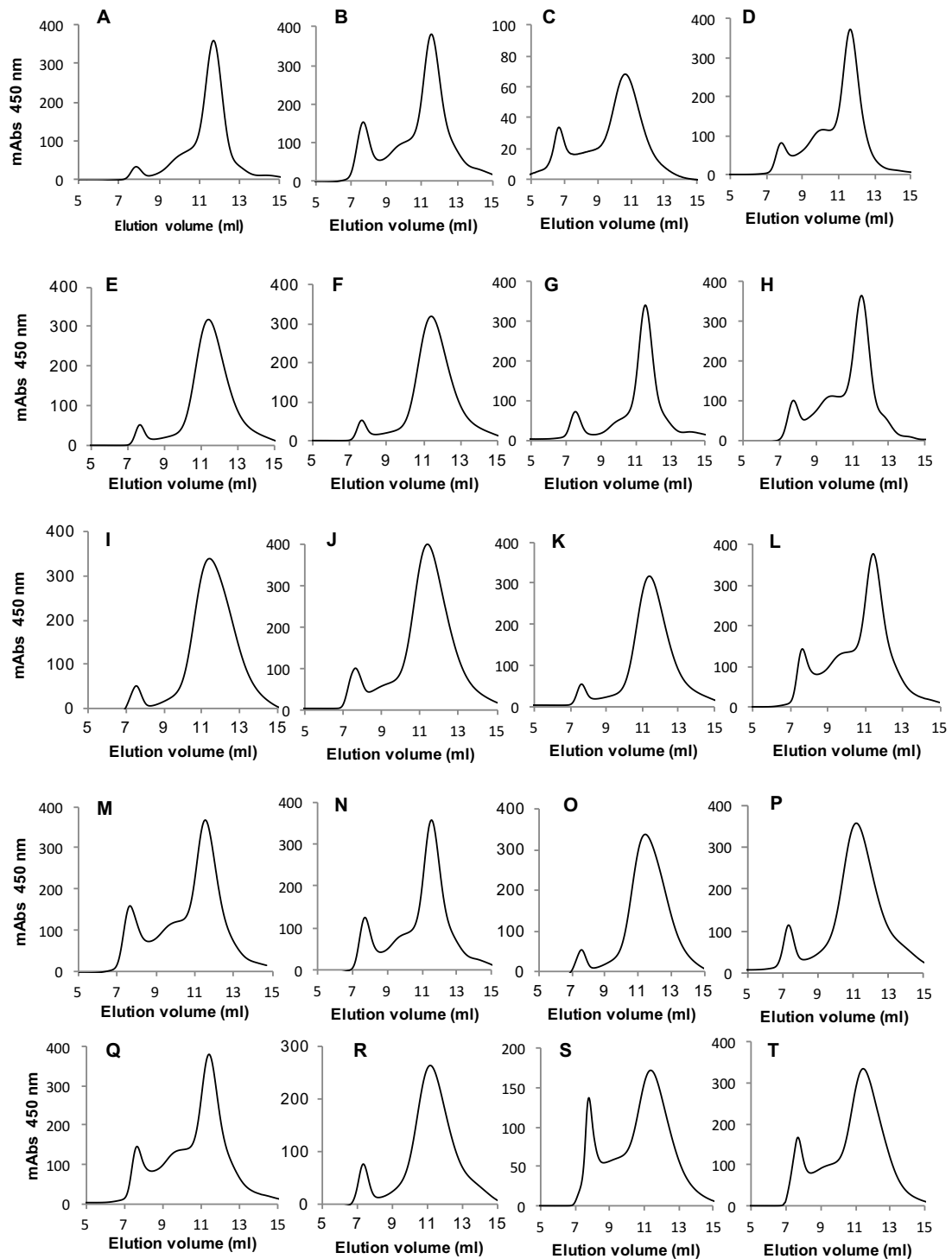


Figure 4. 26. Elution profiles after size exclusion chromatography (superdex200 column) of hAOX1 WT and variants. hAOX1 WT (A), G46E (B), G50D (C), G346R (D), H363Q (E), R433P (F), A437V (G), L438V (H), A439E (I), R1231H (J), K1237N (K), L438F (L), L438K (M), L438A (N), D1234H (O), A437D (P), N436D/A437D (Q), N436D/A437D/L438I (R), N436D/A437D/L438I/I440K (S) and Q434R/N436D/A437D/L438I/I440K (T). All the variants were eluted in 50 mM Tris*HCl, 200 mM NaCl, 1 mM EDTA pH 8.0.

The hAOX1 variants L438A, L438K, L438F and D1234H were all expressed with same yield as the wild type enzyme (Table 12, Fig. 4.26). Overall, the majority of the single mutation inserted into the FAD active site of hAOX1 did not effect the oligomerization state of the purified enzymes. Instead, the multiple hAOX1 variants undergo a stronger impact on the structural organization of the enzyme, leading to a lower yield of purified protein.

Table 12: Protein yield of hAOX1 wild-type and variants^a.

Enzyme	Yield of purified protein (mg/L <i>E. coli</i> culture)
hAOX1 wild-type	1.2 ± 0.3
G46E	0.9 ± 0.2
G50D	0.1 ± 0.05
G346R	1.1 ± 0.2
H363Q	1.2 ± 0.1
R433P	0.8 ± 0.2
A437V	1.2 ± 0.1
L438V	1 ± 0.3
A439E	0.9 ± 0.2
R1231H	0.9 ± 0.3
K1237N	0.7 ± 0.3
D1234H	1.3 ± 0.1
L438A	1 ± 0.05
L438K	1.1 ± 0.1
L438F	0.9 ± 0.1
L344F	n.d.
A437D	1 ± 0.2
N436D/A437D	1.1 ± 0.2
N436D/A437D/L438I	0.3 ± 0.2
N436D/A437D/L438I/I440K	0.2 ± 0.05
Q434R/N436D/A437D/L438I/I440K	0.5 ± 0.2

^aConcentrations measured by absorbance at 450 nm. Data are mean values from three independent measurements (± S.D.).

Notable is the case of the hAOX1 variants N436D/A437D and N436D/A437D/L438I. Although a drastic residue exchange in terms of charge and size, the hAOX1 variant

N436D/A437D showed protein yield comparable to wild type enzyme. Instead, the variant N436D/A437D/L438I, carrying a third mutation Leu to Ile in position 438, shows an impaired folding giving a decreased yield of protein. A similar effect was observed for the variant N436D/A437D/L438I/I440K. Surprisingly, the variant Q434R/N436D/A437D/L438I/I440K partially restored the expression yield to 0.5 mg/L of cell culture.

4.2.2 Characterization of the hAOX1 SNP-based variants

To compare the overall characteristics of the generated hAOX1 variants, UV-Vis spectra were recorded for all the SNP mutants (Fig. 4.27). The UV/Vis spectra of hAOX1 wild type and the SNP variants in their oxidized form displayed the typical features of molybdo-flavoenzymes with a prominent absorption maximum at 450 nm and a shoulder at 550 nm, representing the presence of FAD and the two [2Fe-2S] clusters. No major differences were observed between SNP variants and wild type enzyme (Fig. 4.27).

The Coomassie-stained SDS polyacrylamide gels generally showed that the SNP variants were obtained with high and comparable purity (Fig. 4.27) as the wild type hAOX1, however, the poorly expressed variants generally showed more contaminants, due to the lower expression yield. Particularly, the variants G50D, N436D/A437D/L438I and N436D/A437D/L438I/I440K showed more contaminants during the purification in comparison to all the other variants.

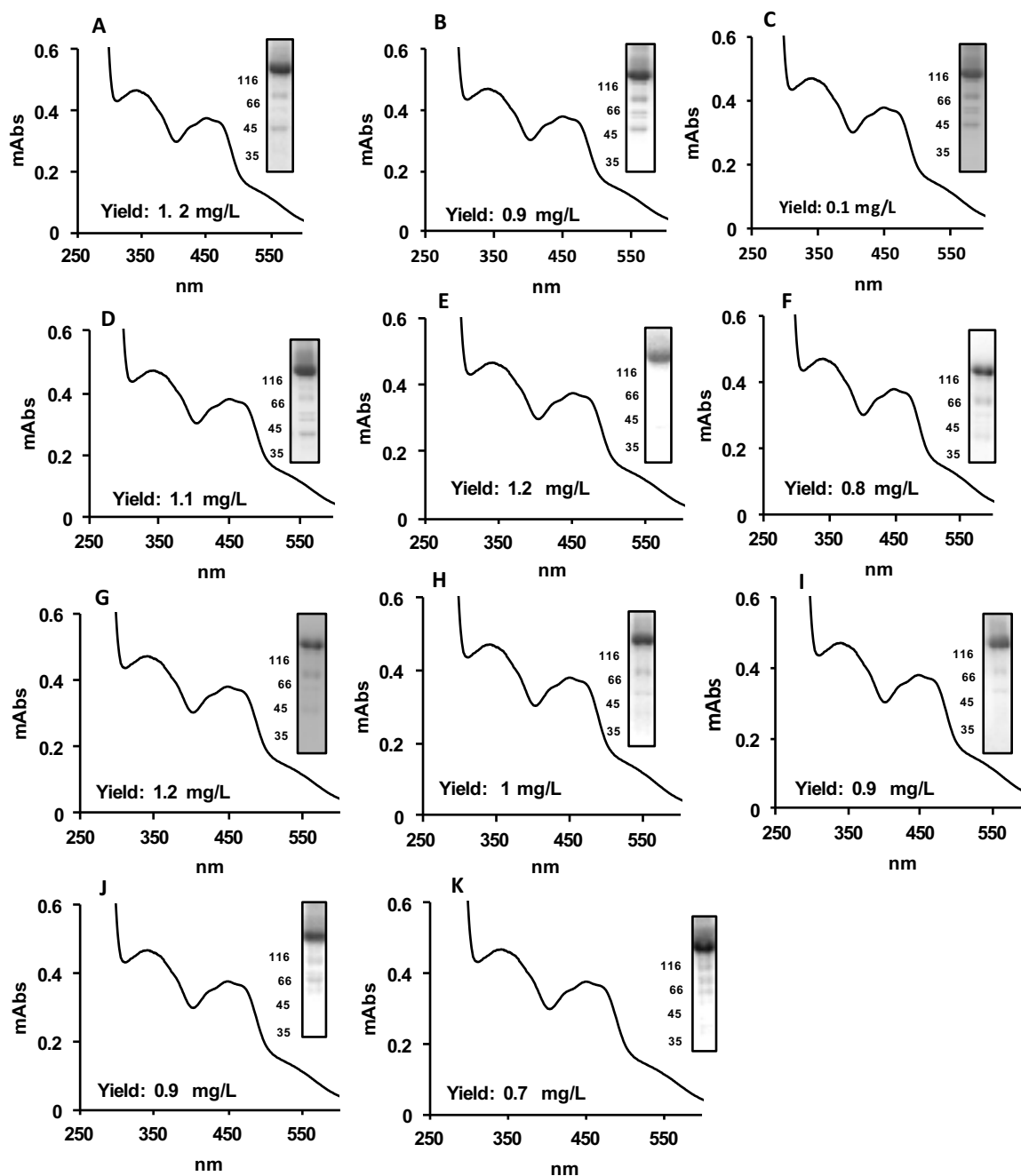


Figure 4.27. Characterization of the hAOX1 SNP-based variants. The main graphs illustrate the UV-Vis spectra of the indicated proteins isolated from *E. coli*. The UV-Vis spectra were recorded using purified air-oxidized hAOX1 proteins in 50 mM Tris, pH 8.0. The yield of protein after purification is indicated. (A) hAOX1 WT; (B) hAOX1 G46E; (C) hAOX1 G50D; (D) hAOX1 G346R; (E) hAOX1 H363Q; (F) hAOX1 R433P; (G) hAOX1 A437V; (H) hAOX1 L438V; (I) hAOX1 A439E; (J) hAOX1 hAOX1 R1231H; (K) hAOX1 K1237N. The 10% SDS-polyacrylamide gels of the indicated proteins after staining with Coomassie blue are shown in the rightmost inset of each panel. The protein concentration for hAOX1 wild type and variants was $\sim 18 \mu\text{M}$.

4.2.2.1 Cofactor content of hAOX1 SNP-based variants

To determine the molybdenum and iron content of the variants of hAOX1, inductively coupled plasma optical emission spectroscopy (IPC-OES) on an Optima 2100 DV was used. As

reference the multi element standard solution XVI (Merck) was used. The calculated saturation (percentage) are related to the theoretical full complement of Moco and the 2×[2Fe-2S] clusters. In comparison to the hAOX1 wild type, the variants have a comparable saturation level of iron, around 70% and molybdenum saturation around 55% (Table 13), indicating that those mutations do not affect the incorporation of the Moco and the other cofactors into the mature protein. Only the variants G346R, L438V and K1237N present a slightly decreased incorporation of Moco. The variant G50D showed a slightly decreased iron content. Instead the variants R433P, R1231H and K1237N showed a lower incorporation of the FAD cofactor.

Table 13: Molybdenum, Iron, FAD and FormA content of hAOX1 wild type and SNP-based variants^a.

Enzyme	Mo content (%)	Fe content (%)	FAD saturation (%)	FormA saturation (LU*s)
hAOX1 WT	62 ± 9	69 ± 8	93.2 ± 4	248.33 ± 31
hAOX1 G46E	55 ± 6	66 ± 5	85.15 ± 7	223.51 ± 26
hAOX1 G50D	63 ± 7	58 ± 13	84.5 ± 10	265.12 ± 34
hAOX1 G346R	49 ± 7	62 ± 6	89.4 ± 5	227.1 ± 19
hAOX1 H363Q	56 ± 11	71 ± 3	90.4 ± 3	233.15 ± 22
hAOX1 R433P	65 ± 12	67 ± 5	79.3 ± 6	277.06 ± 31
hAOX1 A437V	61 ± 5	72 ± 4	82.95 ± 6	228.26 ± 27
hAOX1 L438V	49 ± 10	65 ± 5	94.9 ± 2	236.19 ± 29
hAOX1 A439E	51 ± 8	71 ± 6	86.25 ± 5	236.73 ± 15
hAOX1 R1231H	57 ± 9	64 ± 5	75.52 ± 12	266.9 ± 33
hAOX1 K1237N	48 ± 6	65 ± 7	79.3 ± 9	221.3 ± 28

^aData are mean values from three independent measurements (± S.D.).

To further verify the correct incorporation of the molybdenum cofactor and to prove that the molybdenum content of the enzyme is not originated from unspecific bound molybdenum on the protein, FormA content was measured by high-performance liquid chromatography (HPLC). By this method the molybdenum cofactor is converted to its fluorescent product Form A and used for semiquantitative detection of the protein Moco (Johnson *et al.*, 1984). Form A is an oxidative product of molybdopterin which can be hydrolysed to Form A (dephospho) and phosphate by alkaline phosphatase. The enzymes were additionally compared by their saturation with Mo-MPT cofactors after conversion to its fluorescent derivative (FormA), to exclude the unspecific incorporation with molybdenum, and the results showed comparable levels of the cofactor in consistency with the molybdenum levels (Table 13). The saturation levels with iron were around 65% for all the enzymes and reflected the saturation with $2 \times [2\text{Fe-2S}]$ clusters. Additionally, the loading of the enzymes with FAD was quantified. The results in Table 13 show that all hAOX1 variants have FAD saturation of around 85%, similar to the hAOX1 wild-type, revealing that the introduced amino acid exchanges did not influence the overall cofactor saturation levels of the enzymes. The relative molybdopterin content was confirming a correct insertion of the molybdenum cofactor and the specificity of the molybdenum bound to the enzyme (Table 13).

4.2.2.2 Kinetic parameters of hAOX1 SNP-based variants

To compare the kinetic parameters of hAOX1 wild-type and the variants, steady-state kinetics with phenanthridine as substrate and oxygen as electron acceptor were performed. The kinetics constants for the variants were determined by quantification of the product phenanthridinone following the absorbance increase at 321 nm. The K_M and k_{cat} values calculated for each hAOX1 variant are shown in Table 14. To obtain better comparability of the data among the variants, the kinetic constants were corrected and normalized for a 100% molybdenum saturation level of the purified enzymes (Table 14). While the K_M values of the variants were comparable to the one of the wild-type enzyme and ranged around 6-14 μM , the k_{cat} values showed some differences. In the case of variants G50D, G346R, R433P, A439E, R1231H and K1237N, k_{cat} was significantly reduced with values around 20-50% of the value determined for the wild type enzyme. In contrast, the amino acid exchanges G46E and L438V resulted in

a 2-fold and 1.2-fold increase in k_{cat} , respectively, while the k_{cat} of variants H363Q and A437V was not changed in comparison to the wild-type enzyme.

Table 14: Steady state kinetic parameters of hAOX1 wild-type and variants^a.

Enzyme	k_{cat} (min^{-1})	K_{M} (μM)
hAOX1 wild-type	273 ± 36	9 ± 4
G46E	534 ± 35	14 ± 5
G50D	58 ± 15	12 ± 4
G346R	61 ± 17	6 ± 1
H363Q	271 ± 23	13 ± 4
R433P	68 ± 4	8 ± 1
A437V	281 ± 23	11 ± 3
L438V	343 ± 59	10 ± 3
A439E	49 ± 3	10 ± 2
R1231H	132 ± 46	9 ± 2
K1237N	76 ± 6	6 ± 2

^aKinetics performed using phenanthridine as substrate (1-100 μM) and oxygen as electron acceptor. Proteins concentration were around 200 nM in the assay. Data are mean values from three independent measurements (\pm S.D.).

To analyze the influences of the amino acid exchanges on the enzyme activity, we determined the phenanthridine:DCPIP reactivities of the variants in the presence or absence of DPI. Especially the phenanthridine:DCPIP reaction of the DPI-FAD inhibited enzymes, directly occurs at the Moco site and does not involve intramolecular electron transfer through the other cofactors and therefore a direct comparison with the data of the phenanthridine: O_2 activities was carried out (Table 8). The data provide insights regarding the impact of the mutation on the intramolecular electron transfer pathway and the electron transfer from the reduced FAD to molecular oxygen. The results in Fig. 4.28 show that the specific activities of all hAOX1 variants were not influenced by the presence of DPI. In similarity with the turnover numbers determined for the oxygen reactivity, the specific activities with DCPIP show some differences between the variants (Figure 4.28).

In the case of variants G50D, G346R, R433P, A439E, R1231H and K1237N specific activities were reduced with values around 50-75% of the value determined for the wild type enzyme. In contrast, the amino acid exchange G46E resulted in a 1.5-fold increase in specific activity,

while the values of variants H363Q, A437V and L438V were comparable to the ones of the wild-type. In total, these results show that the differences in enzymatic activities detected for the variants are not based on an altered electron transfer from FAD to O₂ but are rather based on differences at the Moco site, which might be due to different sulfuration levels of the enzyme variants or alterations on the redox potentials of the cofactors.

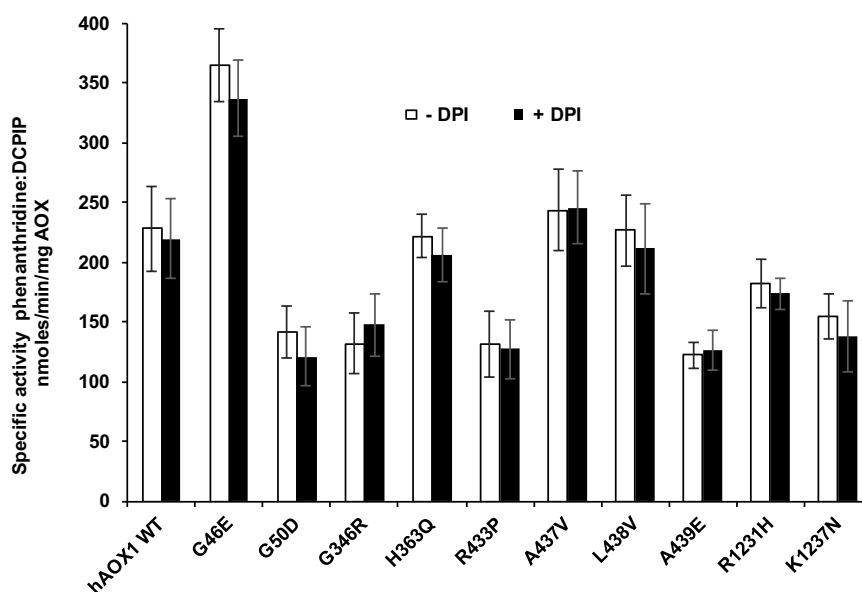


Figure 4. 28. The effect of diphenyleiodonium on the activity of hAOX1 variants. Specific activities of hAOX1 wild-type and SNP-based variants with 80 μ M phenanthridine as substrate and 100 μ M 2,6-dichlorophenolindophenol (DCPIP) as electron acceptor in absence or presence of 5 μ M diphenyleiodonium (DPI). Protein concentrations Proteins concentration were around 200 nM in the assay.

4.2.2.3 UV/VIS monitored redox titrations of hAOX1 G46E and L438V

UV-VIS monitored redox titrations of the hAOX1 SNP variant G46E and L438V were performed at the Nippon medical school (Tokyo, Japan) in the laboratory of Dr. Prof. Takeshi Nishino under the supervision of Dr. Prof. Ken Okamoto together with Yuko Yamaguchi. The experiments were carried out in strictly anaerobic conditions at RT (Shimadzu UV photometer). Firstly, the protein was deoxygenated by means of a glass-pipes system allowing the degassing of hAOX1 by several cycles of vacuum/Argon saturated atmosphere. During the de-oxygenation procedure, the hAOX1 sample was placed in a quartz UV cuvette, fused with a glass pipe system having a Hamilton syringe connected at the top. The top syringe allowed the injection of defined amount of certain reagents, e.g. sodium dithionite or substrate, into the

hAOX1 solution. After injection, the protein was carefully mixed with the reagent and then UV/Vis spectra were measured over time. The hAOX1 SNP variant G46E and L438V together with the wild type enzyme were titrated using sodium dithionite. Subsequently, the same titration experiment was carried out using the substrate phenanthridine (Fig. 4.29). The amount of $\text{Na}_2\text{S}_2\text{O}_4$ employed was determined by standard curve measurements with riboflavin.

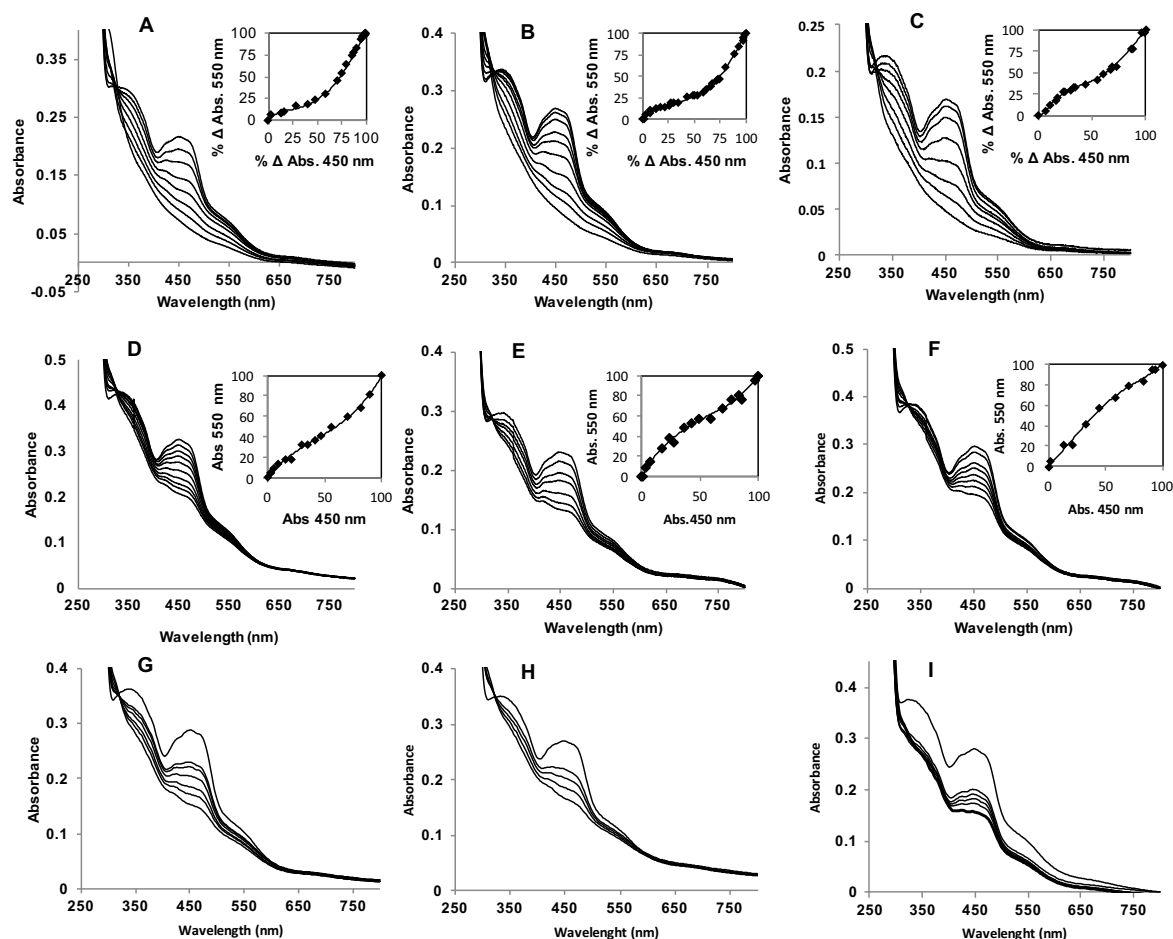


Figure 4. 29. Redox titration using sodium dithionite of hAOX1 WT (A) and the SNP variants L438V (B) and G46E (C). Redox titration by progressive addition of the substrate phenanthridine of hAOX1 WT (D), L438V (E) and G46E (F). Reduction spectra by addition of 100 μM phenanthridine to hAOX1 WT (G), L438V (H) and G46E (I). All the experiments were performed under strict anaerobic condition at room temperature or at 8°C.

The results show comparable redox titration pattern of hAOX1 WT, L438V and G46E. Only the variant hAOX1 G46E shows differences in the absorbance ratio 550/450 nm (Fig. 4.29 C inset) indicating a shift in the redox potential due to the amino acid exchange. Apart minor alterations in hAOX1 G46E variant, none of them showed major changes in the absorbance spectra and no typical absorbance at 620 nm for the semiquinone radical was detected.

Compared to bXO, the hAOX1 enzymes show a slightly higher redox potential for the FAD cofactor (Nishino *et al.*, 1989; Barber *et al.*, 1982; Marho *et al.*, 2013).

4.2.3 Characterization of FAD loop hAOX1 variants

The hAOX1 FAD loop single and multiple variants were expressed and purified following the same procedure as for hAOX1 WT and hAOX1 SNP-variants. All the variants were expressed mainly in a dimeric form, as shown by size exclusion chromatography (Fig. 4.26).

The purity of the hAOX1 variants is strictly related to the yield of protein expressed. Higher yield of protein leads purer expressed enzyme (Fig. 4.30).

The protein yield of the single and double mutants was comparable to the wild type protein (Fig. 4.30 B-C), consisting of around 1 mg of hAOX1 per liter of *E.coli* TP1000 cell culture. The hAOX1 variants N436D/A437D/L438I and N436D/A437D/L438I/I440K, showed a significant decrease in protein yield (Fig. 4.30 D-E). Contrarily, hAOX1 Q434R/N436D/A437D/L438I/I440K, partially restored the expressed protein yield. The UV/Vis spectra of the hAOX1 variants showed no major differences. All the variants showed comparable absorbance peaks at 450 nm and 550 as for the wild type enzyme. Only the quadruple hAOX1 variants showed slightly shifted FAD maximum absorption peak (Fig. 4.30 D).

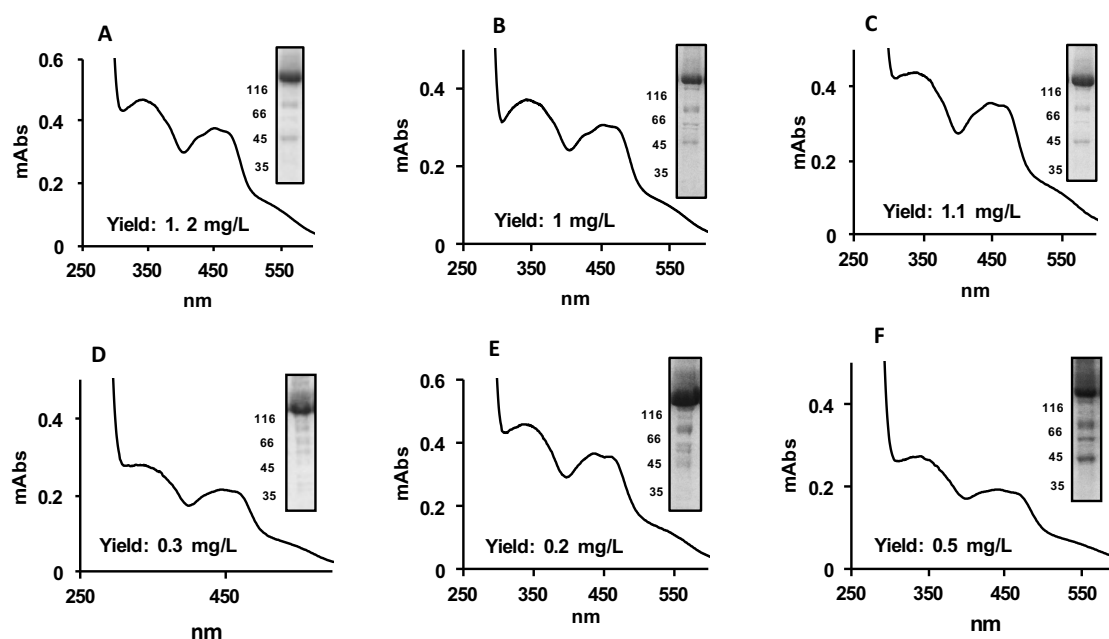


Figure 4.30. UV/Vis spectra of the indicated proteins isolated from *E. coli*. The UV-Vis spectra were recorded using purified air-oxidized hAOX1 proteins in 50 mM Tris, pH 8.0. The yield of protein after purification is indicated. (A) hAOX1 WT; (B) hAOX1 A437D; (C) hAOX1 N436D/A437D; (D) hAOX1 N436D/A437D/L438I; (E) hAOX1 N436D/A437D/L438I/I440K; (F) hAOX1 Q434R/N436D/A437D/L438I/I440K; The 10% SDS-polyacrylamide gels of the indicated proteins after staining with Coomassie blue are shown in the rightmost inset of each panel.

4.2.3.1. Kinetics constants for FAD loop hAOX1 variants

The FAD loop hAOX1 variants were quantified for molybdenum and iron content using inductively coupled plasma optical emission spectroscopy (IPC-OES) on Optima 2100 DV.

The variants tested showed a saturation of molybdenum and iron highly comparable to the hAOX1 wild type (Table 15). In all cases the molybdenum saturation was between 50-70 % and the iron saturation between 65-75%. Despite the fact that some of the variants showed a decreased expression, the metal content for all of them showed no alterations.

The catalytic activity was tested for all the hAOX1-FAD loop variants. The turn over number (k_{cat}) of the variants was altered in a similar trend as for the expressed yield of protein. The variants A437D and N436D/A437D showed k_{cat} values of 287 and 301 min^{-1} , highly comparable to the wild type enzyme. Instead, the N436D/A437D/L438I and N436D/A437D/L438I/I440K mutants had clear decreased in the turn over number up to 52 and 6 min^{-1} , respectively around 5-fold and 40-fold lower than the wild type enzyme. The Q434R/N436D/A437D/L438I/I440K variants partially restored the catalytic activity up to 79 min^{-1} . Contrarily, the K_M values showed no significant differences within all the variants in

comparison to the wild type enzyme, showing a range between 4 and 9 μM toward phenanthridine as substrate.

Table 15: Steady state kinetic parameters of hAOX1 wild-type and variants and data for saturation with molybdenum and iron^a.

Enzyme	^a k_{cat} (min^{-1})	K_{M} (μM)	Mo content (%)	Fe content (%)
hAOX1 wild-type	273 \pm 36	9 \pm 4	62 \pm 9	69 \pm 8
A437D	287 \pm 41	6 \pm 3	56 \pm 9	75 \pm 12
N436D/A437D	301 \pm 35	7 \pm 4	56 \pm 11	77 \pm 14
N436D/A437D/L438I	52 \pm 9	5 \pm 1	72 \pm 13	79 \pm 15
N436D/A437D/L438I/I440K	6 \pm 2	4 \pm 1	65 \pm 7	73 \pm 9
Q434R/N436D/A437D/L438I/I440K	79 \pm 4	6 \pm 2	52 \pm 10	66 \pm 8

^aKinetics performed using phenanthridine as substrate and oxygen as electron acceptor. Proteins concentration were around 200 nM in the assay. Data are mean values from three independent measurements (\pm S.D.).

Notably, the double mutant hAOX1 N436D/A437D showed highly comparable features as the wild type enzyme. Despite the substitution of an Ala and Asn to two Glu residues, the overall properties of the enzyme did not significantly changed. Instead, the insertion of the third and fourth mutation disrupted the structural/functional stability of the enzyme. Surprisingly, the fifth inserted mutation partially recovered the stability of the enzyme.

4.2.4 Characterization of additional variants of the FAD site of hAOX1

Additional hAOX1 FAD variants were expressed, purified and the kinetics parameters were determined as for the wild type enzyme and the other variants. The hAOX1 variants L438A, L438K, L438F and D1234H showed expression yield, UV/Vis spectra and purity similar to the wild-type protein and with only minor differences (Fig. 4.31). Contrarily, the hAOX1 variant L344F did not yield a stable enzyme and therefore, no data are reported.

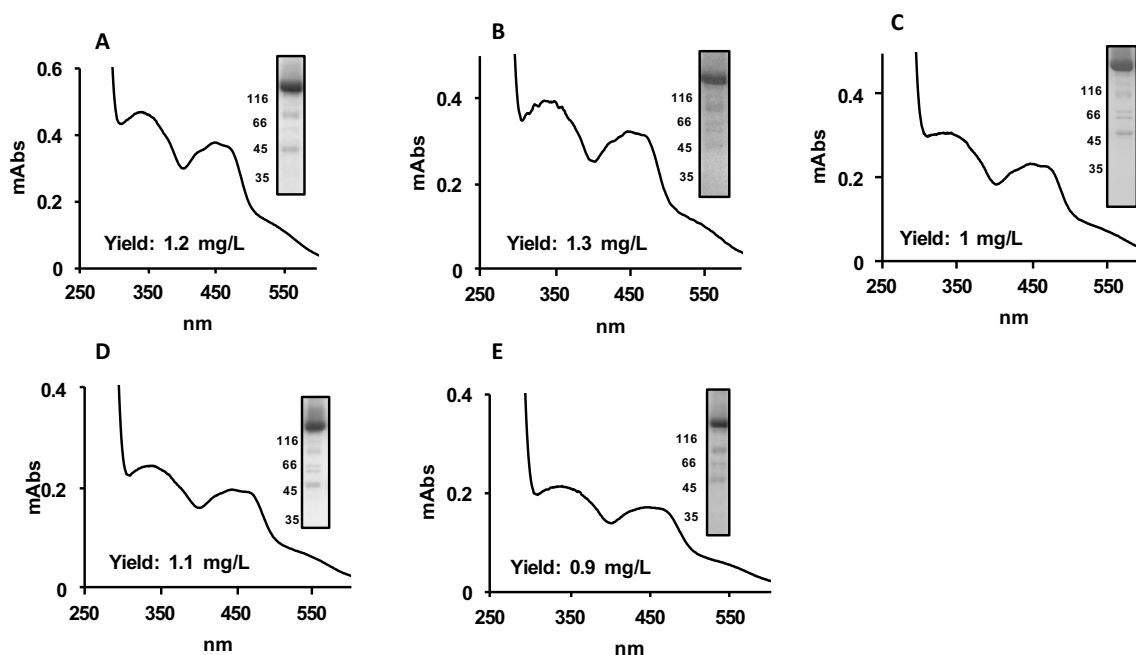


Figure 4.31. UV/Vis spectra of the indicated proteins isolated from *E. coli*. The UV-Vis spectra were recorded using purified air-oxidized hAOX1 proteins in 50 mM Tris, pH 8.0. The yield of protein after purification is indicated. (A) hAOX1 WT; (B) hAOX1 D1234H; (C) hAOX1 L438A; (D) hAOX1 L438F; (E) hAOX1 L438K. The 10% SDS-polyacrylamide gels of the indicated proteins after staining with Coomassie blue are shown in the rightmost inset of each panel.

The metal saturation for all the expressed variants was comparable to the wild-type enzyme, having a molybdenum and iron saturation of around 55% and 65% respectively (Table 16). The kinetics constant k_{cat} and K_m were also comparable to the wild type enzyme. The variants D1234H, L438K and L438F showed respectively values of 281 min^{-1} , 261 min^{-1} and 269 min^{-1} as turn over numbers. Only the variant L438A showed a slightly increased catalytic activity than the other variants, with a k_{cat} of 351 min^{-1} (Table 16). The K_m values for the presented variants ranged from 7 to $14 \mu\text{M}$. The enzymatic activity was measured using phenanthridine as substrate and oxygen as electron acceptor, with the same condition as above described for all the other variants.

Table 16: Steady state kinetic parameters of hAOX1 wild-type and variants and data for saturation with molybdenum and iron^a.

Enzyme	^a k _{cat} (min ⁻¹)	^a K _M (μM)	Mo content (%)	Fe content (%)
hAOX1 wild-type	273 ± 36	9 ± 4	62 ± 9	69 ± 8
D1234H	281 ± 27	10 ± 2	50 ± 7	66 ± 9
L438A	351 ± 28	14 ± 5	52 ± 8	67 ± 11
L438K	261 ± 36	8 ± 2	57 ± 9	71 ± 12
L438F	269 ± 22	7 ± 3	61 ± 8	63 ± 13
L344F	n.d.	n.d.	n.d.	n.d.

^aKinetics performed using phenanthridine as substrate and oxygen as electron acceptor. Proteins concentration were around 200 nM in the assay. Data are mean values from three independent measurements (± S.D.).

As for the substitution L438V, the variant L438A shows a 1.2-fold increase enzymatic activity compared to the wild type enzyme, suggesting an modulating role of the residue Leu438 in relation to the space surrounding the FAD cofactor and particularly to the hydrophobicity around the FAD-N5 location within the active site.

4.3 Reactive oxygen species (ROS) production by hAOX1

4.3.1 hAOX1 and O₂ reactivity

Molecular oxygen is the electron acceptor in the reaction catalyzed by hAOX1 and it can undergo a two-electron reduction, to produce H₂O₂, or a single electron reduction to produce O₂⁻. The anion superoxide is potentially more toxic than hydrogen peroxide within the cell, due to its high reactivity against the cellular structures, leading oxidative damage to the cell (Ray *et al.*, 2012).

Considering that no published data about ROS production by the human AOX1 are available, experiments using the Pt-electrode for H₂O₂ and the cytochrome c reduction assay to measure the rate of H₂O₂/O₂⁻ production by hAOX1 were performed. Detection of superoxide in this assay is based on its ability to reduce ferricytochrome c.

4.3.2 Hydrogen peroxide production by hAOX1 WT

For qualitative measurements of hydrogen peroxide production by hAOX1, activity experiments were performed using a Pt-electrode system. This electrochemical method permits to follow the reaction by detection of the production of hydrogen peroxide, a side product of AOX reaction. On the Pt-electrode surface occurs the oxidation of the H_2O_2 with consequent detectable electron transfer. The potential used for the electrochemical measurements was +600 mV, typical for hydrogen peroxide detection. The results showed a clear production of hydrogen peroxide from hAOX1 after addition of the substrate (phenanthridine) into the reaction solution (Fig. 4.32). The decrease of the signal reflects the consumption of the substrate and therefore a decreased production of detectable hydrogen peroxide in solution.

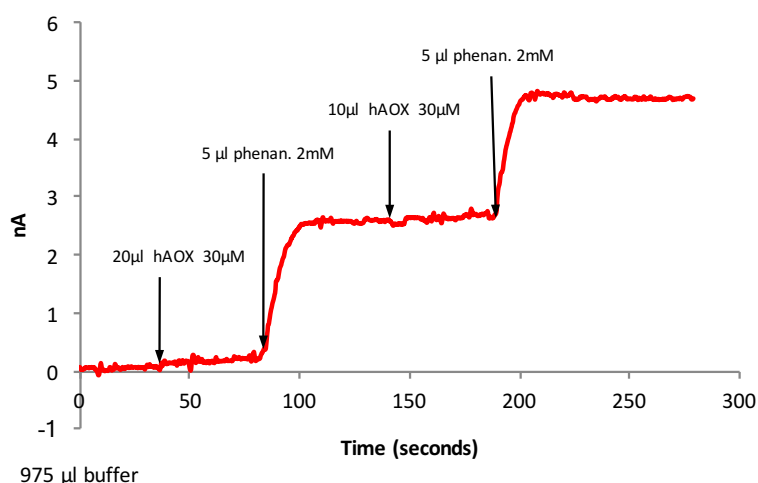


Figure 4. 32. Electrochemical measurements of hydrogen peroxide produced by the human AOX1 using and phenanthridine as substrates.

Those experiments confirm the production of hydrogen peroxide from the hAOX1. Furthermore, hAOX1 showed high stability in presence of H_2O_2 . The enzyme showed catalytical activity up to 5 mM of hydrogen peroxide in the solution assay. However, further quantitative experiments are needed to specifically understand the impact of the oxygen radical on hAOX1 reactivity and stability.

4.3.3 Superoxide production by hAOX1 WT and variants

AOXs have been reported to produce H_2O_2 as the final reaction product, however, studies on the amount of superoxide production of the purified human enzyme have not been performed so far. The production of $O_2^{\cdot-}$ can be conveniently monitored by including cytochrome-c in the reaction mixture. In fact, cytochrome-c reduction by $O_2^{\cdot-}$ is considerably faster than spontaneous $O_2^{\cdot-}$ dismutation. The amount of $O_2^{\cdot-}$ produced in the reaction mixture can be estimated by comparison to a blank reaction run under the same conditions in the presence of superoxide dismutase. The reduction of cytochrome c was almost completely quenched by superoxide dismutase 1 (Fig. 4.33). Since hAOX1 also catalyzes the two-electron reduction of molecular oxygen to H_2O_2 , which in turn can re-oxidize Fe^{2+} cytochrome c to Fe^{3+} cytochrome c, the reaction was performed in the presence of catalase (100 U/mL) that completely decomposes H_2O_2 (Fig. 4.33).

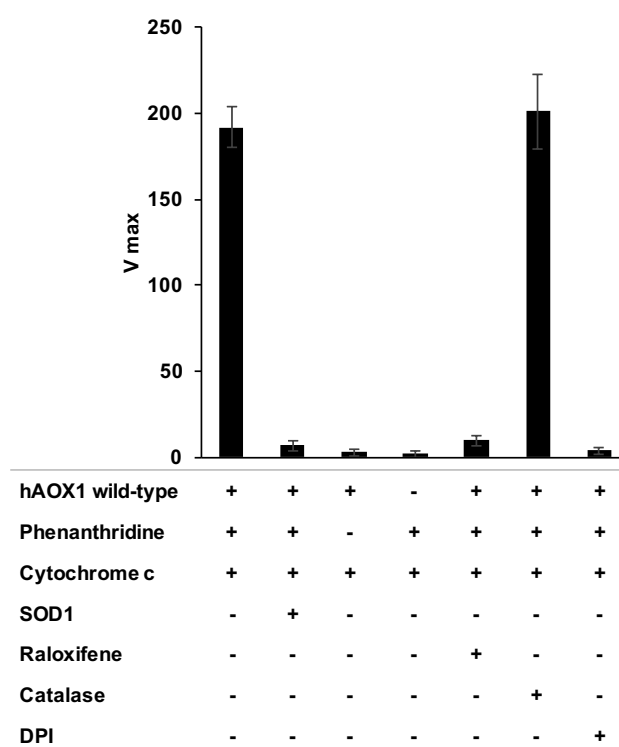


Figure 4. 33. Superoxide production by hAOX1 wild-type. Superoxide production of enzymes were calculated by following the reduction of 100 μ M cytochrome c at 550 nm in the presence of 50 μ M phenanthridine in 50 mM Tris, pH 8.0. 20 μ M superoxide dismutase 1 (SOD1), 10 μ M raloxifene, 25 μ M catalase and 5 μ M diphenyleneiodonium (DPI) were included in the assays as indicated.

To confirm further that the observed cytochrome c reduction is based on the activity of hAOX1, the reaction was carried out in the presence of the inhibitor raloxifene, which readily inhibited

the reaction. As further control, the FAD site was inhibited with DPI, which completely abolished cytochrome c reduction. In addition to the reduction of cytochrome c, another assay was applied for superoxide detection, which is based on the reduction of NBT to formazan (Masuoka & Kubo, 2016). By this assay comparative results with the cytochrome c reduction assay were obtained. To obtain the percentage of $O_2^{\cdot-}$ production for hAOX1 wild-type and the variants, the reduction of cytochrome c ($U/\mu\text{mol enzyme}$) was related to the overall rate of phenanthridinone production ($U/\mu\text{mol enzyme}$) (Table 17).

4.3.4 Superoxide and hAOX1 variants

The more relevant aspect of all the variants tested in this work resulted to be the production of superoxide anion as side product of the oxygen reduction by hAOX1. The hAOX1 wild-type enzyme is characterized by a percentage of superoxide production of $11\% \pm 3$. While the variants G46E, G50D and R433P showed similar values to the wild-type enzyme, the rate of superoxide production was slightly increased in the variants G346R, A439E, R1231H and K1237N with ratios around 15-18% and an even higher increased rate in variant A437V with 25% (Table 17). Interestingly, an imposing increased rate of superoxide production was obtained for the variant L438V with $72\% \pm 10$. The leucine residue in position 438 is located within the flexible loop I ($Q_{430}AQRQENALAI_{440}$) and in proximity of 3.42 Å to the N5 of the isoalloxazine ring (being stacked between residues L344 and L438). In addition to phenanthridine, the rate of superoxide production was also followed with phthalazine and 4-dimethylaminocinnamaldehyde (p-DMAC) as substrates, resulting in comparable numbers of superoxide produced.

Table 17: Rates of superoxide production from hAOX1 wild type and SNP variants^a

Enzyme	Specific activity phenanthridine:O ₂ (nmoles/min/mg of enzyme)	Specific activity phenanthridine:cyt c (nmoles/min/mg of enzyme)	O ₂ ⁻ production ratio (%)
hAOX1 wild-type	1148 ± 151	126 ± 16	11 ± 3
G46E	2131 ± 177	256 ± 31	12 ± 3
G50D	272 ± 57	28 ± 7	10 ± 4
G346R	302 ± 41	45 ± 9	15 ± 3
H363Q	1291 ± 73	168 ± 36	13 ± 11
R433P	266 ± 31	32 ± 6	12 ± 2
A437V	1192 ± 95	298 ± 39	25 ± 3
L438V	1423 ± 193	1025 ± 141	72 ± 10
A439E	209 ± 45	33 ± 5	16 ± 4
R1231H	689 ± 104	124 ± 35	18 ± 7
K1237N	287 ± 53	43 ± 12	15 ± 5

^aThe ratio of superoxide production was calculated as ratio of the specific activity phenanthridine:O₂ (nmoles/min/mg of enzyme) and Specific activity phenanthridine:cyt c (nmoles/min/mg of enzyme). The substrate phenanthridine concentration was 80 μM and cytochrome c 250 μM in the assay. Proteins concentration were around 200 nM in the assay. Data are mean values from three independent measurements (± S.D.).

The FAD loop multiple variants did not show alterations in superoxide production. Only the variant hAOX1 N436D/A437D showed a slightly decreased superoxide production of around 3-5% (Table 18).

Further insights were obtained by the measurement of the superoxide rate from the variants hAOX L438F, hAOX1 L438K, L438A. The variants which had a substituted Leu438 residue showed an altered superoxide production (Table 18). The variant hAOX1 L438K showed a superoxide production of around the 36% on the total oxygen reduced. The variant L438F (residue present in mAOX3) showed a O₂⁻ production ratio of around 63%. The highest superoxide rate production was shown from the variant L438A, producing 83% superoxide from the reducing equivalent obtained by the oxidation of the substrate at the molybdenum center. Variant hAOX1 D1234H showed a superoxide production comparable to the wild type enzyme, of around 13%.

Table 18: Rates of superoxide production from hAOX1 wild type and XOR-FAD single and multiple variants^a

Enzyme	O ₂ ⁻ production ratio (%)
hAOX1 wild-type	11 ± 3
A437D	21 ± 5
N436D/A437D	5 ± 3
N436D/A437D/L438I	9 ± 4
N436D/A437D/L438I/I440K	11 ± 4
L438A	83 ± 9
L438F	63 ± 8
L438K	36 ± 5
D1234H	13 ± 4

^aThe ratio of superoxide production was calculated as ratio of the specific activity phenanthridine:O₂ (nmoles/min/mg of enzyme) and Specific activity phenanthridine:cyt c (nmoles/min/mg of enzyme). The substrate phenanthridine concentration was 80 μM and cytochrome c 250 μM in the assay. Proteins concentration were around 200 nM in the assay. Data are mean values from three independent measurements (± S.D.).

Although the substitutions L438V and L438A do not insert large changes in terms of size and charge of the residues, their impact in superoxide production is considerable. Instead, the substitutions L438F and L438K gained lower amount of superoxide production but significantly higher than the wild type enzyme.

5. Discussion

5.1 Optimization of the expression of hAOX1

Evidences exist that low-frequency usage codons within a coding sequence can provide the genetic instruction modulating the rate of protein synthesis (Purvis *et al.*, 1987; Marin & Xia, 2008). Studies on the *E. coli* genome and protein structure database identified that high-frequency-usage codons are mainly associated with structural elements, such as alpha helices, whereas clusters of lower frequency usage codons are more likely to be associated with beta-strands and random coils (Thanaraj & Argos, 1996). It was confirmed that the positioning and clustering of codons with different usage frequencies is non-random and plays a role in gene expression (Ikemura, 1981; Bulmer, 1987; Wolin & Walter, 1988). Genetic redundancy at the codon level increases the organism's resistance to mutations, however, even a single nucleotide exchange can effect protein expression, protein structure and function (Lithwick & Margalit, 2003; Plotkin & Kudla, 2011). From a practical point of view, the common causes for failures in heterologous gene expression are primarily related to the disparities in codon bias, mRNA secondary structure and stability, gene product toxicity, and product solubility (Makrides, 1996; Gustafsson *et al.*, 2004). Nowadays, it is accepted that non-optimal codon content can limit expression of heterologous proteins due to limiting available congenial tRNAs in the expression host. Inserting of rare codons that are incongruent with the native gene sequence during heterologous expression can lead to reduced translation rates and overall expression levels (Kane, 1995; Goldman & Wilson, 1995). The disparities in codon usage can cause significant stress on host cell metabolism and translational processes (Angov *et al.*, 2011). Several strategies have been employed to minimize the bias codon usage for heterologous expressions, as codon optimization and codon harmonization (Angov *et al.*, 2011).

Previous expression systems for the heterologous expression of hAOX1 in *E. coli* resulted in a low yield of protein of about 50 μg per liter of *E. coli* cell culture (Hartmann *et al.*, 2012). Here, we have used a *hAOX1* codon-optimized gene to increase the expression yield of the purified protein. The results obtained reveal the importance in the selection of the strategies for heterologous expression of complex human Moco-containing proteins in *E. coli*. In the case of hAOX1, the number of rare codons resulted in low expression levels of the gene, which can be

overcome by introducing codons more commonly used in *E. coli* into the respective gene sequence.

The expression of the codon-optimized hAOX1 resulted in a protein yield of around 1 mg per liter of *E. coli* culture, which is about 10- to 20-fold higher than the yield obtained using the native gene sequence in the same expression vector. With this higher level of protein expression and higher protein concentration in the *E. coli* extracts, the purification of the protein was additionally facilitated and a two-step purification by Ni-NTA chromatography and size exclusion chromatography was sufficient to yield a highly pure protein, which could be used for further studies.

The purified protein was mainly in a dimeric form, the active form of the enzyme, and lower portions of monomeric and multimeric hAOX1 were separated by size-exclusion chromatography. Subsequently, the purified hAOX1 derived from the codon optimized expression system was compared to the one expressed by the native *hAOX1* gene. The saturation for molybdenum was calculated to be around 50% whereas around 60% was the saturation for iron (calculated to both $2 \times [2\text{Fe}-2\text{S}]$ cluster). As supposed, both expression systems revealed the same cofactor content in hAOX1. The absorption spectra resulted in a typical molybdo-flavoenzyme absorption spectrum. FAD and iron sulfur clusters ($2 \times [2\text{Fe}2\text{S}]$) showed the characteristic absorption maxima at 450 nm and 550 nm.

However, the main problem remained to obtain a 100% active enzyme after expression of hAOX1 in *E. coli*. This drawback is related to the low saturation of the molybdenum cofactor, considering that the specific system for Moco sulfuration of the human protein is not present in *E. coli* (Mendel & Leimkuhler, 2015). The sulfuration is the last important step of the biosynthesis of the mono-oxo molybdenum cofactor in the xanthine oxidase family of molybdoenzymes. To have an active enzyme, it is necessary the fully sulfuration of the cofactor, with a sulfido ligand bound to the molybdenum atom at the equatorial position.

In order to obtain an active sulfurated *R. capsulatus* XDH, *E. coli* needs to express a protein capable of donating the terminal sulfur ligand to form active XDH. For the maturation of *R. capsulatus* XDH expressed in *E. coli*, XdhC was shown to be required for the sulfuration of Moco. XDH expressed heterologously in the absence of XdhC was shown to contain a desulfurated form of Moco (Leimkühler *et al.*, 2003).

Unfortunately, attempts to co-express the human Moco sulfurase (Peretz *et al.*, 2007) in *E. coli* to increase the sulfuration levels have failed, owing to its expression in inclusion bodies (Hartmann, 2010). To overcome this low enzyme activity of the purified protein, a chemical sulfuration step was included during the purification procedure (Massey and Edmondson,

1970; Wahl and Rajagopalan, 1982). The chemical sulfuration proved to be successful and resulted in a 10-fold increase in enzyme activity (Foti *et al.*, 2016).

The purified protein from the codon-optimized construct showed a correct folding of the protein, insertion of the cofactors (Moco, FAD, and the 2[2Fe–2S] clusters), in addition to the level of Moco sulfuration and the overall activities. Also, the chemical sulfuration of the protein yielded 10-fold increase of enzyme activity with every substrate tested. Thus, with this protein all further characterizations were performed.

Considering together the emerging importance of aldehyde oxidase in the metabolism of xenobiotics (Hutzler *et al.*, 2013) and the specie-specific barrier for studies in model organisms (Dalvie *et al.*, 2010), a functional heterologous expression system for hAOX1 facilitates new detailed *in vitro* investigations for a better understanding about this enzyme. In particular, the availability of purified hAOX1 in large scale may be needful for screenings of drugs as substrates and inhibitors, and therefore, to carry the *in vitro* experimental data toward a pharmacological and medical application in the future.

5.2 Characterization of the enzymatic activity of the hAOX1

In the work presented here, kinetic characterizations of the human AOX1 and activity measurements at the Moco active site were performed. To date, most of the data for substrate specificity regarding the hAOX1 were obtained using human liver cell lysate, S9 liver fractions or partially purified protein (Kitamura & Tatsumi, 1984; Beedham *et al.*, 1995; Clarke *et al.*, 1995; Kawashima *et al.*, 1999; Obach *et al.*, 2004; Panoutsopoulos *et al.*, 2004; Kitamura *et al.*, 2008; Dalvie *et al.*, 2010; Barr & Jones, 2011; Linton *et al.*, 2011; Zhang *et al.*, 2011; Hutzler *et al.*, 2013). The majority of those studies show kinetic data detected using a liquid chromatography-tandem mass spectrometry assay that monitored the formation of the product after the enzymatic reaction.

Only few studies were performed using purified human protein from heterologous expression systems (Alfaro *et al.*, 2009; Hartmann *et al.*, 2012). In a previous work (Hartmann *et al.*, 2012), the recombinant hAOX1 was measured with benzaldehyde, phthalazine, phenanthridine and chloroquinazolinone as substrates using DCPIP and oxygen (only for phenanthridine) as electron acceptors. The turnover numbers ranged from 5.6 min⁻¹ for chloroquinazolinone to 12.2 min⁻¹ for phenanthridine. In another work, the recombinant hAOX was measured using several synthesized 6-substituted quinazolinones as substrates showing K_m in a range from 27

μM for R=Cl up to $399 \mu\text{M}$ for R=H (Alfaro *et al.*, 2009). Both studies showed enzymatic activity in the order of 10-15 fold lower compared to the study presented here, due to a less functional expression system (Alfaro *et al.*, 2009) or for the inhibitory effect of the electron acceptor DCPIP (Hartmann *et al.*, 2012). More data are available about recombinant AOXs from other organisms as cynomolgus Monkey AOX1 (Hoshino *et al.*, 2007; Fukiya *et al.*, 2010), rat AOX1 (Adachi *et al.*, 2007), bovine AOX1 (Calzi *et al.*, 1995), murine AOX1 (Vila *et al.*, 2004; Schumann *et al.*, 2009), murine AOX3 (Terao *et al.*, 2001; Vila *et al.*, 2004), murine AOX4 (Terao *et al.*, 2009), murine AOX2 (formerly AOX311) (Kurosaki *et al.*, 2004) and rabbit AOX1 (Hurwitz, 1955; Rajagopalan *et al.*, 1962; Rajagopalan & Handler, 1964; Krenitsky *et al.*, 1972; Tomita *et al.*, 1993; Itoh *et al.*, 2009).

The kinetic data for the recombinant hAOX1 presented in this work were measured using phenanthridine, phthalazine and benzaldehyde as substrates and oxygen, DCPIP and ferricyanide as electron acceptors. The highest catalytic activity was obtained for the reaction phenanthridine:oxygen with a k_{cat} of 306 min^{-1} . Ferricyanide used as electron acceptor increased the K_{M} for all the substrates tested, from $25 \mu\text{M}$ for phenanthridine to $196 \mu\text{M}$ for phthalazine. The lowest catalytic efficiency ($k_{\text{cat}}/K_{\text{M}}$) was obtained for the reactions DCPIP:phthalazine and ferricyanide:phthalazine with $1.2 \text{ min}^{-1}\mu\text{M}^{-1}$ and $1.4 \text{ min}^{-1}\mu\text{M}^{-1}$ respectively.

The catalytic activity of hAOX1 was also studied using phenanthridine as substrate and PMS, methyl viologen and benzyl viologen as electron acceptors. The reaction of phenanthridine with PMS, methyl viologen and benzyl viologen as electron acceptors was not detectable in aerobic conditions due to the fast re-oxidation of the electron acceptors in presence of oxygen. Instead, under anaerobic conditions hAOX1 gained a considerable specific activity, particularly with PMS as electron acceptor ($2380 \pm 149 \text{ mU/mg hAOX1}$). The reaction phenanthridine:methyl viologen ($1610 \pm 121 \text{ mU/mg hAOX}$) showed a specific activity comparable to oxygen or ferricyanide (1420 ± 110 and $1350 \pm 127 \text{ mU/mg hAOX}$, respectively). Contrarily, benzyl viologen showed slightly lower catalytic activity (1210 mU/mg of hAOX1).

5.3 Structural insights of hAOX1 free and complexed with substrate-inhibitor

The mouse AOX3 was the first enzyme belonging to the aldehyde oxidase class to be crystallized, revealing its overall 3D-structure (Coelho *et al.*, 2012). mAOX3 showed to have

a molecular structure consistent with the xanthine oxidase enzyme family, however, important differences were identified regarding the Moco active site and the FAD binding site (Coelho *et al.*, 2012). Although all the mammalian aldehyde oxidases have common origins, derived from a duplication event of a XDH ancestor gene (Rodriguez-Trelles *et al.*, 2003; Garattini *et al.*, 2008), several AOX isoforms are present in different organisms. The number of the AOXs ranges from the four isoforms present in rodents to the single active gene present in humans (Garattini & Terao, 2011). Due to this inter-specific diversity, species-specific information are necessary to uncover the functions of AOXs in the different organisms.

The crystal structure of the hAOX1 free and the complex hAOX1-phthalazine-thioridazine (Coelho *et al.*, 2015) contributed with new insights for the human AOX1. The overall crystal structure of hAOX1 resulted to be similar to the other enzymes of the same family with some important difference at the active site, the substrate funnel and the FAD binding site (Coelho *et al.*, 2015). Furthermore, it was shown that in the complex hAOX1-substrate-inhibitor, the inhibitor thioridazine bound in proximity to the dimer interface in a groove at the enzyme surface and it is stacked between two loops (formed by residues 570–580 and 1058–1067) that define the binding pocket of the tricyclic phenothiazine moiety (Fig. 5.1). Upon inhibitor binding, the side chains from His575 and Glu577 moved, turning the binding pocket more accessible to the inhibitor. Residues 570 and 571 are disordered in the hAOX1-free structure, but after thioridazine binding, they become better structured and define one helical turn close to the thioridazine inhibitor-binding site (Fig. 5.1). Although some of the residues forming the inhibitor binding pocket are polar, the tricyclic aromatic moiety interacts mostly with the main chain atoms via hydrophobic interactions.

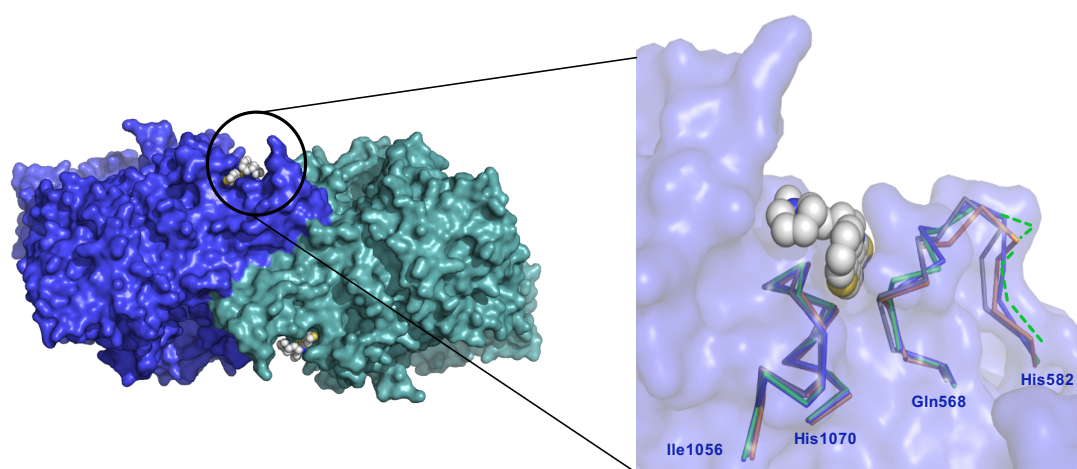


Figure 5. 1. Structure of the hAOX1 homodimer highlighting the inhibitor thioridazine binding pocket (left). The zoom-in (right) shows the thioridazine molecule, represented in space-filling-mode, into the binding pocket overlay of hAOX1 (blue), mAOX3 (orange) and bXDH (green). Picture produced by Pymol Mac 6.1 (adapted from Coelho *et al.*, 2015).

The binding of the substrate phthalazine molecule involved repositioning of two conserved aromatic residues, Phe885 and Phe923, highly important for substrate orientation toward the Moco catalytic site. There is a structural similarity for the inhibitor-binding pockets found in complexes that have been already reported, in particular for prion protein (PrP) with promazine and chlorpromazine (Baral *et al.*, 2014) and for human MALT1 caspase with thioridazine (Schlauderer *et al.*, 2013). These findings strongly suggest that the inhibitor-binding site may also be common for phenothiazine-derived drugs and that this might have a relevant impact on drug-drug interactions and should be considered in the development of target-specific drugs. The existence of this inhibitor-binding site far from the hAOX1 active site was unexpected and might be helpful for studies on novel therapeutic compounds.

5.4 Inhibition studies

An increasing number of compounds of medical and pharmaceutical interest resulted to be inhibitors of hAOX1 (Obach *et al.*, 2004). Aldehyde oxidase are involved in phase I drug metabolism, performing its role in alternative or cooperative metabolic pathway in relation to cytochromes (Kitamura *et al.*, 2006; Pryde *et al.*, 2010; Barr & Jones, 2011). Selective inhibitors resulted to be crucial for pre-clinical studies and for *in vivo* investigations (Garattini & Terao, 2011). Many molecules have failed in the clinic trials because the clearance or toxicity is underestimated by preclinical species (Barr *et al.*, 2014). Furthermore, the functional comparison to XOR is only partially useful due to the diversity of their active sites. In general, AOX enzymes have a broader substrate specificity, acting on aldehydes, purines, and heterocyclic compounds as substrates, whereas the selectivity of XOR enzymes is restricted to mainly purines as specific substrates.

To further characterize the substrate and inhibitor binding modes, structural and kinetic data from the complex of hAOX1 with phthalazine (substrate) and thioridazine (inhibitor) provided crucial information about this enzyme (Coelho *et al.*, 2015). To test the impact of thioridazine inhibition on these enzymes, we performed steady-state kinetic measurements with hAOX1 and mAOX3, using phthalazine as a substrate, and with bXO using xanthine as a substrate. Our observations suggest a noncompetitive type of inhibition for the phthalazine-thioridazine

inhibition of hAOX1 and mAOX3, using ferricyanide as electron acceptor. The inhibition constants were K_{iThi} of $1.3 \pm 0.3 \mu\text{M}$ for hAOX1 and K_{iThi} of $16.4 \pm 1.4 \mu\text{M}$ for mAOX3. The kinetics of the xanthine-thioridazine inhibition of bXO with molecular oxygen as electron acceptor showed a mixed type of inhibition instead. The inhibition was about 10- to 20-fold weaker than the phthalazine-thioridazine inhibition of hAOX1 and mAOX3, with $K_{iThi} = 440 \pm 31 \mu\text{M}$ and $K_{iiThi} = 70 \pm 9 \mu\text{M}$. These observations suggested a tight binding of the inhibitor to hAOX1 far from the active site and less effective in mAOX3 and in bXO. Although the binding of thioridazine to the inhibitor-binding pocket of hAOX1 and mAOX3 occurs to the same range in the free and substrate-bound enzymes, in bXO the inhibition constants are different. The mixed-inhibition mode suggested that binding of substrate to the active site influenced the affinity of the inhibitor for the inhibitor-binding site.

Taken together, the kinetic data revealed a noncompetitive mode of inhibition for the human and mouse enzymes and a mixed inhibition type for bXO. Although the high similarity, the different inhibition mode might be explained with the structural and catalytic differences present between these enzymes. Further inhibition studies on hAOX1 by loxapine, a thioridazine-related molecule (Sperry *et al.*, 1984), confirmed the same type of noncompetitive inhibition. Notably, there is a large number of widespread phenothiazine-derived drugs, mostly with antipsychotic and antihistaminic effects but also some that are antibiotics, anticancer or antiprion agents, which are commonly used for treatment of several diseases (Declercq *et al.*, 2013).

The structural similarity among the members of the XO family suggested previously that it may underlie a more general mechanism of enzyme inhibition. Therefore, other drugs or drug-like molecules with a tricyclic ring system similar to that of thioridazine might exhibit a similar mode of inhibition of hAOX1 by binding to the same site. However, it should be tested in future studies.

Moreover, our data are consistent with inhibition studies on hAOX1 by DCPIP which has been reported before (Barr & Jones, 2011). The steady-state kinetics experiments and the inhibition studies showed that DCPIP acts as an uncompetitive inhibitor of the human AOX1. DCPIP is frequently used as electron acceptor in enzyme-catalyzed oxidation reactions. For bovine xanthine oxidase, the rate of electron transfer from conventional substrates to DCPIP approximates that for electron transfer to the physiologic acceptor, molecular oxygen (Bray, 1959). The electron transfer of the reducing equivalents from the substrate to oxygen takes place at the FAD site (Komai *et al.*, 1969), whereas DCPIP directly receive the electrons from the reduced molybdenum atom (Massey *et al.*, 1970). In hAOX1, the mode of inhibition was

shown to be uncompetitive, and our data interpretation suggests DCPIP binding only to the reduced enzyme. Furthermore, bXO was tested for the reaction xanthine:DCPIP and no inhibition was detected. The differences between hAOX1 and bovine XO can be explained by the different surrounding of the active site and resulting in charge differences, also revealed by the different substrate specificity of both enzymes. The uncompetitive inhibition type suggests that DCPIP binds to the reduced Moco and prevents the electron transfer from reduced form of enzyme to molecular oxygen. Furthermore, the structure of DCPIP suggests its access and interaction within the active site of hAOX1.

5.5 Interaction of hAOX1 with NADH

In the crystal structure of human AOX1, the flexible loop II in proximity of the FAD pocket (T₁₂₃₀RGPDQ₁₂₃₅) is flipped by almost 180° to the relative in bXOR (Coelho *et al.*, 2015). Interestingly, the conformation of this loop is unique in human AOX1, and occupies almost the same position as the nicotinamide ring in the bXDH-NADH complex (Fig. 5.2) thereby blocking access to the isoalloxazine ring (Ishikita *et al.*, 2012). To better understand this unique loop II orientation and role, we further investigated the NADH oxidase activity of hAOX1. NADH is found in all living cells and it is the major source of the electrons transported by the mitochondria and responsible for the synthesis of ATP. Murine hepatic AOX preparations have been shown to oxidize NADH generating the reducing equivalents necessary for O₂^{•-} production from molecular oxygen (Kundu *et al.*, 2007; Maia & Moura, 2011; Choughule *et al.*, 2015). Maia *et al.*, suggested the involvement AOX in nitric oxide (NO) metabolism in the cell (Maia *et al.*, 2015). Notably, Kundu *et al.*, proposed AOX as novel NADH oxidase enzyme with an eventual important role in the cell physiology (Kundu *et al.*, 2012).

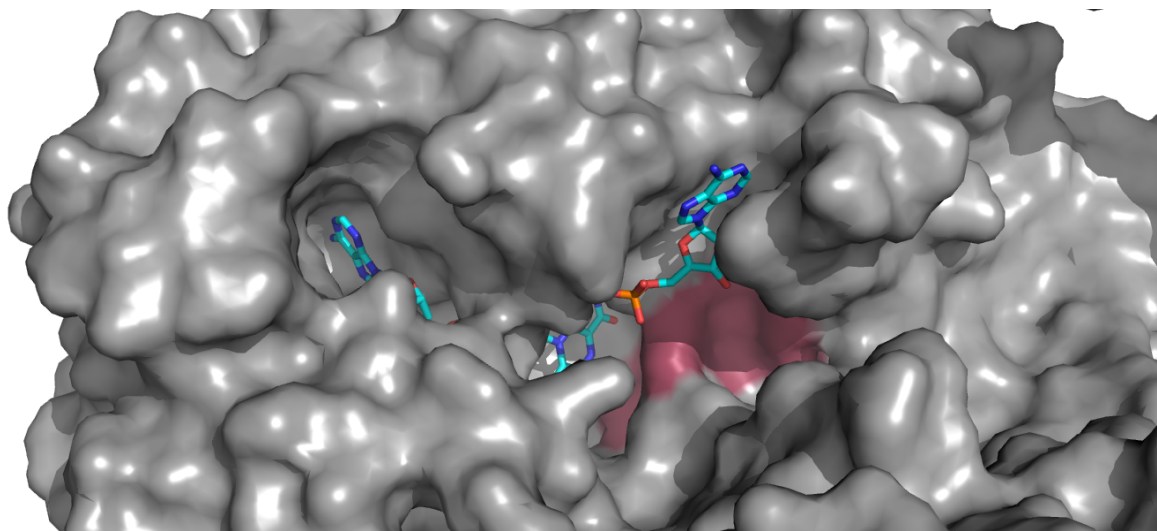


Figure 5. 2. Structure of bXDH-NADH complex. bXDH structure shown in surface and FAD-NADH structures in sticks (PDB:3UNI). Shown as red surface is the exposed moiety of the FAD flexible loop I (Q423-K433) of bXDH (Ishikita *et al.*, 2012). Picture produced by Pymol Mac 6.1.

Our results, however, show that the human AOX1 does not react with NADH. Hence, it is not possible that hAOX1 acts as a NADH oxidase due to electrochemical and structural incompatibility. In previous studies mainly rat, rabbit and mouse enzymes were considered, for which a NADH oxidase activity has been obtained (Kundu *et al.*, 2012; Mahro *et al.*, 2013). Thus, the investigations on AOX enzymes need to be clearly divided into studies on the human enzyme, containing only one AOX orthologue and studies on the rodent enzymes, containing four orthologues with a significantly different substrate spectrum. As shown in Fig 5.3, the hAOX1 presents a different structural arrangement at the FAD binding site in comparison to mAOX3 and bXDH.

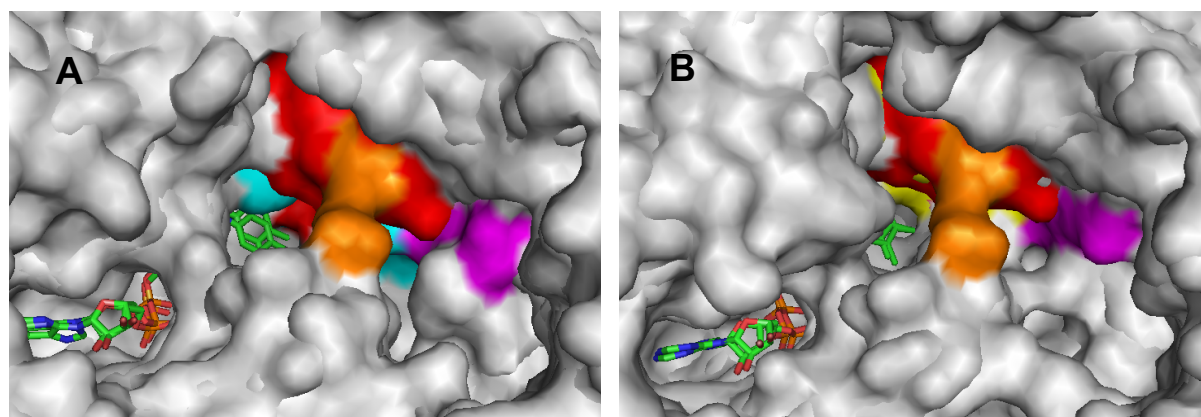


Figure 5. 3. Surface superimposition of the FAD binding site of hAOX1-mAOX3 (A) and hAOX1-bXDH (B). In panel A the red-orange portion represents the FAD flexible loops I and II of hAOX1 and light blue and magenta portions represent FAD flexible loops I and II of mAOX3. In panel B the red-orange portion represents the FAD flexible loops I and II of hAOX1 and yellow and magenta portions represent FAD flexible loops I and

II of bXDH. The FAD structures are shown in sticks. Pictures produced by Pymol Mac 6.1. (Coelho *et al.*, 2012; Ishikita *et al.*, 2012; Coelho *et al.*, 2015).

Particularly, an Arg residue blocks the access to NAD⁺/NADH to the FAD cofactor. Beyond that, the residues composition and overall charge of the FAD flexible loops is different among hAOX1, mAOX3 and bXDH (Coelho *et al.*, 2015). Especially in case of the bXDH, more negatively charged residues are present on the FAD flexible loop I (Q423-K433) coordinating a suitable electrostatic environment around the FAD cofactor for the interaction toward NAD⁺ or NADH.

5.6 Studies at the FAD active site of hAOX1

Phylogenetic studies by Rodriguez-Trelles *et al.*, suggested that a selective amino acids replacement at the FAD active site in AOXs is an evolutionary process promoting the switch from NAD⁺ to dioxygen as the final electron acceptor of those enzymes (Rodriguez-Trelles *et al.*, 2003).

XOR is known to be available in two inter-convertible forms, xanthine dehydrogenase (XDH) and xanthine oxidase (XO) (Ishikita *et al.*, 2012). Bovine XDH W336 is implicated in the conformational changes of the active-site loop Q423-K433 around the FAD cofactor, which causes the conversion of XDH into the XO form in mammals, and vice versa (Enroth *et al.*, 2000; Kuwabara *et al.*, 2003; Ishikita *et al.*, 2012). This structural rearrangement blocks the approach of NAD⁺ to FAD, changes the electrostatic potential around FAD, and opens the gate for the solvent channel, making it easier for dioxygen to reach the reduced cofactor (Kuwabara *et al.*, 2003). Furthermore, cysteine residues responsible for the conversion of XDH to XO, identified as C535 and C992, are well conserved in all mammalian XDH. Notably, in AOXs these residues are replaced by tyrosine residues excluding the conversion process for AOX enzymes. While in their FAD domain all mammalian XOR proteins are endowed with a particular tyrosine residue responsible for the binding of NAD⁺, AOXs lacks this tyrosine residue (Parks *et al.*, 1988; Nishino & Nishino, 1989; Nishino *et al.*, 2005). These selective differences at the FAD region between those enzymes occurred in both invertebrate and vertebrate AOX paralogs originated from XDH by duplications about 1 billion years ago (Rodriguez-Trelles *et al.*, 2003).

The cofactors reactivity and orientation in AOXs and XOR are related to the flow of electrons, which are generated at the Mo active site during the substrate oxidation and then passed through

the two FeS centers and to the FAD, from where they are released to the terminal electron acceptor. XDH uses NAD^+ as the physiological oxidizing substrate and the enzyme can be converted into the XO form which utilizes molecular oxygen as the electron acceptor (D/O conversion) (Enroth *et al.*, 2000). In addition, the inter-conversion of XDH into XO requires structural rearrangements of an eleven-residue loop (FAD variable loop Q₄₂₃ASRREDDAK₄₃₃). The loop movement leads to a change in the electrostatic environment around the FAD cofactor (Ishikita *et al.*, 2012). In the XO conformation, the loop blocks access of NAD^+ to its binding site and as a consequence the enzyme uses oxygen as the final electron acceptor.

Unlike XOR, AOXs cannot use NAD^+ as the final electron acceptor and they transfer the electrons generated during the enzymatic reaction only to molecular oxygen. Consistent with this, the amino acid composition of the Q₄₂₃ASRREDDAK₄₃₃ loop is very different in human AOX1, mouse AOX3 and XORs of different origin. In the crystal structure of human AOX1 another loop close to the FAD pocket (T₁₂₃₀RGPDQ₁₂₃₅) is flipped by almost 180° relative to mouse AOX3 and bovine XOR. Interestingly, the conformation of this loop is unique in human AOX1, as it occupies almost the same position as the nicotinamide ring in the bXDH-NADH complex structure and blocks access to the isoalloxazine ring (Fig. 5.2-5.3). The reason why this conformation is observed only in human AOX1 remains to be clarified. In the hAOX1 structure, the middle domain accommodates the FAD cofactor, with FAD isoalloxazine ring stacked between two leucine residues (Leu344 and Leu438).

Our observations reveal the complexity of the equilibrium at the FAD active site and its specific characteristics differ from the enzymes of the xanthine oxidase family.

The hAOX1 variants generated in this work are divided in three groups: I) hAOX1 single nucleotide polymorphisms (SNP); II) XOR-FAD loop hAOX1 variants; III) additional single point hAOX1 variants. Our results show that the residue composition of the hAOX1 flexible loop I (Q₄₃₀AQRQENALAI₄₄₀) and loop II (T₁₂₃₀RGPDQ₁₂₃₅) is modulating the overall enzymatic activity of hAOX1 and the electron transfer from the reduced FAD to the terminal electron acceptor as molecular oxygen. Although alterations at the redox potential at the FAD binding site are probable, the mechanism behind the impairment caused by those residues exchanges remains unclear and further investigations are required.

5.6.1 Single nucleotide polymorphisms (SNPs) at the FAD active site of hAOX1

Single nucleotide polymorphisms are allelic variations between the human populations, typically in one geographical or ethnic group (Nachman, 2001). Variations in the DNA sequences of humans can affect how humans develop diseases and respond to pathogens, chemicals, drugs, vaccines, and other agents. SNPs are also critical for personalized medicine (Varela & Amos, 2010). Some SNPs are associated with alterations in the metabolism of different drugs (Goldstein, 2001; Lee, 2004; Yanase *et al.*, 2006). The association of a wide range of human diseases like cancer, infectious diseases autoimmune, neuropsychiatric and many other diseases, with different SNPs can be considered as relevant pharmacogenomic targets for drug therapy studies (Nachman, 2001).

Here we report ten new hAOX1 SNP variants with a single point mutation in residues located around the FAD binding site (central domain). The SNP-variants produced are hAOX1 R1231H, A439E, R433P, G46E, L438V, G346R, H363Q, K1237N, A437V and G50D. Those variants are present: 1) on the variable loops 1 and 2 (hAOX1 R1231H, hAOX1 A439E, hAOX1 R433P, hAOX1 L438V, hAOX1 K1237N and hAOX1 A437V); 2) in close proximity of the FAD cofactor (hAOX1 G346R, hAOX1 H363Q); 3) between the FeS center II and the FAD center (hAOX1 G46E, hAOX1 G50D). The reported experiments are focused on the general characterization of the hAOX1 variants based on expression, purification and enzyme activity. Furthermore, ROS production from hAOX1 WT and variants were investigated.

All hAOX1 SNP variants were heterogously expressed mostly in a dimeric form and with a rather high purity level. Only the variant hAOX1 G50D showed less purity and decreased protein yield. The residue G50, highly conserved in hAOX1, mAOX3, hXOR and bXOR, seems to be involved in the coordination of the FeS II structure and its substitution to an Asp residue prevents a correct insertion of the cofactor into the apo-protein with consequent instability and degradation of the enzyme. However, further studies need to be performed to clarify this aspect. The variant hAOX1 R1231H showed around 50% activity than wild type enzyme. The residue R1231 gives a specific conformation to the flexible loop II (T₁₂₃₀RGPDQ₁₂₃₅) forming a bridge at the entrance of the FAD active site and preventing the access to large molecule e.g. NAD⁺ or NADH (Fig.5.4).

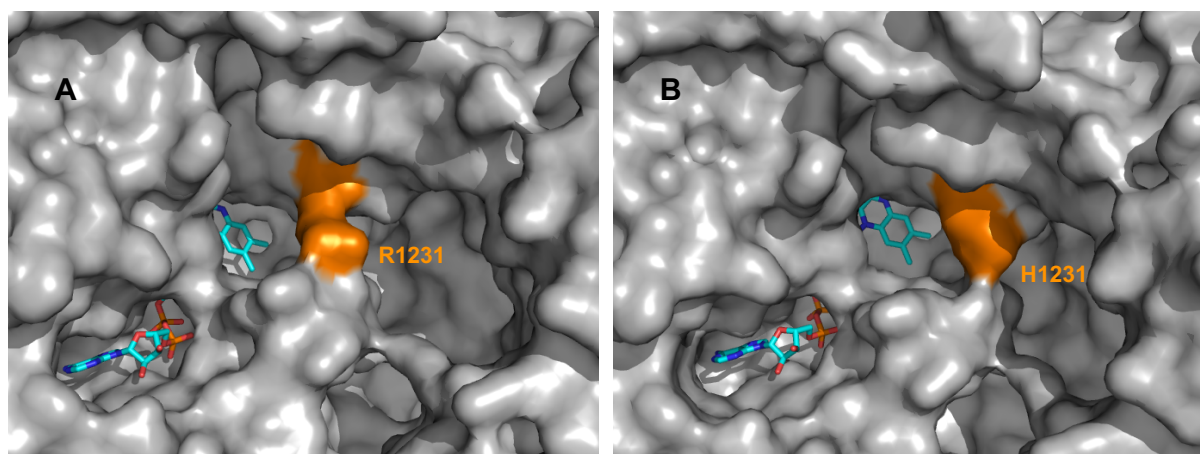


Figure 5. 4. Shown are the FAD active site of the hAOX1 wild type (A) and a model of the structure of hAOX1 R1231H SNP variant (B). The residue R1231 and H1231 are represented in orange. The FAD structure is shown in sticks. The figure was created using MacPymol.

The variant hAOX1 R1231H was tested for reactivity toward NAD^+ and NADH but no electron transfer was observed.

Further two residues showed to be relevant in the organization of the FAD active site of hAOX1, R433 and A439. Both residues are highly conserved in hAOX1, mAOX3, hXOR and bXOR. The SNP variants hAOX1 A439E and R433P showed a decreased catalytic activity around 5-fold lower than the wild type hAOX1. The nature of the substitutions, in terms of charge and size, showed a strong impact in the catalytic properties of the FAD active site. The SNP variant hAOX1 K1237N and G346R resulted also in poorly active hAOX1 variants. Interestingly, the SNP variant hAOX1 G46E showed twice the activity as compared to the wild type enzyme. Such variant resulted in a “XO-like hAOX1” enzyme. The residue G46 in hAOX1 is a glutamate in bXOR and hXOR. The redox titration of the variant G46E shows a reduction profile with more similarities to XO compared hAOX1 (see results section). Those evidences propose an important role of this Glu residue to facilitate the electron transfer through the FeS II and the FAD cofactor.

The variants hAOX1 L438V showed a 20 % increased activity as the hAOX1 wild type. The variants hAOX1 H363Q and A437V showed comparable enzymatic activity as hAOX1 wild type. The variants showed similar activity level either with O_2 or ferricyanide as electron acceptors. These results point out the hypothesis that those mutations at the FAD site effect not just the electron transfer to O_2 from FAD, but also the overall enzyme activity. The comparable values obtained using diverse electron acceptors suggest that the entire internal electron transfer can be affected. However, another possible reason for the altered enzymatic activity regards the sulfuration level of the variants. The hAOX1 variants present amino acid exchange

only in the surround of the FAD cofactor, however, such mutations can affect the overall structure of the protein with consequences on the Moco sulfuration level.

The mechanistic reasons for the altered catalytic activities remain to be clarified, although the modified redox potentials of the variants seem to have a crucial role. A different sulfuration level among the variants can also have an effect on the divergent parameters.

5.6.2 Insertion of the bXOR FAD flexible loop I into the hAOX1 FAD active site

As previously described, the flexible loop (Q₄₂₃ASRREDDIAK₄₃₃ in bXOR) surrounding the FAD cofactor and its conformational changes leads to the XO/XDH interconversion (Enroth *et al.*, 2000). The loop is a cluster of several residues which modulate the redox potential and the structural conformation at the FAD binding site (Nishino *et al.*, 2005).

To better understand the role of these loops on the activity of hAOX1, additional hAOX1 FAD site directed variants were generated, with the final goal of inserting the flexible loop I of bXOR in hAOX1.

The produced hAOX1 FAD multiple variants are: A437D, N436D/A437D, N436D/A437D/L438I, N436D/A437D/L438I/I440K, Q434R/N436D/A437D/L438I/I440K. The hAOX1 A437D and N436D/A437D variants showed characteristics, in terms of yield, purity and catalytic activity, comparable to hAOX1 WT. The N436D/A437D/L438I and especially the N436D/A437D/L438I/I440K mutant showed decreased yield, purity and catalytic activity. The turn over number for hAOX1 N436D/A437D/L438I was around 52 min⁻¹ and for hAOX1 N436D/A437D/L438I/I440K was 6 min⁻¹. The hAOX1 Q434R/N436D/A437D/L438I/I440K variant partially restored yield of protein and enzymatic activity relative to wild-type, with a k_{cat} value of about 56 min⁻¹. For all the hAOX1 FAD multiple variants the K_M values were between 4 and 13 μ M for the substrate phenanthridine. Thus, the affinity toward the substrate was not significantly changed. Taken together those results confirm the importance of the FAD loops surrounding the FAD binding site, especially the residue Leu438 which seems to be the crucial residue stabilizing and coordinating the electron transfer through the FAD cofactor.

5.7 Reactive Oxygen Species (ROS) and hAOX1

ROS represent prominent key molecules in physiological and pathological conditions in the cell (Hayyan *et al.*, 2016). Under controlled and physiological conditions, ROS are essential species involved in homeostatic cellular processes as cell cycle, redox signaling and defense against pathogens (Ray *et al.*, 2012). In contrast, as the intracellular ROS concentration increases, they are a dangerous source of damage to several molecules within the cell. ROS can cause damage to the DNA, leading to an oncogenic effect, damage to lipids with consequent peroxidation and damage to residues or cofactors of proteins, e.g. iron-sulfur clusters (Holmstrom & Finkel, 2014). So far mainly XOR has been implicated to generate significant amounts of $O_2^{\bullet-}$ during the course of their catalytic activity against recognized substrates (Kundu *et al.*, 2007). A report by Kundu *et al.* 2012 suggested, however, that hAOX1 represents a significant source of ROS in the cytosol and plays a critical role in in ROS-mediated tissue injury under specific conditions (Kundu *et al.*, 2012). This suggestion was based on the levels of enzymatic activity of XOR and AOX in human liver, where AOX1 has been calculated to have 24-fold higher enzyme activity than XOR (Krenitsky *et al.*, 1972). However, the reports by Kundu 2007 and 2012 investigated the rat liver AOX enzymes, which represented a mixture of all four AOX isoenzymes since the isoenzymes were not separated during purification. Further existing studies investigating the amount of ROS production by AOX enzymes in the literature were also performed on either the rat, rabbit or mouse enzymes, species containing various isoenzymes with different activities which were not investigated separately (Kundu *et al.*, 2012; Maia *et al.*, 2015). Studies on the rate of superoxide production by the human AOX1 enzyme have not been performed so far. In our study, the wild-type hAOX1 enzyme was shown to produce superoxide radical with a rate of around 10% as compared to the overall reaction. This value, however, is lower than the Kundu, *et al.* 2012 reported rates by Kundu, *et al.* (2012) of 16-20% for bXO and significantly lower than the rates of 32% for the rat AOXs. Thus, hAOX1 as major superoxide producing source should be analyzed carefully, since the $k_{cat} = 273 \text{ min}^{-1}$ with phenanthridine of the enzyme is significantly lower than the $k_{cat} = 1100 \text{ min}^{-1}$ of human XO with xanthine (Yamaguchi *et al.*, 2007). However, hAOX1 exists always in the oxidase form and does not need a conversion for oxygen reactivity and further exists in 24-fold higher amount than XOR in the cell, thus, being a factor to be considered for ROS generation in the cell.

In this study, we combined the study of hAOX1 SNPs variants and their effect on superoxide generation. Among the ten SNPs located around the FAD site, the amino acid exchange L438V

proved to be the most interesting one, since this variant produced a rate of around 75% of superoxide radical. The unbalanced superoxide production by the L438V amino acid exchange was unexpected considering the high similarity between the leucine and valine residues, both with a hydrophobic side chain but with valine having a shorter side chain (Fig. 5.4).

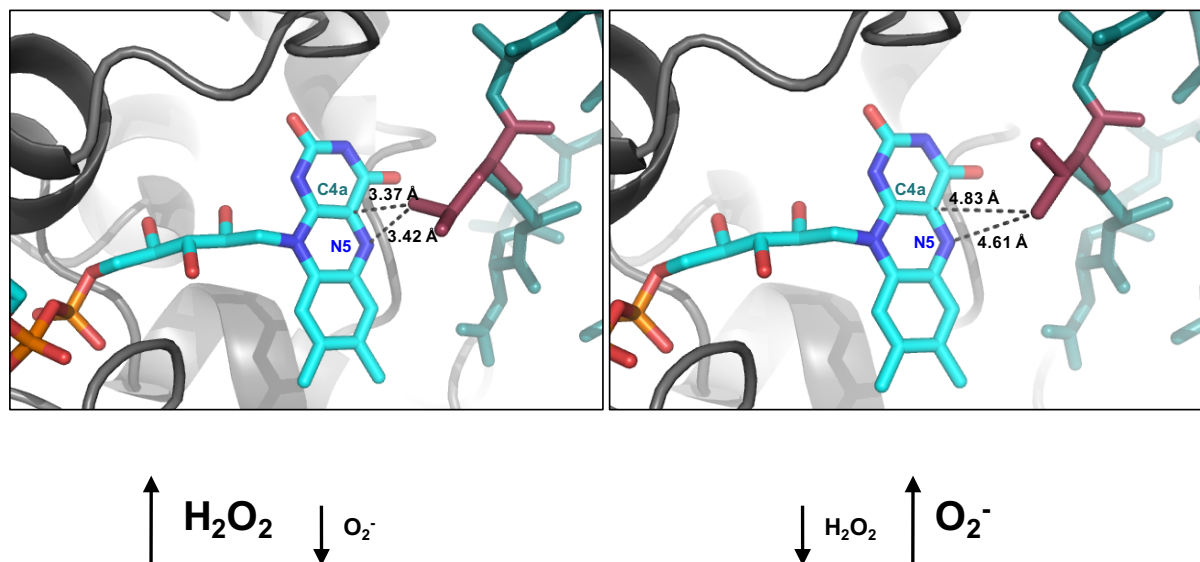


Figure 5. 5. Model of the FAD environment surrounding the residue Val in position 438 (right) in comparison to the wild type (left). Figures were created with MacPymol built 0.99rc6.

Considering the high toxicity of the superoxide anion in the cell, the hAOX1-L438V SNP variant should be considered an eventual candidate for critical or pathological roles of this natural variant within the human population. Alterations can be caused by high and uncontrolled oxygen radical production, particularly under pharmacological treatments where aldehyde oxidase is especially active and catalyzing the reduction of molecular oxygen in human liver hepatocytes (Garattini *et al.*, 2008). All other SNP based amino acid exchanges in the FAD loop I or loop II did not change the rate of superoxide production significantly, even when the amino acid exchange was located directly in vicinity to the amino acid L438.

By comparison, an amino acid substitution in rat XO has been reported which resulted also in an increased rate of superoxide production. A variant of rat XOR containing the amino acid exchanges W335A/F336L resulted in a form of the enzyme that is stably locked in the oxidase form. This enzyme variant was reported to produce $\text{O}_2^{\cdot -}$ and H_2O_2 in a ratio of 6:1 (Asai, 2007). The high rate of superoxide formation and the inability of the double variant to be converted to the dehydrogenase form has been explained by significant changes at the FAD site. Consequently, in the double variant a positive shift of the redox potential of the FAD cofactor

was determined, with the result of the increased O_2 reactivity of the enzyme. In native XOR, the reduction potential of the FeSI cluster and FAD are similar. Based on the thermodynamic equilibrium of the electrons introduced into the wild-type enzyme, the FAD cofactor was shown exists in both the $FADH_2$ and $FADH^\bullet$ states in XO, which led to the H_2O_2 and $O_2^{\bullet-}$ produced, respectively. Due to the increase in the FAD midpoint potential in the W335A/F336L variant, the electrons were explained to be more easily transferred from FeSI to the FAD in a one-electron transfer step, resulting in the formation of more $FADH^\bullet$ and thus a higher $O_2^{\bullet-}$ production rate. In AOX, however, stabilization of the $FADH^\bullet$ has not been observed so far, thus, other factors than the stabilization of the $FADH^\bullet$ contribute to the increased rate of $O_2^{\bullet-}$ production.

Unlike XOR, AOXs cannot use NAD^+ as the final electron acceptor and they transfer the electrons generated during the enzymatic reaction only to molecular oxygen (Johns, 1967). Consistent with this, the amino acid composition of the $Q_{423}ASRREDDIAK_{433}$ flexible loop I is different in human AOX1 and XORs. In the crystal structure of hAOX1, the flexible loop II in proximity of the FAD pocket ($T_{1230}RGPDQ_{1235}$) has a different orientation than to the relative in bXOR.

Hepatic AOX preparations have been shown to oxidize NADH generating the reducing equivalents necessary for $O_2^{\bullet-}$ production from molecular oxygen (Kundu *et al.*, 2007; Maia & Moura, 2011). Our results, however, show that hAOX1 does not react with NADH. It is not possible that hAOX1 acts as a NADH oxidase which is capable of producing significant amounts of $O_2^{\bullet-}$ in tissues. In previous studies mainly rat, rabbit and mouse enzymes were considered, for which a NADH oxidase activity has been obtained.

The hAOX1 WT and the new hAOX1 variants were tested for production of superoxide radical using the cytochrome C reduction assay. All the enzymes, WT and mutants, showed production of superoxide radical. To prove the specific superoxide production by hAOX1 WT and all the variants, several experiments were performed. As control, the reduction of cytochrome c was totally inhibited by SOD1. SOD1 is an enzyme that catalyzes the dismutation of the superoxide ($O_2^{\bullet-}$) radical into either molecular oxygen (O_2) or hydrogen peroxide (H_2O_2).

The most relevant result was obtained by the SNP variant hAOX1 L438V. The variant L438V produced 75% of superoxide radical during the catalysis, then producing just a minor amount of hydrogen peroxide. This result highlights two interesting points: 1) the crucial relevance of the residue L438 in the coordination of the FAD cofactor and 2) the possible toxic effect of the SNP L438V mutant within the human cells. The reason for the variant L438V to produce such high superoxide radical is still unclear. Probably the coordination role of this residue is crucial

for the stabilization of the FAD cofactor in the active site. The leucine in position 438 is the closest residue within the flexible FAD loop (430-440), having a distance of only 3.37 Å to the N5 and 3.42 Å to the C4a of the FAD isoalloxazine ring. Notable of attention is that, from the 3D crystal structure, the FAD cofactor resulted to be stacked between two leucine residues, located in position 438 and 344 (Fig. 5.6). Furthermore, in bXO/XDH the residues having the same location, I431 and F336, have an important role in the coordination of the FAD cofactor. A probable explanation for these alterations could be related with the redox potential at the FAD binding site.

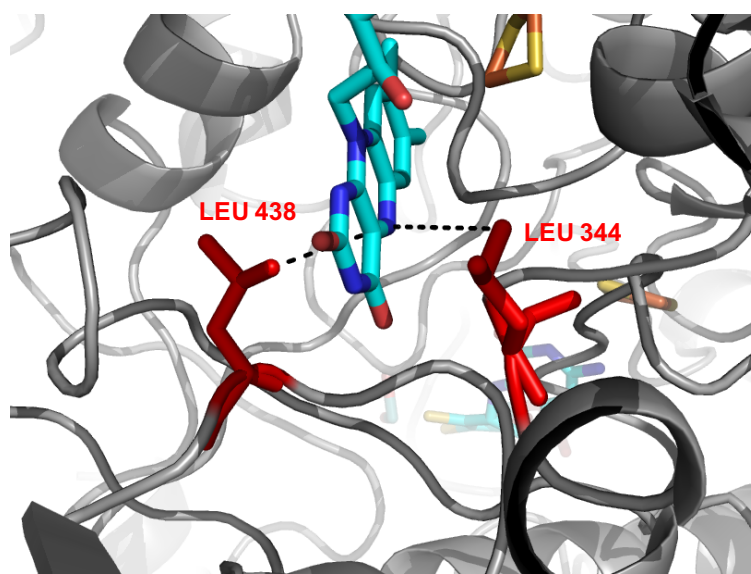


Figure 5. 6. Location of the FAD cofactor between Leu438 and Leu344. Shown are the residues Leu438 and Leu344 (red sticks), FAD and FeSII (sticks). Figures were created with MacPymol built 0.99rc6.

5.7.1 Mutagenesis of Leu438 and ROS overproduction

The reaction of oxygen at the flavin active site of enzymes is still an intriguing question. Presently, more than 100 000 protein sequences are deposited in the NCBI database classified as flavoenzymes (Chaiyen *et al.*, 2012). Flavins as FAD and FMN are redox cofactors able to get up to two electrons from reducing substrates and releasing them to electron acceptors of diverse chemical nature (Palfey & McDonald, 2010). Oxygen is essential in aerobic organisms, and therefore it is commonly used as electron acceptor in flavoenzyme catalysis to generate hydrogen peroxide (H_2O_2), which is emerging as a key cell signaling molecule (Forman *et al.*, 2010). These proteins are involved in networks of redox reactions playing essential roles in

cellular physiology. Flavoenzymes are also among the most active generators of ROS, for example NADPH oxidases (Drummond *et al.*, 2011), mitochondrial electron chain enzymes (Pryde & Hirst, 2011), and monoamine oxidases (Binda *et al.*, 2011). Reaction rates of reduced flavin with oxygen are very different among the various flavo-enzymes (Palfey & McDonald, 2010). This biochemical issue is gaining further interest because of its direct connection to ROS physiology, and because of its relevance to redox cellular homeostasis.

The mechanism of how the reduced cofactor in flavo-enzymes reacts with oxygen, a hydrophobic molecule by nature, is one of the most controversial and actively investigated questions in enzymology and biochemistry (Nishino, 1989; Hunt & Massey, 1994; Mattevi, 2006). It is generally believed that flavin and oxygen undergo an initial one electron transfer to generate a radical pair between the neutral flavin semiquinone (one electron reduced) and superoxide radical (Chaiyen *et al.*, 2012). This initiating step is chemically required to bypass the spin-inversion barrier, which is inherent to a reaction between molecules that are in singlet (reduced flavin) and triplet (molecular oxygen) states. Because of its intrinsic instability, the radical pair intermediate has never been captured and characterized (Chaiyen *et al.*, 2012).

A protonated active site histidine was identified as the crucial positively charged group that contributes to facilitate the formation of the anionic superoxide radical (Klinman, 2007). Instead in the monomeric sarcosine oxidase, the crystal structure originally displayed a conserved Lys residue interacting with the flavin N5 atom via a water-mediated hydrogen bond, a feature conserved in many amine oxidases (Kommoju *et al.*, 2011). Site directed mutagenesis to replace the Lys side chain with Met decreased the rate constant for flavin oxidation by approximately 8000-fold (Zhao *et al.*, 2008).

A clearly emerging question is that the reaction is primarily affected by changes in the local environment of the flavin N5-C4a locus. This is the site that is directly involved in the reaction with oxygen, and changes in its environment and accessibility are the central factors that control reactivity with oxygen and the outcome of the reaction.

Considering the crucial role of the residue Leu438 at the FAD active site of hAOX1 regarding the oxygen radicals formation, further variants were produced and analyzed: hAOX1 L438A, L438K and L438F. The residue Leu438 has a distance of 3.37 and 3.42 Å from the N5 and C4a respectively (Fig. 5.7).

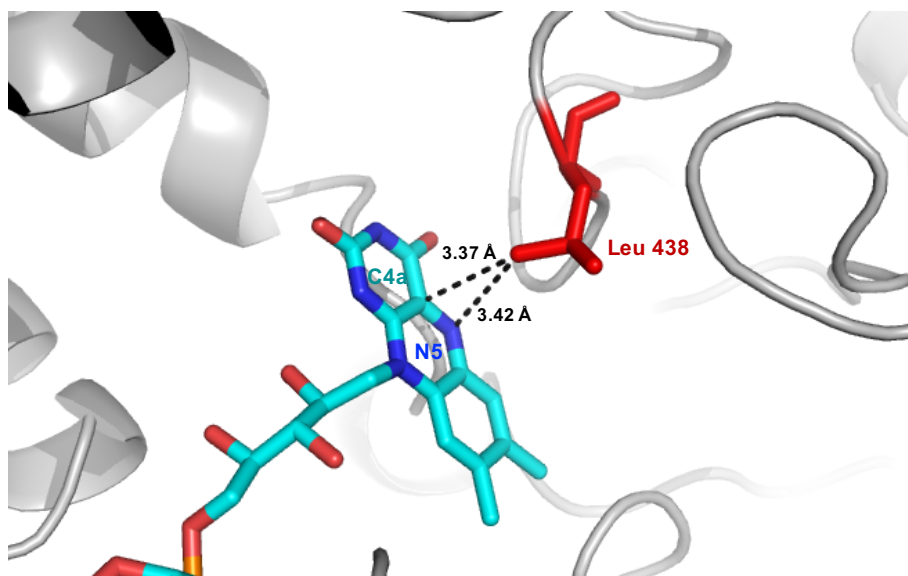


Figure 5. 7. Location of the residue Leu438 in hAOX1 and distances to the N5-C4a locus. Figures were created with MacPymol built 0.99rc6.

The substitution Leu to Ala increase the superoxide up to 80-90% of the total electrons coming from the Moco. Leu to Lys resulted in around 65% and Leu to Phe in around 35% of superoxide respectively. Those results confirmed the previous observations made on other enzyme that such reaction is primarily affected by changes in the local environment of the flavin N5-C4a locus. This is the site that is directly involved in the reaction with oxygen, and changes in its environment and accessibility are the central factors that control reactivity with oxygen and the outcome of the reaction.

6. Outlook

In this work on the human AOX1 new aspects regarding the catalytic activity, the structure-function relationship and the reactive oxygen species (ROS) production were investigated.

By single point mutagenesis, twenty new hAOX1 variants carrying mutations in the surrounding environment of the FAD cofactor were generated and characterized. Notably, ten of those variants are single nucleotide polymorphisms (SNP) variants present within the human population. The flexible loops in the vicinity of the FAD cofactor display similarity and partial superimposition within the xanthine oxidase enzyme family. Those flexible moieties play a crucial role during the interconversion XDH/XO, changing orientation and modulating the enzyme for the reaction toward NAD^+ or molecular oxygen. hAOX1 variants on these flexible loops showed altered enzymatic activity, revealing the importance of the residues Gly46, Gly 50, Gly346, Arg433, Ala439, Arg1231 and Lys1237, effecting the environment of the FAD active site. Still unclear remains the mechanistic reason for the alteration of the electron transfer pathway and the effect of different sulfuration levels within the variants analyzed.

Further studies are necessary to reveal more aspects regarding the FAD active site in the hAOX1. Stopped flow anaerobic kinetics might be needful to understand whether these alterations effect the oxidative or reductive half reactions, or both together. The separation of the two half reactions, obtaining the k_{red} and k_{ox} , may clarify which part of the reaction is mainly effected from the residues exchanges in the variants. Furthermore, stopped-flow enzyme kinetics may be performed using the reduced enzyme toward controlled concentrations of molecular oxygen. Of great utility will be the obtaining of the deflavo-hAOX1 form, as control for the steady-state kinetics experiments.

Another important aspect regards the redox potential of the hAOX1 cofactors. As shown from Martin Mahro (2013) the cofactor reduction potentials of hAOX1, mAOX3 and bXOR display interesting differences (Fig. 6.1). XORs are characterized to have similar values for the molybdenum reduction potentials, whereas AOXs shows a considerable discrepancy of the molybdenum reduction potentials. Unique to AOXs is a FeSI reduction potential that is higher than that of FeSII. In XDHs, the FAD/ FADH_2 pair has an unusually low reduction potential, which shifts of around 180 mV positively upon NAD^+ binding (Barber *et al.*, 1982; Hunt *et al.*, 1993; Ishikita *et al.*, 2012). Alterations of these reduction potential pairs would result in differences in the electron transfer pathway and catalytic rate.

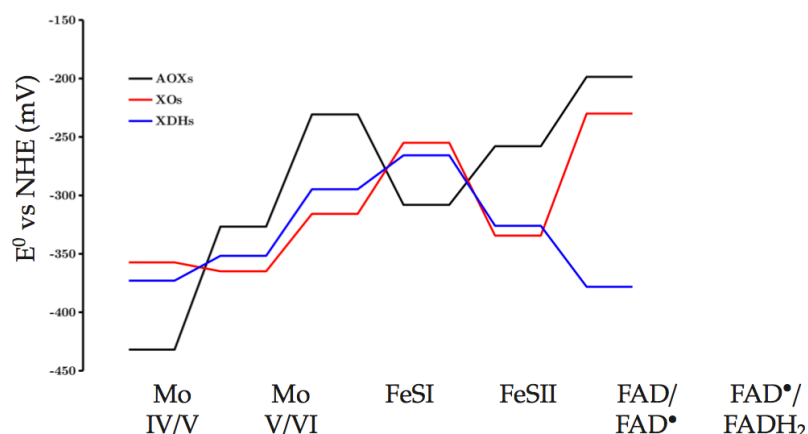


Figure 6. 1. Cofactor reduction potential of AOXs, XOs and XDHS (adapted from PhD thesis of Dr. Martin Mahro, 2013). Values of published cofactor reduction potentials of AOX (Barber & Siegel, 1982) XOs (Cammack, 1976; Porras & Palmer, 1982; Barber *et al.*, 1982; Harris *et al.*, 1999) and XDHS (Barber, 1977; Barber *et al.*, 1980; Parschat *et al.*, 2001) are plotted according to their position in the protein electron transfer chain. Values obtained by redox titration or EPR spectroscopy. Unique to AOXs is the degeneration of both molybdenum reduction potentials and the more positive FeSI reduction potential in comparison to FeSII. XDHS are characterized by a more negative FAD[•]/FADH₂ reduction potential in comparison to FAD/FAD[•].

The hAOX1 shows the more positive reduction potential for the FAD in comparison to the other enzyme of the same family and it might explain the high reactivity of the hAOX1 toward molecular oxygen. However, further studies are necessary for the correct understanding of the impact of the FAD redox potential on the reaction with oxygen. Determination of the redox potentials by electrochemical approaches or electron paramagnetic resonance (EPR) measurements might provide a breakthrough toward a better understanding of the redox properties of hAOX1, especially regarding the hAOX1 FAD variants which show clear alterations in enzyme activity and ROS production.

The diversity in residues composition and spatial orientation of those flexible loops among the XO enzyme family explains the different redox properties, and consequently the different reactivity at the FAD cofactor toward oxygen or NAD⁺. As opposed to mAOX3, bXO and bXDH, the hAOX1 is unable to react with NADH. This information discards the possibilities to consider the hAOX1 as a physiologically relevant NADH oxidase enzyme.

The hAOX1 variants generated in this work revealed interesting properties regarding reactive oxygen species (ROS) production.

The variants L438V, L438A, L438K and L438F showed unbalanced ratio of H₂O₂/O₂⁻ production with an overproduction of superoxide anion (3-8 fold higher compared to the wild type). For future studies the generation of new Leu438 variants may explain the correlation between the substituted residue and the rate of superoxide production. Interestingly, the

variants L438V results from polymorphism identified in a human individual. The overproduction of superoxide by this SNP variant might cause an alteration in the oxidative stress of those individuals carrying the mutation. This aspect employs future investigations at the cellular level. Studies on human cell cultures represent a further step in the research on the hAOX1 that might provide insights about the physiological relevance of the knowledge obtained by *in vitro* investigations. Although hAOX1 is an enzyme evidently involved in the phase I of the metabolism of xenobiotics, it performs the catalysis of only a small minority (<1%) of the reactions that occur in the drug metabolism (Sanoh *et al.*, 2015). The main characters of the drug metabolism pathways are the cytochrome enzyme families, which present alternative or complementary reaction pathways with the hAOX1. Therefore, another cellular function for the hAOX1 might be reasonable. Indeed, the role of hAOX1 in the cell is still unclear. Considering the species-specific differences for AOXs, the investigations on AOX enzymes need to be clearly divided into studies on the human enzyme, containing only one AOX orthologue and studies on other organisms containing more orthologues with a significantly different in substrates and inhibitors spectrum. The generation of knock-out cell lines or genetically modified cell lines expressing the SNP L438V overproducing superoxide, might provide insights regarding a potential role of hAOX1 in oxidative stress and oxidative signaling in the cell.

7. Conclusion

The focus of this study was to understand the catalytic mechanism of hAOX1 with special interest at the FAD reactivity toward oxygen and consequent oxygen radicals production. The human AOX1 was compared to enzyme of the same family as murine AOX3 and bovine XOR. Our results showed for the first time the complexity of the FAD active site of hAOX1 and its role in the overall enzyme activity and superoxide anion formation.

Starting from the available information about the FAD active site of bXOR and its importance in the interconversion dehydrogenase/oxidase form, we elaborated a strategy to uncover the role of crucial residues coordinating the FAD cofactor in hAOX1. Particularly, the focus of the study was to understand the relevance of the flexible loop I (Q₄₃₀AQRQENALAI₄₄₀) and the flexible loop II (T₁₂₃₀RGPDQ₁₂₃₅) in relation to the overall enzyme reactivity and its impact on the oxygen reduction. hAOX1 variants on these flexible loops displayed impaired catalytic activity, revealing the importance of the residues Gly46, Gly 50, Gly346, Arg433, Ala439, Arg1231 and Lys1237, indicating a novel role for this residues cluster in the structure-function relation in the FAD active site of hAOX1. Among the twenty new hAOX1 variants generated in this study, of particular interest resulted to be the residue Leu438.

Four hAOX1 variants were produced on this residue: L438V, L438A, L438F and L438K. Those variants did not show important alterations in catalytic activity, expression level, dimerization ratio and metal content but revealed a prominent overproduction of superoxide anion as side product of the hAOX1 catalytic activity. In the case of the variants L438V and L438A, the superoxide rate produced was 70-90% of the total reducing equivalent generated from the oxidation of the substrate. The L438K mutant showed around 65% of superoxide production and the variant L438F around 35%. Clearly, the Leu438 coordinates the reaction between the isoalloxazine ring of the FAD cofactor and molecular oxygen. Structural data confirm the vicinity of this Leu residue to the N5 (3.42 Å) and to the C4a (3.37 Å) atoms of the FAD alloxazine ring. This idea is supported by the observation that the locus N5-C4a of the FAD alloxazine ring plays the crucial role in the interaction with oxygen and consequent formation of the superoxide anion.

Several studies from V. Massey and coworkers focused on the interaction FAD:Oxygen in xanthine oxidoreductases. It was shown that the primary pathway in the oxidation of xanthine

oxidase during the rapid phase of the reaction is a 2-electron transfer to form hydrogen peroxide. Since the slow phase of the enzyme reaction is thought to reflect the oxidation of 1-electron reduced xanthine oxidase molecules, superoxide anions was proposed to be generated during this step. Indeed, the stabilization of the semiquinone FADH^{\bullet} seems to be necessary to gain superoxide anion production (Komai *et al.*, 1969; Fridovich, 1970; Olson *et al.*, 1974). Asai *et al.*, generated a bXOR W335A/F336L mutant with the ability to produce a much higher ratio of $\text{O}_2^{\bullet-}$. This feature is caused by its conformation, which is strongly shifted towards the XO form and its FAD redox potential is higher than that of the wild type enzyme. By this mechanism, $\text{O}_2^{\bullet-}$ is formed by the reaction of FADH^{\bullet} with molecular oxygen. In the double mutant bXOR W335A/F336L, the FAD redox potential changes to a higher value, and during the catalytic turnover FAD can receive only one electron from Fe/S II to form FADH^{\bullet} , which readily react with oxygen and $\text{O}_2^{\bullet-}$ is produced (Nishino *et al.*, 1989; Harris and Massey, 1997; Asai *et al.*, 2007). Analysis of the hAOX1 variants overproducing superoxide did not show clear stabilization of semiquinone FADH^{\bullet} by spectro-photometric detection. It might be due to the inability to detect the semiquinone FADH^{\bullet} with the methods employed. The substitution Leu to Val or Leu to Ala in hAOX1 creates a larger and hydrophobic space around the N5 of the FAD isoalloxazine ring facilitating the formation of superoxide. Notably, in the variant L438A three consecutive Alanine residues (Ala437-Ala438-A439) surround the N5-C4a moiety of the FAD creating an even larger and hydrophobic environment in the vicinity of the FAD. The contribution of those results is amplified considering that the mechanism and the effect of the production of oxygen radicals in living organism is still one of the biggest open questions in biochemistry and cell biology (Winterbourn, 2008; Winterbourn & Hampton, 2008).

8. Summery

In this work the human AOX1 was characterized and detailed aspects regarding the expression, the enzyme kinetics and the production of reactive oxygen species (ROS) were investigated. The hAOX1 is a cytosolic enzyme belonging to the molybdenum hydroxylase family. Its catalytically active form is a homodimer with a molecular weight of 300 kDa. Each monomer (150 kDa) consists of three domains: a N-terminal domain (20 kDa) containing two [2Fe-2S] clusters, a 40 kDa intermediate domain containing a flavin adenine dinucleotide (FAD), and a C-terminal domain (85 kDa) containing the substrate binding pocket and the molybdenum cofactor (Moco). The hAOX1 has an emerging role in the metabolism and pharmacokinetics of many drugs, especially aldehydes and N- heterocyclic compounds.

In this study, the hAOX1 was heterologously expressed in *E. coli* TP1000 cells, using a new codon optimized gene sequence which improved the expressed protein yield of around 10-fold compared to the previous expression systems for this enzyme. To increase the catalytic activity of hAOX1, an in vitro chemical sulfuration was performed to favor the insertion of the equatorial sulfido ligand at the Moco with consequent increased enzymatic activity of around 10-fold. Steady-state kinetics and inhibition studies were performed using several substrates, electron acceptors and inhibitors. The recombinant hAOX1 showed higher catalytic activity when molecular oxygen was used as electron acceptor. The highest turn over values were obtained with phenanthridine as substrate. Inhibition studies using thioridazine (phenothiazine family), in combination with structural studies performed in the group of Prof. M.J. Romão, Nova Universidade de Lisboa, showed a new inhibition site located in proximity of the dimerization site of hAOX1. The inhibition mode of thioridazine resulted in a noncompetitive inhibition type. Further inhibition studies with loxapine, a thioridazine-related molecule, showed the same type of inhibition. Additional inhibition studies using DCPIP and raloxifene were carried out.

Extensive studies on the FAD active site of the hAOX1 were performed. Twenty new hAOX1 variants were produced and characterized. The hAOX1 variants generated in this work were divided in three groups: I) hAOX1 single nucleotide polymorphisms (SNP) variants; II) XOR-FAD loop hAOX1 variants; III) additional single point hAOX1 variants. The hAOX1 SNP variants G46E, G50D, G346R, R433P, A439E, K1231N showed clear alterations in their

catalytic activity, indicating a crucial role of these residues into the FAD active site and in relation to the overall reactivity of hAOX1.

Furthermore, residues of the bovine XOR FAD flexible loop (Q₄₂₃ASRREDDIAK₄₃₃) were introduced in the hAOX1. FAD loop hAOX1 variants were produced and characterized for their stability and catalytic activity. Especially the variants hAOX1 N436D/A437D/L438I, N436D/A437D/L438I/I440K and Q434R/N436D/A437D/L438I/I440K showed decreased catalytic activity and stability. hAOX1 wild type and variants were tested for reactivity toward NADH but no reaction was observed.

Additionally, the hAOX1 wild type and variants were tested for the generation of reactive oxygen species (ROS). Interestingly, one of the SNP variants, hAOX1 L438V, showed a high ratio of superoxide production. This result showed a critical role for the residue Leu438 in the mechanism of oxygen radicals formation by hAOX1. Subsequently, further hAOX1 variants having the mutated Leu438 residue were produced. The variants hAOX1 L438A, L438F and L438K showed superoxide overproduction of around 85%, 65% and 35% of the total reducing equivalent obtained from the substrate oxidation.

The results of this work show for the first time a characterization of the FAD active site of the hAOX1, revealing the importance of specific residues involved in the generation of ROS and effecting the overall enzymatic activity of hAOX1. The hAOX1 SNP variants presented here indicate that those allelic variations in humans might cause alterations ROS balancing and clearance of drugs in humans.

References

- Achiron A, Aviv U, Mendel L & Burgansky-Eliash Z (2015) Acute angle closure glaucoma precipitated by olanzapine. *Int J Geriatr Psychiatry* **30**: 1101-1102.
- Adachi M, Itoh K, Masubuchi A, Watanabe N & Tanaka Y (2007) Construction and expression of mutant cDNAs responsible for genetic polymorphism in aldehyde oxidase in Donryu strain rats. *J Biochem Mol Biol* **40**: 1021-1027.
- Alfaro JF, Joswig-Jones CA, Ouyang W, Nichols J, Crouch GJ & Jones JP (2009) Purification and mechanism of human aldehyde oxidase expressed in *Escherichia coli*. *Drug Metab Dispos* **37**: 2393-2398.
- Amrani L, Primus J, Glatigny A, Arcangeli L, Scazzocchio C & Finnerty V (2000) Comparison of the sequences of the aspergillus nidulans *hxB* and drosophila melanogaster *ma-l* genes with *nifS* from *Azotobacter vinelandii* suggests a mechanism for the insertion of the terminal sulphur atom in the molybdopterin cofactor. *Mol Microbiol* **38**: 114-125.
- Angov E (2011) Codon usage: nature's roadmap to expression and folding of proteins. *Biotechnology journal* **6**: 650-659.
- Angov E, Legler PM & Mease RM (2011) Adjustment of codon usage frequencies by codon harmonization improves protein expression and folding. *Methods in molecular biology* **705**: 1-13.
- Asai R, Nishino T, Matsumura T, Okamoto K, Igarashi K, Pai EF & Nishino T (2007) Two mutations convert mammalian xanthine oxidoreductase to highly superoxide-productive xanthine oxidase. *J Biochem (Tokyo)* **141**: 525-534.
- Asakawa T, Itoh K, Adachi M, Hoshino K, Watanabe N & Tanaka Y (2008) Properties of 130 kDa subunit of monkey aldehyde oxidase. *Biological & pharmaceutical bulletin* **31**: 380-385.
- Baral PK, Swayampakula M, Rout MK, Kav NN, Spyropoulos L, Aguzzi A & James MN (2014) Structural basis of prion inhibition by phenothiazine compounds. *Structure* **22**: 291-303.
- Barber MJ & Siegel LM (1982) Oxidation-reduction potentials of molybdenum, flavin, and iron-sulfur centers in milk xanthine oxidase: variation with pH. Vol. 21 p.^pp. 1638-1647.
- Barber MJ, Coughlan MP, Kanda M & Rajagopalan KV (1980) Electron paramagnetic resonance properties and oxidation-reduction potentials of the molybdenum, flavin, and iron-sulfur centers of chicken liver xanthine dehydrogenase. Vol. 201 p.^pp. 468-475.
- Barber MJ, Coughlan MP, Rajagopalan KV & Siegel LM (1982) Rabbit liver aldehyde oxidase: reduction potentials and spectroscopic properties. Vol. 21 p.^pp. 805-809.
- Baron R, McCammon JA & Mattevi A (2009) The oxygen-binding vs. oxygen-consuming paradigm in biocatalysis: structural biology and biomolecular simulation. *Current opinion in structural biology* **19**: 672-679.

- Baron R, Binda C, Tortorici M, McCammon JA & Mattevi A (2011) Molecular mimicry and ligand recognition in binding and catalysis by the histone demethylase LSD1-CoREST complex. *Structure* **19**: 212-220.
- Barr JT & Jones JP (2011) Inhibition of human liver aldehyde oxidase: implications for potential drug-drug interactions. *Drug metabolism and disposition: the biological fate of chemicals* **39**: 2381-2386.
- Barr JT, Choughule KV, Nepal S, *et al.* (2014) Why do most human liver cytosol preparations lack xanthine oxidase activity? *Drug metabolism and disposition: the biological fate of chemicals* **42**: 695-699.
- Beedham C (1997) The role of non-P450 enzymes in drug oxidation. *Pharmacy world & science : PWS* **19**: 255-263.
- Beedham C, Critchley DJ & Rance DJ (1995) Substrate specificity of human liver aldehyde oxidase toward substituted quinazolines and phthalazines: a comparison with hepatic enzyme from guinea pig, rabbit, and baboon. *Archives of biochemistry and biophysics* **319**: 481-490.
- Beedham C, Bruce SE, Critchley DJ & Rance DJ (1990) 1-substituted phthalazines as probes of the substrate-binding site of mammalian molybdenum hydroxylases. *Biochemical pharmacology* **39**: 1213-1221.
- Bendotti C, Prosperini E, Kurosaki M, Garattini E & Terao M (1997) Selective localization of mouse aldehyde oxidase mRNA in the choroid plexus and motor neurons. *Neuroreport* **8**: 2343-2349.
- Berger R, Mezey e, Clancy KP, Harta G, Wright RM, Repine JE, Brown RH, Brownstein M & Patterson D (1995) Analysis of aldehyde oxidase and xanthine dehydrogenase/oxidase as possible candidate genes for autosomal recessive familial amyotrophic lateral sclerosis. *Somat Cell Mol Genet* **21**: 121-131.
- Binda C, Aldeco M, Geldenhuys WJ, Tortorici M, Mattevi A & Edmondson DE (2011) Molecular Insights into Human Monoamine Oxidase B Inhibition by the Glitazone Anti-Diabetes Drugs. *ACS medicinal chemistry letters* **3**: 39-42.
- Bittner F, Oreb M & Mendel RR (2001) ABA3 is a molybdenum cofactor sulfurase required for activation of aldehyde oxidase and xanthine dehydrogenase in *Arabidopsis thaliana*. *J Biol Chem* **276**: 40381-40384.
- Boyington JC, Gladyshev VN, Khangulov SV, Stadtman TC & Sun PD (1997) Crystal structure of formate dehydrogenase H: catalysis involving Mo, molybdopterin, selenocysteine, and an Fe₄S₄ cluster. *Science* **275**: 1305-1308.
- Braman J, Papworth C & Greener A (1996) Site-directed mutagenesis using double-stranded plasmid DNA templates. *Methods in molecular biology* **57**: 31-44.
- Branzoli U & Massey V (1974) Preparation of aldehyde oxidase in its native and deflavo forms. Comparison of spectroscopic and catalytic properties. *J Biol Chem* **249**: 4399-4345.
- Bray RC (1959) The chemistry of xanthine oxidase. 6. Variations in stability and the presence of an inhibitor in certain preparations. *Biochem J* **73**: 690-694.
- Bruckner C & Checchi F (2011) Detection of infectious disease outbreaks in twenty-two fragile states, 2000-2010: a systematic review. *Conflict and health* **5**: 13.
- Bulmer M (1987) A statistical analysis of nucleotide sequences of introns and exons in human genes. *Molecular biology and evolution* **4**: 395-405.

- Calzi ML, Raviolo C, Ghibaudi E, de Gioia L, Salmona M, Cazzaniga G, Kurosaki M, Terao M & Garattini E (1995) Purification, cDNA cloning, and tissue distribution of bovine liver aldehyde oxidase. *J Biol Chem* **270**: 31037-31045.
- Chaiyen P, Fraaije MW & Mattevi A (2012) The enigmatic reaction of flavins with oxygen. *Trends in biochemical sciences* **37**: 373-380.
- Chakraborty S & Massey V (2002) Reaction of reduced flavins and flavoproteins with diphenyliodonium chloride. *J Biol Chem* **277**: 41507-41516.
- Chan MK, Mukund S, Kletzin A, Adams MWW & Rees DC (1995) Structure of a hyperthermophilic tungstopterin enzyme, aldehyde ferredoxin oxidoreductase. *Science* **267**: 1463-1469.
- Choughule KV, Joswig-Jones CA & Jones JP (2015) Interspecies differences in the metabolism of methotrexate: An insight into the active site differences between human and rabbit aldehyde oxidase. *Biochemical pharmacology* **96**: 288-295.
- Clarke SE, Harrell AW & Chenery RJ (1995) Role of aldehyde oxidase in the in vitro conversion of famciclovir to penciclovir in human liver. *Drug metabolism and disposition: the biological fate of chemicals* **23**: 251-254.
- Coelho C, Foti A, Hartmann T, Santos-Silva T, Leimkuhler S & Romao MJ (2015) Structural insights into xenobiotic and inhibitor binding to human aldehyde oxidase. *Nat Chem Biol* **11**: 779-783.
- Coelho C, Mahro M, Trincao J, Carvalho AT, Ramos MJ, Terao M, Garattini E, Leimkuhler S & Romao MJ (2012) The first mammalian aldehyde oxidase crystal structure: insights into substrate specificity. *The Journal of biological chemistry* **287**: 40690-40702.
- Dalvie D, Zhang C, Chen W, Smolarek T, Obach RS & Loi CM (2010) Cross-species comparison of the metabolism and excretion of zonisamide: contribution of aldehyde oxidase to interspecies differences. *Drug metabolism and disposition: the biological fate of chemicals* **38**: 641-654.
- Declercq T, Petrovic M, Azermai M, Vander Stichele R, De Sutter AI, van Driel ML & Christiaens T (2013) Withdrawal versus continuation of chronic antipsychotic drugs for behavioural and psychological symptoms in older people with dementia. *The Cochrane database of systematic reviews* CD007726.
- Dobbek H, Gremer L, Kiefersauer R, Huber R & Meyer O (2002) Catalysis at a dinuclear [CuSMo(=O)OH] cluster in a CO dehydrogenase resolved at 1.1-Å resolution. *Proc Natl Acad Sci U S A* **99**: 15971-15976.
- Drummond GR, Selemidis S, Griendling KK & Sobey CG (2011) Combating oxidative stress in vascular disease: NADPH oxidases as therapeutic targets. *Nature reviews Drug discovery* **10**: 453-471.
- Enroth C, Eger BT, Okamoto K, Nishino T & Pai EF (2000) Crystal structures of bovine milk xanthine dehydrogenase and xanthine oxidase: structure-based mechanism of conversion. *Proc Natl Acad Sci U S A* **97**: 10723-10728.
- Finnegan S, Agniswamy J, Weber IT & Gadda G (2010) Role of valine 464 in the flavin oxidation reaction catalyzed by choline oxidase. *Biochemistry* **49**: 2952-2961.
- Forman HJ, Maiorino M & Ursini F (2010) Signaling functions of reactive oxygen species. *Biochemistry* **49**: 835-842.

- Foti A, Hartmann T, Coelho C, Santos-Silva T, Romao MJ & Leimkuhler S (2016) Optimization of the Expression of Human Aldehyde Oxidase for Investigations of Single-Nucleotide Polymorphisms. *Drug Metab Dispos* **44**: 1277-1285.
- Fridovich I (1997) Superoxide anion radical (O₂⁻), superoxide dismutases, and related matters. *J Biol Chem* **272**: 18515-18517.
- Fukiya K, Itoh K, Yamaguchi S, Kishiba A, Adachi M, Watanabe N & Tanaka Y (2010) A single amino acid substitution confers high cinchonidine oxidation activity comparable with that of rabbit to monkey aldehyde oxidase 1. *Drug Metab Dispos* **38**: 302-307.
- Gadda G (2012) Oxygen activation in flavoprotein oxidases: the importance of being positive. *Biochemistry* **51**: 2662-2669.
- Garattini E & Terao M (2006) Granulocytic maturation in cultures of acute myeloid leukemia is not always accompanied by increased apoptosis. *Leukemia research* **30**: 519-520.
- Garattini E & Terao M (2011) Increasing recognition of the importance of aldehyde oxidase in drug development and discovery. *Drug metabolism reviews* **43**: 374-386.
- Garattini E, Fratelli M & Terao M (2008) Mammalian aldehyde oxidases: genetics, evolution and biochemistry. *Cellular and molecular life sciences : CMLS* **65**: 1019-1048.
- Garattini E, Mendel R, Romao MJ, Wright R & Terao M (2003) Mammalian molybdo-flavoenzymes, an expanding family of proteins: structure, genetics, regulation, function and pathophysiology. *Biochem J* **372**: 15-32.
- Garattini E, Parrella E, Diomede L, *et al.* (2004) ST1926, a novel and orally active retinoid-related molecule inducing apoptosis in myeloid leukemia cells: modulation of intracellular calcium homeostasis. *Blood* **103**: 194-207.
- Gatchel RJ, Mayer TG, Capra P, Barnett J & Diamond P (1986) Million Behavioral Health Inventory: its utility in predicting physical function in patients with low back pain. *Archives of physical medicine and rehabilitation* **67**: 878-882.
- Goldman MJ & Wilson JM (1995) Expression of alpha v beta 5 integrin is necessary for efficient adenovirus-mediated gene transfer in the human airway. *Journal of virology* **69**: 5951-5958.
- Goldstein JA (2001) Clinical relevance of genetic polymorphisms in the human CYP2C subfamily. *British journal of clinical pharmacology* **52**: 349-355.
- Gustafsson C, Govindarajan S & Minshull J (2004) Codon bias and heterologous protein expression. *Trends in biotechnology* **22**: 346-353.
- Hanahan D (1983) Studies on transformation of *Escherichia coli* with plasmids. *Journal of molecular biology* **166**: 557-580.
- Harkness RA, McCreanor GM, Simpson D & MacFadyen IR (1986) Pregnancy in and incidence of xanthine oxidase deficiency. *J Inher Metab Dis* **9**: 407-408.
- Harris CM, Sanders SA & Massey V (1999) Role of the flavin midpoint potential and NAD binding in determining NAD versus oxygen reactivity of xanthine oxidoreductase. *J Biol Chem* **274**: 4561-4569.
- Hartmann T, Terao M, Garattini E, Teutloff C, Alfaro JF, Jones JP & Leimkuhler S (2012) The impact of single nucleotide polymorphisms on human aldehyde oxidase. *Drug metabolism and disposition: the biological fate of chemicals* **40**: 856-864.

- Hayyan M, Hashim MA & AlNashef IM (2016) Superoxide Ion: Generation and Chemical Implications. *Chemical reviews* **116**: 3029-3085.
- Heidenreich T, Wollers S, Mendel RR & Bittner F (2005) Characterization of the NifS-like domain of ABA3 from *Arabidopsis thaliana* provides insight into the mechanism of molybdenum cofactor sulfuration. *J Biol Chem* **280**: 4213-4218.
- Henderson Pozzi M & Fitzpatrick PF (2010) A lysine conserved in the monoamine oxidase family is involved in oxidation of the reduced flavin in mouse polyamine oxidase. *Archives of biochemistry and biophysics* **498**: 83-88.
- Hernandez-Ortega A, Borrelli K, Ferreira P, Medina M, Martinez AT & Guallar V (2011) Substrate diffusion and oxidation in GMC oxidoreductases: an experimental and computational study on fungal aryl-alcohol oxidase. *Biochem J* **436**: 341-350.
- Hille R (1996) The mononuclear molybdenum enzymes. *Chemical Rev* **96**: 2757-2816.
- Hille R (1999) Molybdenum enzymes. *Essays in biochemistry* **34**: 125-137.
- Hille R (2002) Molybdenum and Tungsten in Biology. *Trends in biochemical sciences* **27**: 360-367.
- Hille R (2002) Molybdenum enzymes containing the pyranopterin cofactor: An overview. Vol. 39 p.^pp. 187-226.
- Holland HD (2006) The oxygenation of the atmosphere and oceans. *Philosophical transactions of the Royal Society of London Series B, Biological sciences* **361**: 903-915.
- Holmes RS (1979) Genetics, ontogeny, and testosterone inducibility of aldehyde oxidase isozymes in the mouse: evidence for two genetic loci (Aox-I and Aox-2) closely linked on chromosome 1. *Biochemical genetics* **17**: 517-527.
- Holmstrom KM & Finkel T (2014) Cellular mechanisms and physiological consequences of redox-dependent signalling. *Nature reviews Molecular cell biology* **15**: 411-421.
- Hoshino K, Itoh K, Masubuchi A, Adachi M, Asakawa T, Watanabe N, Kosaka T & Tanaka Y (2007) Cloning, expression, and characterization of male cynomolgus monkey liver aldehyde oxidase. *Biological & pharmaceutical bulletin* **30**: 1191-1198.
- Huang DY, Furukawa A & Ichikawa Y (1999) Molecular cloning of retinal oxidase/aldehyde oxidase cDNAs from rabbit and mouse livers and functional expression of recombinant mouse retinal oxidase cDNA in *Escherichia coli*. *Archives of biochemistry and biophysics* **364**: 264-272.
- Hunt J & Massey V (1994) Studies of the reductive half-reaction of milk xanthine dehydrogenase. *J Biol Chem* **269**: 18904-18914.
- Hunt J, Massey V, Dunham WR & Sands RH (1993) Redox potentials of milk xanthine dehydrogenase. Room temperature measurement of the FAD and 2Fe/2S center potentials. *J Biol Chem* **268**: 18685-18691.
- Hunt J, Massey V, Dunham WR & Sands RH (1993) Redox potentials of milk xanthine dehydrogenase. Room temperature measurement of the FAD and iron-sulfur (2Fe/2S) center potentials. Vol. 268 p.^pp. 18685-18691.
- Hurwitz J (1955) Inhibition studies on aldehyde oxidase. *J Biol Chem* **212**: 757-769.
- Hutzler JM, Obach RS, Dalvie D & Zientek MA (2013) Strategies for a comprehensive understanding of metabolism by aldehyde oxidase. *Expert opinion on drug metabolism & toxicology* **9**: 153-168.

- Ichida K, Matsumura T, Sakuma R, Hosoya T & Nishino T (2001) Mutation of human molybdenum cofactor sulfurase gene is responsible for classical xanthinuria type II. *Biochem Biophys Res Commun* **282**: 1194-1200.
- Ikemura T (1981) Correlation between the abundance of Escherichia coli transfer RNAs and the occurrence of the respective codons in its protein genes: a proposal for a synonymous codon choice that is optimal for the E. coli translational system. *Journal of molecular biology* **151**: 389-409.
- Ishikita H, Eger BT, Okamoto K, Nishino T & Pai EF (2012) Protein conformational gating of enzymatic activity in xanthine oxidoreductase. *Journal of the American Chemical Society* **134**: 999-1009.
- Itoh K, Adachi M, Sato J, Shouji K, Fukiya K, Fujii K & Tanaka Y (2009) Effects of selenium deficiency on aldehyde oxidase 1 in rats. *Biological & pharmaceutical bulletin* **32**: 190-194.
- Johns DG (1967) Human liver aldehyde oxidase: differential inhibition of oxidation of charged and uncharged substrates. *J Clin Invest* **46**: 1492-1505.
- Johnson JL & Rajagopalan KV (1982) Structural and metabolic relationship between the molybdenum cofactor and urothione. *Proc Natl Acad Sci U S A* **79**: 6856-6860.
- Johnson JL, Hainline BE, Rajagopalan KV & Arison BH (1984) The pterin component of the molybdenum cofactor. Structural characterization of two fluorescent derivatives. *J Biol Chem* **259**: 5414-5422.
- Jorns MS, Chen ZW & Mathews FS (2010) Structural characterization of mutations at the oxygen activation site in monomeric sarcosine oxidase. *Biochemistry* **49**: 3631-3639.
- Kane JF (1995) Effects of rare codon clusters on high-level expression of heterologous proteins in Escherichia coli. *Current opinion in biotechnology* **6**: 494-500.
- Karrasch M, Börner G & Thauer RK (1990) The molybdenum cofactor of formylmethanofuran dehydrogenase from *Methanosarcina barkeri* is a molybdopterin guanine dinucleotide. *FEBS Lett* **274**: 48-52.
- Kawashima K, Hosoi K, Naruke T, Shiba T, Kitamura M & Watabe T (1999) Aldehyde oxidase-dependent marked species difference in hepatic metabolism of the sedative-hypnotic, zaleplon, between monkeys and rats. *Drug Metab Dispos* **27**: 422-428.
- Kisker C, Schindelin H, Pacheco A, Wehbi WA, Garrett RM, Rajagopalan KV, Enemark JH & Rees DC (1997) Molecular basis of sulfite oxidase deficiency from the structure of sulfite oxidase. *Cell* **91**: 973-983.
- Kitamura S & Tatsumi K (1984) Reduction of tertiary amine N-oxides by liver preparations: function of aldehyde oxidase as a major N-oxide reductase. *Biochem Biophys Res Commun* **121**: 749-754.
- Kitamura S, Sugihara K & Ohta S (2006) Drug-metabolizing ability of molybdenum hydroxylases. *Drug metabolism and pharmacokinetics* **21**: 83-98.
- Kitamura S, Nitta K, Tayama Y, Tanoue C, Sugihara K, Inoue T, Horie T & Ohta S (2008) Aldehyde oxidase-catalyzed metabolism of N1-methylnicotinamide in vivo and in vitro in chimeric mice with humanized liver. *Drug Metab Dispos* **36**: 1202-1205.
- Klinman JP (2007) How do enzymes activate oxygen without inactivating themselves? *Accounts of chemical research* **40**: 325-333.

- Kobayashi K, Miki M, Okamoto K & Nishino T (1993) Electron transfer process in milk xanthine dehydrogenase as studied by pulse radiolysis. *J Biol Chem* **268**: 24642-24646.
- Komai H, Massey V & Palmer G (1969) The preparation and properties of deflavo xanthine oxidase. *J Biol Chem* **244**: 1692-1700.
- Kommoju PR, Chen ZW, Bruckner RC, Mathews FS & Jorns MS (2011) Probing oxygen activation sites in two flavoprotein oxidases using chloride as an oxygen surrogate. *Biochemistry* **50**: 5521-5534.
- Krenitsky TA, Neil SM, Elion GB & Hitchings GH (1972) A comparison of the specificities of xanthine oxidase and aldehyde oxidase. *Arch Biochem Biophys* **150**: 585-599.
- Krüger B & Meyer O (1986) The pterin (bactopterin) of carbon monoxide dehydrogenase from *Pseudomonas carboxydoflava*. *Eur J Biochem* **157**: 121-128.
- Krüger B, Meyer O, Nagel M, Andreesen JR, Meincke M, Bock E, Blümle S & Zumft WG (1987) Evidence for the presence of bactopterin in the eubacterial molybdoenzymes nicotinic acid dehydrogenase, nitrite oxidoreductase, and respiratory nitrate reductase. *FEMS Microbiol Lett* **48**: 225-227.
- Kundu TK, Velayutham M & Zweier JL (2012) Aldehyde oxidase functions as a superoxide generating NADH oxidase: an important redox regulated pathway of cellular oxygen radical formation. *Biochemistry* **51**: 2930-2939.
- Kundu TK, Hille R, Velayutham M & Zweier JL (2007) Characterization of superoxide production from aldehyde oxidase: an important source of oxidants in biological tissues. *Archives of biochemistry and biophysics* **460**: 113-121.
- Kurosaki M, Demontis S, Barzago MM, Garattini E & Terao M (1999) Molecular cloning of the cDNA coding for mouse aldehyde oxidase: tissue distribution and regulation in vivo by testosterone. *Biochem J* **341**: 71-80.
- Kurosaki M, Demontis S, Barzago MM, Garattini E & Terao M (1999) Molecular cloning of the cDNA coding for mouse aldehyde oxidase: tissue distribution and regulation in vivo by testosterone. Vol. 341 p.^pp. 71-80.
- Kurosaki M, Terao M, Barzago MM, Bastone A, Bernardinello D, Salmona M & Garattini E (2004) The aldehyde oxidase gene cluster in mice and rats. Aldehyde oxidase homologue 3, a novel member of the molybdo-flavoenzyme family with selective expression in the olfactory mucosa. *J Biol Chem* **279**: 50482-50498.
- Kuwabara Y, Nishino T, Okamoto K, Matsumura T, Eger BT, Pai EF & Nishino T (2003) Unique amino acids cluster for switching from the dehydrogenase to oxidase form of xanthine oxidoreductase. *Proc Natl Acad Sci U S A* **100**: 8170-8175.
- Laemmli UK (1970) Cleavage of structural proteins during the assembly of the head of bacteriophage T4. *Nature* **227**: 680-685.
- Lee CR (2004) CYP2C9 genotype as a predictor of drug disposition in humans. *Methods and findings in experimental and clinical pharmacology* **26**: 463-472.
- Lee MC, Velayutham M, Komatsu T, Hille R & Zweier JL (2014) Measurement and characterization of superoxide generation from xanthine dehydrogenase: a redox-regulated pathway of radical generation in ischemic tissues. *Biochemistry* **53**: 6615-6623.
- Leferink NG, Jose MD, van den Berg WA & van Berkel WJ (2009) Functional assignment of Glu386 and Arg388 in the active site of L-galactono-gamma-lactone dehydrogenase. *FEBS letters* **583**: 3199-3203.

- Leferink NG, Fraaije MW, Joosten HJ, Schaap PJ, Mattevi A & van Berkel WJ (2009) Identification of a gatekeeper residue that prevents dehydrogenases from acting as oxidases. *J Biol Chem* **284**: 4392-4397.
- Leimkühler S, Hodson R, George GN & Rajagopalan KV (2003) Recombinant *Rhodobacter capsulatus* xanthine dehydrogenase, a useful model system for the characterization of protein variants leading to xanthinuria I in humans. *J Biol Chem* **278**: 20802-20811.
- Leimkühler S, Stockert AL, Igarashi K, Nishino T & Hille R (2004) The role of active site glutamate residues in catalysis of *Rhodobacter capsulatus* xanthine dehydrogenase. *J Biol Chem* **279**: 40437-40444.
- Linton A, Kang P, Ornelas M, Kephart S, Hu Q, Pairish M, Jiang Y & Guo C (2011) Systematic structure modifications of imidazo[1,2-a]pyrimidine to reduce metabolism mediated by aldehyde oxidase (AO). *Journal of medicinal chemistry* **54**: 7705-7712.
- Lithwick G & Margalit H (2003) Hierarchy of sequence-dependent features associated with prokaryotic translation. *Genome research* **13**: 2665-2673.
- Luo S, Wehr NB & Levine RL (2006) Quantitation of protein on gels and blots by infrared fluorescence of Coomassie blue and Fast Green. *Analytical biochemistry* **350**: 233-238.
- Maeda K, Ohno T, Igarashi S, Yoshimura T, Yamashiro K & Sakai M (2012) Aldehyde oxidase 1 gene is regulated by Nrf2 pathway. *Gene* **505**: 374-378.
- Mahro M, Bras NF, Cerqueira NM, Teutloff C, Coelho C, Romao MJ & Leimkühler S (2013) Identification of crucial amino acids in mouse aldehyde oxidase 3 that determine substrate specificity. *PloS one* **8**: e82285.
- Maia LB & Moura JJ (2011) Nitrite reduction by xanthine oxidase family enzymes: a new class of nitrite reductases. *J Biol Inorg Chem* **16**: 443-460.
- Maia LB, Pereira V, Mira L & Moura JJ (2015) Nitrite reductase activity of rat and human xanthine oxidase, xanthine dehydrogenase, and aldehyde oxidase: evaluation of their contribution to NO formation in vivo. *Biochemistry* **54**: 685-710.
- Makarov V, Manina G, Mikusova K, *et al.* (2009) Benzothiazinones kill Mycobacterium tuberculosis by blocking arabinan synthesis. *Science* **324**: 801-804.
- Makrides SC (1996) Strategies for achieving high-level expression of genes in *Escherichia coli*. *Microbiological reviews* **60**: 512-538.
- Marin A & Xia X (2008) GC skew in protein-coding genes between the leading and lagging strands in bacterial genomes: new substitution models incorporating strand bias. *Journal of theoretical biology* **253**: 508-513.
- Massey V, Schopfer LM & Nishino T (1989) Differences in protein structure of xanthine dehydrogenase and xanthine oxidase revealed by reconstitution with flavin active site probes. *J Biol Chem* **264**: 10567-10573.
- Massey V, Komai H, Palmer G & Elion GB (1970) The existence of nonfunctional active sites in milk xanthine oxidase: reaction with functional active site inhibitors. *Vitam Horm* **28**: 505-531.
- Masuoka N & Kubo I (2016) Suppression of superoxide anion generation catalyzed by xanthine oxidase with alkyl caffeates and the scavenging activity. *International journal of food sciences and nutrition* **67**: 283-287.

- Mattevi A (2006) To be or not to be an oxidase: challenging the oxygen reactivity of flavoenzymes. *Trends in biochemical sciences* **31**: 276-283.
- McCord JM & Fridovich I (1969) Superoxide dismutase. An enzymic function for erythrocyte hemoglobin. *J Biol Chem* **244**: 6049-6055.
- McDonald CA, Fagan RL, Collard F, Monnier VM & Palfey BA (2011) Oxygen reactivity in flavoenzymes: context matters. *Journal of the American Chemical Society* **133**: 16809-16811.
- Mendel RR & Leimkuhler S (2015) The biosynthesis of the molybdenum cofactors. *J Biol Inorg Chem* **20**: 337-347.
- Mullis K, Faloona F, Scharf S, Saiki R, Horn G & Erlich H (1992) Specific enzymatic amplification of DNA in vitro: the polymerase chain reaction. 1986. *Biotechnology* **24**: 17-27.
- Nachman MW (2001) Single nucleotide polymorphisms and recombination rate in humans. *Trends in genetics : TIG* **17**: 481-485.
- Neumann M, Stöcklein W & Leimkühler S (2007) Transfer of the Molybdenum Cofactor Synthesized by *Rhodobacter capsulatus* MoeA to XdhC and MobA. *J Biol Chem* **282**: 28493-28500.
- Neumeier M, Weigert J, Schaffler A, Weiss TS, Schmidl C, Buttner R, Bollheimer C, Aslanidis C, Scholmerich J & Buechler C (2006) Aldehyde oxidase 1 is highly abundant in hepatic steatosis and is downregulated by adiponectin and fenofibric acid in hepatocytes in vitro. *Biochem Biophys Res Commun* **350**: 731-735.
- Nishino T & Nishino T (1989) The nicotinamide adenine dinucleotide-binding site of chicken liver xanthine dehydrogenase. Evidence for alteration of the redox potential of the flavin by NAD binding or modification of the NAD-binding site and isolation of a modified peptide. *J Biol Chem* **264**: 5468-5473.
- Nishino T, Schopfer LM & Massey V (1989) The reactivity of chicken liver xanthine dehydrogenase with molecular oxygen. *J Biol Chem* **264**: 2518-2527.
- Nishino T, Nishino T, Schopfer LM & Massey V (1989) Reactivity of chicken liver xanthine dehydrogenase containing modified flavins. Vol. 264 p. pp. 6075-6085.
- Nishino T, Okamoto K, Eger BT & Pai EF (2008) Mammalian xanthine oxidoreductase - mechanism of transition from xanthine dehydrogenase to xanthine oxidase. *The FEBS journal* **275**: 3278-3289.
- Nishino T, Okamoto K, Kawaguchi Y, Hori H, Matsumura T, Eger BT, Pai EF & Nishino T (2005) Mechanism of the conversion of xanthine dehydrogenase to xanthine oxidase: identification of the two cysteine disulfide bonds and crystal structure of a non-convertible rat liver xanthine dehydrogenase mutant. *J Biol Chem* **280**: 24888-24894.
- Obach RS, Huynh P, Allen MC & Beedham C (2004) Human liver aldehyde oxidase: inhibition by 239 drugs. *Journal of clinical pharmacology* **44**: 7-19.
- Okamoto K, Eger BT, Nishino T & Pai EF (2008) Mechanism of inhibition of xanthine oxidoreductase by allopurinol: crystal structure of reduced bovine milk xanthine oxidoreductase bound with oxipurinol. *Nucleosides, nucleotides & nucleic acids* **27**: 888-893.
- Okamoto K, Matsumoto K, Hille R, Eger BT, Pai EF & Nishino T (2004) The crystal structure of xanthine oxidoreductase during catalysis: implications for reaction mechanism and enzyme inhibition. *Proc Natl Acad Sci U S A* **101**: 7931-7936.

- Olson JS, Ballou DP, Palmer G & Massey V (1974) The reaction of xanthine oxidase with molecular oxygen. *The journal of biological chemistry* **249**: 4350-4362.
- Pablos MI, Chuang J, Reiter RJ, Ortiz GG, Daniels WM, Sewerynek E, Melchiorri D & Poeggeler B (1995) Time course of the melatonin-induced increase in glutathione peroxidase activity in chick tissues. *Biological signals* **4**: 325-330.
- Palfey BA & McDonald CA (2010) Control of catalysis in flavin-dependent monooxygenases. *Archives of biochemistry and biophysics* **493**: 26-36.
- Palmer T, Santini C-L, Iobbi-Nivol C, Eaves DJ, Boxer DH & Giordano G (1996) Involvement of the *narJ* and *mob* gene products in the biosynthesis of the molybdoenzyme nitrate reductase in *Escherichia coli*. *Mol Microbiol* **20**: 875-884.
- Panoutsopoulos GI, Kouretas D & Beedham C (2004) Contribution of aldehyde oxidase, xanthine oxidase, and aldehyde dehydrogenase on the oxidation of aromatic aldehydes. *Chemical research in toxicology* **17**: 1368-1376.
- Parks DA, Williams TK & Beckman JS (1988) Conversion of xanthine dehydrogenase to oxidase in ischemic rat intestine: a reevaluation. *The American journal of physiology* **254**: G768-774.
- Parschat K, Canne C, Huttermann J, Kappl R & Fetzner S (2001) Xanthine dehydrogenase from *Pseudomonas putida* 86: specificity, oxidation-reduction potentials of its redox-active centers, and first EPR characterization. Vol. 1544 p.^pp. 151-165.
- Peretz H, Naamati MS, Levartovsky D, Lagziel A, Shani E, Horn I, Shalev H & Landau D (2007) Identification and characterization of the first mutation (Arg776Cys) in the C-terminal domain of the Human Molybdenum Cofactor Sulfurase (HMCS) associated with type II classical xanthinuria. *Molecular genetics and metabolism* **91**: 23-29.
- Plotkin JB & Kudla G (2011) Synonymous but not the same: the causes and consequences of codon bias. *Nature reviews Genetics* **12**: 32-42.
- Porras AG & Palmer G (1982) The room temperature potentiometry of xanthine oxidase. pH-dependent redox behavior of the flavin, molybdenum, and iron-sulfur centers. *J Biol Chem* **257**: 11617-11626.
- Pryde DC, Dalvie D, Hu Q, Jones P, Obach RS & Tran TD (2010) Aldehyde oxidase: an enzyme of emerging importance in drug discovery. *Journal of medicinal chemistry* **53**: 8441-8460.
- Pryde KR & Hirst J (2011) Superoxide is produced by the reduced flavin in mitochondrial complex I: a single, unified mechanism that applies during both forward and reverse electron transfer. *J Biol Chem* **286**: 18056-18065.
- Purvis IJ, Bettany AJ, Santiago TC, Coggins JR, Duncan K, Eason R & Brown AJ (1987) The efficiency of folding of some proteins is increased by controlled rates of translation in vivo. A hypothesis. *Journal of molecular biology* **193**: 413-417.
- Rajagopalan KV & Handler P (1964) Hepatic aldehyde oxidase II. Differential inhibition of electron transfer to various electron acceptors. *J Biol Chem* **239**: 2022-2026.
- Rajagopalan KV & Johnson JL (1992) The pterin molybdenum cofactors. *J Biol Chem* **267**: 10199-10202.

- Rajagopalan KV, Fridovich I & Handler P (1962) Hepatic aldehyde oxidase. I. Purification and properties. *The Journal of biological chemistry* **237**: 922-928.
- Ray PD, Huang BW & Tsuji Y (2012) Reactive oxygen species (ROS) homeostasis and redox regulation in cellular signaling. *Cellular signalling* **24**: 981-990.
- Reiter RJ, Carneiro RC & Oh CS (1997) Melatonin in relation to cellular antioxidative defense mechanisms. *Hormone and metabolic research = Hormon- und Stoffwechselforschung = Hormones et métabolisme* **29**: 363-372.
- Reiter RJ, Melchiorri D, Sewerynek E, Poeggeler B, Barlow-Walden L, Chuang J, Ortiz GG & Acuna-Castroviejo D (1995) A review of the evidence supporting melatonin's role as an antioxidant. *Journal of pineal research* **18**: 1-11.
- Rivera SP, Choi HH, Chapman B, Whitekus MJ, Terao M, Garattini E & Hankinson O (2005) Identification of aldehyde oxidase 1 and aldehyde oxidase homologue 1 as dioxin-inducible genes. *Toxicology* **207**: 401-409.
- Rodriguez R & Redman R (2005) Balancing the generation and elimination of reactive oxygen species. *Proc Natl Acad Sci U S A* **102**: 3175-3176.
- Rodriguez-Trelles F, Tarrío R & Ayala FJ (2003) Convergent neofunctionalization by positive Darwinian selection after ancient recurrent duplications of the xanthine dehydrogenase gene. *Proc Natl Acad Sci U S A* **100**: 13413-13417.
- Rodriguez-Trelles F, Tarrío R & Ayala FJ (2003) Convergent neofunctionalization by positive Darwinian selection after ancient recurrent duplications of the xanthine dehydrogenase gene. *Proceedings of the National Academy of Sciences of the United States of America* **100**: 13413-13417.
- Romão MJ, Archer M, Moura I, Moura JGG, LeGall J, Engh R, Schneider M, Hof P & Huber R (1995) The crystal structure of xanthine oxidase related aldehyde oxidoreductase. Vol. 270 p. pp. 1170-1176.
- Rubio LM & Ludden PW (2008) Biosynthesis of the iron-molybdenum cofactor of nitrogenase. *Annual review of microbiology* **62**: 93-111.
- Rytkönen EMK, Halila R, Laan M, Saksela M, Kallioniemi O-P, Palotie A & Raivio KO (1995) The human gene for xanthine dehydrogenase (XDH) is localized on chromosome band 2p22. *Cytogenet Cell Genet* **68**: 61-63.
- Saam J, Rosini E, Molla G, Schulten K, Pollegioni L & Ghisla S (2010) O₂ reactivity of flavoproteins: dynamic access of dioxygen to the active site and role of a H⁺ relay system in D-amino acid oxidase. *J Biol Chem* **285**: 24439-24446.
- Sagi M, Scazzocchio C & Fluhr R (2002) The absence of molybdenum cofactor sulfuration is the primary cause of the flacca phenotype in tomato plants. *The Plant journal : for cell and molecular biology* **31**: 305-317.
- Saito T, Nishino T & Tsushima K (1989) Interconversion between NAD-dependent and O₂-dependent types of rat liver xanthine dehydrogenase and difference in kinetic and redox properties between them. *Advances in experimental medicine and biology* 179-183.
- Saito T, Nishino T & Massey V (1989) Differences in environment of FAD between NAD-dependent and O₂-dependent types of rat liver xanthine dehydrogenase shown by active site probe study. *J Biol Chem* **264**: 15930-15935.

- Sakamoto N, Yamamoto T, Moriwaki Y, *et al.* (2001) Identification of a new point mutation in the human xanthine dehydrogenase gene responsible for a case of classical type I xanthinuria. *Human genetics* **108**: 279-283.
- Sanoh S, Tayama Y, Sugihara K, Kitamura S & Ohta S (2015) Significance of aldehyde oxidase during drug development: Effects on drug metabolism, pharmacokinetics, toxicity, and efficacy. *Drug Metab Pharmacokinet* **30**: 52-63.
- Satoh T & Kurihara FN (1987) Purification and properties of dimethylsulfoxide reductase containing a molybdenum cofactor from a photodenitrifier, *Rhodopseudomonas sphaeroides* f.sp. *denitrificans*. *J Biochem* **102**: 191-197.
- Schindelin H, Kisker C, Hilton J, Rajagopalan KV & Rees DC (1996) Crystal structure of DMSO reductase: redox-linked changes in molybdopterin coordination. *Science* **272**: 1615-1621.
- Schlauderer F, Lammens K, Nagel D, *et al.* (2013) Structural analysis of phenothiazine derivatives as allosteric inhibitors of the MALT1 paracaspase. *Angewandte Chemie* **52**: 10384-10387.
- Schumann S, Terao M, Garattini E, Saggi M, Lenzian F, Hildebrandt P & Leimkühler S (2009) Site directed mutagenesis of amino acid residues at the active site of mouse aldehyde oxidase AOX1. *PloS one* **4**: e5348.
- Sies H (1993) Strategies of antioxidant defense. *European journal of biochemistry* **215**: 213-219.
- Sperry L, Hudson B & Chan CH (1984) Loxapine abuse. *The New England journal of medicine* **310**: 598.
- Stefansson A, Gunnarsson I & Giroud N (2007) New methods for the direct determination of dissolved inorganic, organic and total carbon in natural waters by Reagent-Free Ion Chromatography and inductively coupled plasma atomic emission spectrometry. *Analytica chimica acta* **582**: 69-74.
- Tayama Y, Miyake K, Sugihara K, Kitamura S, Kobayashi M, Morita S, Ohta S & Kihira K (2007) Developmental changes of aldehyde oxidase activity in young Japanese children. *Clinical pharmacology and therapeutics* **81**: 567-572.
- Temple CA & Rajagopalan KV (2000) Optimization of Expression of Human Sulfite Oxidase and its Molybdenum Domain. *Arch Biochem Biophys* **383**: 281-287.
- Terao M, Kurosaki M, Demontis S, Zanotta S & Garattini E (1998) Isolation and characterization of the human aldehyde oxidase gene: conservation of intron/exon boundaries with the xanthine oxidoreductase gene indicates a common origin. *Biochem J* **332**: 383-393.
- Terao M, Kurosaki M, Saltini G, Demontis S, Marini M, Salmona M & Garattini E (2000) Cloning of the cDNAs coding for two novel molybdo-flavoproteins showing high similarity with aldehyde oxidase and xanthine oxidoreductase. *J Biol Chem* **275**: 30690-30700.
- Terao M, Romao MJ, Leimkuhler S, Bolis M, Fratelli M, Coelho C, Santos-Silva T & Garattini E (2016) Structure and function of mammalian aldehyde oxidases. *Archives of toxicology* **90**: 753-780.
- Terao M, Kurosaki M, Barzago MM, *et al.* (2009) Role of the molybdoflavoenzyme aldehyde oxidase homolog 2 in the biosynthesis of retinoic acid: generation and characterization of a knockout mouse. *Molecular and cellular biology* **29**: 357-377.

- Terao M, Kurosaki M, Marini M, *et al.* (2001) Purification of the aldehyde oxidase homolog 1 (AOH1) protein and cloning of the AOH1 and aldehyde oxidase homolog 2 (AOH2) genes. Identification of a novel molybdo-flavoprotein gene cluster on mouse chromosome 1. *J Biol Chem* **276**: 46347-46363.
- Terao M, Barzago MM, Kurosaki M, *et al.* (2016) Mouse aldehyde-oxidase-4 controls diurnal rhythms, fat deposition and locomotor activity. *Scientific reports* **6**: 30343.
- Thanaraj TA & Argos P (1996) Protein secondary structural types are differentially coded on messenger RNA. *Protein science : a publication of the Protein Society* **5**: 1973-1983.
- Tomita S, Tsujita M & Ichikawa Y (1993) Retinal oxidase is identical to aldehyde oxidase. *FEBS letters* **336**: 272-274.
- Torres Pazmino DE, Winkler M, Glieder A & Fraaije MW (2010) Monooxygenases as biocatalysts: Classification, mechanistic aspects and biotechnological applications. *Journal of biotechnology* **146**: 9-24.
- Varela MA & Amos W (2010) Heterogeneous distribution of SNPs in the human genome: microsatellites as predictors of nucleotide diversity and divergence. *Genomics* **95**: 151-159.
- Vila R, Kurosaki M, Barzago MM, Kolek M, Bastone A, Colombo L, Salmona M, Terao M & Garattini E (2004) Regulation and biochemistry of mouse molybdo-flavoenzymes. The DBA/2 mouse is selectively deficient in the expression of aldehyde oxidase homologues 1 and 2 and represents a unique source for the purification and characterization of aldehyde oxidase. *J Biol Chem* **279**: 8668-8683.
- Wahl RC & Rajagopalan KV (1982) Evidence for the inorganic nature of the cyanolyzable sulfur of molybdenum hydroxylases. *The Journal of biological chemistry* **257**: 1354-1359.
- Wahl RC, Warner CK, Finnerty V & Rajagopalan KV (1982) *Drosophila melanogaster ma-l* mutants are defective in the sulfuration of desulfo Mo hydroxylases. *J Biol Chem* **257**: 3958-3962.
- Warner CK & Finnerty V (1981) Molybdenum hydroxylases in *Drosophila* II. Molybdenum cofactor in xanthine dehydrogenase, aldehyde oxidase and pyridoxal oxidase. *Mol Gen Genet* **184**: 92-96.
- Watanabe T, Ihara N, Itoh T, Fujita T & Sugimoto Y (2000) Deletion mutation in *Drosophila ma-l* homologous, putative molybdopterin cofactor sulfurase gene is associated with bovine xanthinuria type II. *J Biol Chem* in press.
- Winterbourn CC (2008) Reconciling the chemistry and biology of reactive oxygen species. *Nat Chem Biol* **4**: 278-286.
- Winterbourn CC (2016) Revisiting the reactions of superoxide with glutathione and other thiols. *Archives of biochemistry and biophysics* **595**: 68-71.
- Winterbourn CC & Hampton MB (2008) Thiol chemistry and specificity in redox signaling. *Free radical biology & medicine* **45**: 549-561.
- Wolin SL & Walter P (1988) Ribosome pausing and stacking during translation of a eukaryotic mRNA. *The EMBO journal* **7**: 3559-3569.
- Wollers S, Heidenreich T, Zarepour M, Zachmann D, Kraft C, Zhao Y, Mendel RR & Bittner F (2008) Binding of sulfurated molybdenum cofactor to the C-terminal domain of ABA3 from *Arabidopsis thaliana* provides insight into the mechanism of molybdenum cofactor sulfuration. *J Biol Chem*.

- Wright RM, Weigel LK, Varella-Garcia M, Vaitaitis G & Repine JE (1997) Molecular cloning, refined chromosomal mapping and structural analysis of the human gene encoding aldehyde oxidase (AOX1), a candidate for the ALS2 gene. *Redox report : communications in free radical research* **3**: 135-144.
- Xu P, Zhu XL, Huecksteadt TP, Brothman AR & Hoidal JR (1994) Assignment of human xanthine dehydrogenase gene to chromosome 2p22. *Genomics* **23**: 289-291.
- Yamaguchi Y, Matsumura T, Ichida K, Okamoto K & Nishino T (2007) Human xanthine oxidase changes its substrate specificity to aldehyde oxidase type upon mutation of amino acid residues in the active site: roles of active site residues in binding and activation of purine substrate. *Journal of biochemistry* **141**: 513-524.
- Yamamoto T, Moriwaki Y, Takahashi S, Tsutsumi Z, Tuneyoshi K, Matsui K, Cheng J & Hada T (2003) Identification of a new point mutation in the human molybdenum cofactor sulftransferase gene that is responsible for xanthinuria type II. *Metabolism: clinical and experimental* **52**: 1501-1504.
- Yanase K, Tsukahara S, Mitsunashi J & Sugimoto Y (2006) Functional SNPs of the breast cancer resistance protein-therapeutic effects and inhibitor development. *Cancer letters* **234**: 73-80.
- Yasuhara A, Akiba-Goto M & Aisaka K (2005) Cloning and sequencing of the aldehyde oxidase gene from *Methylobacillus* sp. KY4400. *Bioscience, biotechnology, and biochemistry* **69**: 2435-2438.
- Yesbergenova Z, Yang G, Oron E, Soffer D, Fluhr R & Sagi M (2005) The plant Mo-hydroxylases aldehyde oxidase and xanthine dehydrogenase have distinct reactive oxygen species signatures and are induced by drought and abscisic acid. *The Plant journal : for cell and molecular biology* **42**: 862-876.
- Yoshihara S & Tatsumi K (1997) Purification and characterization of hepatic aldehyde oxidase in male and female mice. *Archives of biochemistry and biophysics* **338**: 29-34.
- Zhang X, Liu HH, Weller P, Zheng M, Tao W, Wang J, Liao G, Monshouwer M & Peltz G (2011) In silico and in vitro pharmacogenetics: aldehyde oxidase rapidly metabolizes a p38 kinase inhibitor. *The pharmacogenomics journal* **11**: 15-24.
- Zhao G, Bruckner RC & Jorns MS (2008) Identification of the oxygen activation site in monomeric sarcosine oxidase: role of Lys265 in catalysis. *Biochemistry* **47**: 9124-9135.
- Zientek M, Jiang Y, Youdim K & Obach RS (2010) In vitro-in vivo correlation for intrinsic clearance for drugs metabolized by human aldehyde oxidase. *Drug metabolism and disposition: the biological fate of chemicals* **38**: 1322-1327.

Appendix

Table A 1. List of chemicals used in this work.

Name	Company
2-(N-morpholino)ethanesulfonic acid (MES)	Sigma-Aldrich Corporation
4-(Dimethylamino)cinnamaldehyde	Sigma-Aldrich Corporation
Acetic acid	Sigma-Aldrich Corporation
Agarose SPI	Duchefa Biochemie B.V
Ammonium acetate	Carl Roth GmbH & Co. KG
Benzaldehyde	Sigma-Aldrich Corporation
Benzyl viologen	Sigma-Aldrich Corporation
Calcium chloride dihydrate	VWR International GmbH
Cinnamaldehyde	Sigma-Aldrich Corporation
Coomassie R250 brilliant blue	Ferak Berlin GmbH
Dichlorophenolindophenol	Sigma-Aldrich Corporation
diphenyliodonium chloride	Sigma-Aldrich Corporation
Dimethyl sulfoxide	Carl Roth GmbH & Co. KG
Dipotassium phosphate	Duchefa Biochemie B.V
Dithiothreitol	AppliChem GmbH
Ethanol	VWR International GmbH
Flavin adenine dinucleotide disodium salt	Sigma-Aldrich Corporation
Glycerol (98%)	Sigma-Aldrich Corporation
Hydrochloric acid, 37%	Sigma-Aldrich Corporation
Imidazole	Sigma-Aldrich Corporation
Isopropyl β -D-1-thiogalactopyranoside	Duchefa Biochemie B.V

L-ascorbic acid	Sigma-Aldrich Corporation
Magnesium chloride hexahydrate	Sigma-Aldrich Corporation
Methanol, HPLC grade	VWR International GmbH
Methyl viologen	Sigma-Aldrich Corporation
Monopotassium phosphate	Merck KgaA
NAD ⁺ , hydrate	Sigma-Aldrich Corporation
NADH, disodium salt, grade II	Roche AG
Nitric acid, 65% Suprapur	Millipore
Nitro blue tetrazolium chloride	Sigma-Aldrich Corporation
phenanthridine	Sigma-Aldrich Corporation
phenazine methosulfate	Carl Roth GmbH & Co. KG
phthalazine	Sigma-Aldrich Corporation
Peptone	Duchefa Biochemie B.V
Polyethylene glycol 4000 (PEG4000)	Fermentas Life Sciences
Potassium chloride	VWR International GmbH
Potassium cyanide	Sigma-Aldrich Corporation
Potassium hexacyanoferrate (II) (ferricyanide)	Merck KgaA
Potassium hydroxide	
Potassium iodide	VWR International GmbH
Potassium thiocyanate	Carl Roth GmbH & Co. KG
Riboflavin dihydrate	Sigma-Aldrich Corporation
Riboflavin-5'-monophosphate sodium salt dihydrate	Sigma-Aldrich Corporation
salicylaldehyde	Sigma-Aldrich Corporation
Sodium molybdate dihydrate	Carl Roth GmbH & Co. KG
Sodium acetate	Sigma-Aldrich Corporation
Sodium bicarbonate	Sigma-Aldrich Corporation
Sodium chloride	Duchefa Biochemie B.V

Sodium dithionite	Sigma-Aldrich Corporation
Sodium dodecyl sulfate	AppliChem GmbH
Sodium hydroxide	Carl Roth GmbH & Co. KG
Sodium nitrate	Carl Roth GmbH & Co. KG
Sodium sulfide	Sigma-Aldrich Corporation
Trichloroacetic acid	Duchefa Biochemie B.V
Tris(hydroxymethyl)aminomethane (Tris)	Duchefa Biochemie B.V
Tryptone	Duchefa Biochemie B.V
Yeast Extract	Duchefa Biochemie B.V

Table A 2. List of buffer and solutions used in this work.

Name	Composition	pH	Sterilization	Storage
A1	TE + 1:100 RNase premix	8.00	filtration	4 °C
A2	200 mM NaOH, 1.25% w/v SDS	-	filtration	> 22 °C
AGE-loading buffer	50% v/v glycerol, 40 mM Tris x Ac, 1 mM Na ₂ H ₂ EDTA	8.00	-	4 °C
Coomassie (de-) staining solution	40% v/v MeOH, 10 % v/v acetic acid, (0.25 Coomassie-	-	-	RT
K-MES	500 mM KOH x 2-(N-morpholino)-ethanesulfonic acid	6.3	filtration	-20 °C
lysis buffer	300 mM NaCl, 50 mM NaH ₂ PO ₄	8.00	filtration	RT
MES-buffer	12% w/v glycerol, 50 mM CaCl ₂ , 45 mM MnCl ₂ , 2% v/v K-MES	6.3	filtration	4 °C
Mini-prep Tris EDTA buffer	50 mM Tris x HCl, 1 mM Na ₂ H ₂ EDTA	8.00	autoclave	RT
native-/(SDS)-PAGE-loading buffer	250 mM Tris x HCl, 30% w/v glycerol, 0.25% w/v brom- phenyl-blue, (10% v/v β- mercaptoethanol, 3% w/v SDS)	6.8	-	4 °C

native-/ (SDS)- PAGE running buffer	192 mM glycine, 25 mM Tris, (0.1 % w/v SDS)	8.2	-	RT
NTA elution buffer	50 mM NaH ₂ PO ₄ , 300 mM NaCl, 250 mM imidazole	8.0	filtration	4 °C
NTA washing buffer I	50 mM NaH ₂ PO ₄ , 300 mM NaCl, 10 mM imidazole	8.0	filtration	4 °C
NTA washing buffer II	50 mM NaH ₂ PO ₄ , 300 mM NaCl, 20 mM imidazole	8.0	filtration	4 °C
standard assay buffer	50 mM Tris x HCl, 200 mM, NaCl, 1 mM EDTA	8.0	filtration	RT
storage buffer	50 mM Tris x HCl, 200 mM, NaCl, 1 mM EDTA	8.0	filtration	RT
sulfuration buffer	50 mM K _x H _{3-x} PO ₄ , Na ₂ H ₂ EDTA	7.4	filtration	RT

Table A 3. Oligonucleotides used in this study. Primers were synthesized and desalted by BioTez (BioTeZ Berlin-Buch GmbH).

oligonucleotide	sequence	purpose
hAOX1co_NdeI_For	CACCATATGAAACAGGATCG	Sequencing
hAOX1co_int1_For	ATCGTATTGAAGAACTGAGCG	Sequencing
hAOX1co_int2_For	CCGATTGGTCATCCGATTATGC	Sequencing
hAOX1co_int3_For	GATGGTCGTATTCTGGCACTGG	Sequencing
hAOX1co_int4_For	GGCACAGACCGCATTGATGAA	Sequencing
hAOX1co_Int1_Rv	AAT CAG ACA TGC ATT TGC CG	Sequencing
hAOX1co_G1269R_For1	CAGCAAAGGTCTGCGTGAAAG CGGTG	Cloning
hAOX1co_G1269R_Rev1	CACCGCTTTCACGCAGACC TTTGCTG	Cloning
hAOX1co_G46E_For	CAAATATGGTTGTGGTGAGGGTGG TTGTGGTGCATG	Cloning
hAOX1co_G46E_Rev	CATGCACCACAACCACCTCACCA CAACCATATTTG	Cloning
hAOX1co_G346R_For	TGGGCACCCTGGCACGTAGCC	Cloning

	AGATTCGTA	
hAOX1co_G346R_Rev	TACGAATCTGGCTACGTGCCAG GGTGCCCA	Cloning
hAOX1co_L438V_For	GCGTCAAGAAAATGCAGTGGCAA TTGTTAATAGC	Cloning
hAOX1co_L438V_Rev	GCTATTAACAATTGCCACTGCATT TTCTTGACGC	Cloning
hAOX1co_H363Q_For	GGTCATATTATTAGCCGTCAGCCA GATAGCGATCTGAATC	Cloning
hAOX1co_H363Q_Rev	GATTCAGATCGCTATCTGGCTGAC GGCTAATAATATGACC	Cloning
hAOX1co_K1237N_For	GGTCCAGATCAGTATAACATT CCGGCAATTTGTG	Cloning
hAOX1co_K1237N_Rev	CACAAATTGCCGGAATGTTA TACTGATCTGGACC	Cloning
hAOX1co_G50D_For	GGTGGTGGTGGTTGTGATGC GTGTACCGTTATG	Cloning
hAOX1co_G50D_Rev	CATAACGGTACACGCATCAC AACCACCACCACC	Cloning
hAOX1co_L438A_For	CGT CAA GAA AAT GCA GCG GCA ATT GTT AAT AG	Cloning
hAOX1co_L438A_Rev	CTA TTA ACA ATT GCC GCT GCA TTT TCT TGA CG	Cloning
hAOX1co_L344F_For	AAA CAT CTG GGC ACC TTT GCA GGT AGC CAG	Cloning
hAOX1co_L344F_Rev	CTG GCT ACC TGC AAA GGT GCC CAG ATG TTT	Cloning
hAOX1co_A437V_For	CAA GAA AAT GCA CTG GTG ATT GTT AAT AGC	Cloning
hAOX1co_A437V_Rev	GCT ATT AAC AAT CAC CAG TGC ATT TTC TTG	Cloning
hAOX1co_L438K_For	CGT CAA GAA AAT GCA AAA GCA ATT GTT AAT AGC	Cloning
hAOX1co_L438K_Rev	GCT ATT AAC AAT TGC TTT TGC ATT TTC TTG ACG	Cloning
hAOX1co_L438F_For	CGT CAA GAA AAT GCA TTC GCA ATT GTT AAT AGC	Cloning
hAOX1co_L438F_Rev	GCT ATT AAC AAT TGC GAA TGC ATT TTC TTG ACG	Cloning
hAOX1co_R433P_For	CGTCAGGCACAGCCTCAA GAAAATGCAC	Cloning
hAOX1co_R433P_Rev	GTGCATTTTCTTGAGGCTG TGCTGACG	Cloning
hAOX1co_A439E_For	CGTCAAGAAAATGCACTGGAAA TTGTTAATAGCGGTATGC	Cloning
hAOX1co_A439E_Rev	GCATACCGCTATTAACAATTTCC AGTGCATTTTCTTGACG	Cloning
hAOX1co_R1231H_For	GGTATTCTGCATACCCATGG TCCGGATCAGTA	Cloning
hAOX1co_R1231H_Rev	TACTGATCCGGACCATGGGTA TGCAGAATACC	Cloning

hAOX1co_D1234H_For	CAT ACC CGT GGT CCG CAT CAG TAT AAA ATT CCG	Cloning
hAOX1co_D1234H_Rev	CGG AAT TTT ATA CTG ATG CGG ACC ACG GGT ATG	Cloning
hAOX1co_A437D_For	AAA CAT CTG GGC ACC TTT GCA GGT A	Cloning
hAOX1co_A437D_Rev	TAC CTG CAA AGG TGC CCA GAT GTT T	Cloning
hAOX1co_N436D/A437D_For	GCA CAG CGT CAA GAA GAT GAT CTG GCA ATC GTT AAT AGC GGT	Cloning
hAOX1co_N436D/A437D_Rev	ACC GCT ATT AAC GAT TGC CAG ATC ATC TTC TTG ACG CTG TGC	Cloning
hAOX1co_N436D/A437D/L438I_For	AAT TTG TTA GCG CAT TTC GTC AGG CAA GCC GT	Cloning
hAOX1co_N436D/A437D/L438I_Rev	ACG GCT TGC CTG ACG AAA TGC GCT AAC AAA TT	Cloning
hAOX1co_N436D/A437D/L438I/ I440 K_For	AAT TTG TTA GCG CAT TTC GTC AGG CAT CG	Cloning
hAOX1co_N436D/A437D/L438I/ I440 K_Rev	CGA TGC CTG ACG AAA TGC GCT AAC AAA TT	Cloning
hAOX1co_Q434R/N436D/A437D/ L438I/I440 K_For	CAC AGC GTC GAG AAG ATG ATA TCG CAA AAG	Cloning
hAOX1co_Q434R/N436D/A437D/ L438I/I440 K_Rev	CTT TTG CGA TAT CAT CTT CTC GAC GCT GTG	Cloning
hAOX1co-Q-For	GGC AGC CAT ATG GAT CGT GCA AGC GAA	Cloning and sequencing
hAOX1co-Q-Rev	TTC GCT TGC ACG ATC CAT ATG GCT GCC	Cloning and sequencing
hAOX1co-Q2-For	CAT ATG GAT CGT GCA AGC GAA CTG CTG TTT TAT	Cloning and sequencing
hAOX1co-Q2-Rev	ATA AAA CAG CAG TTC GCT TGC ACG ATC CAT ATG	Cloning and sequencing
hAOX1co_L438QII_For	CGC GGC AGC CAT ATG GAT CGT GCA AGC GAA	Cloning and sequencing
hAOX1co_L438QII_Rev	TTC GCT TGC ACG ATC CAT ATG GCT GCC GCG	Cloning and sequencing

Table A 4. Plasmids used in this study.

name	plasmid	Selection marker
pTHcoaox	pTrcHis-hAOX1 codon optimized	Amp
pFA03	pTrcHis-hAOX1 G1269R codon optimized	Amp
pFA04	pTrcHis-hAOX1 G46E codon optimized	Amp

pFA05	pTrcHis-hAOX1 G50D codon optimized	Amp
pFA06	pTrcHis-hAOX1 G346R codon optimized	Amp
pFA07	pTrcHis-hAOX1 H363Q codon optimized	Amp
pFA08	pTrcHis-hAOX1 R433P codon optimized	Amp
pFA09	pTrcHis-hAOX1 A437V codon optimized	Amp
pFA10	pTrcHis-hAOX1 L438V codon optimized	Amp
pFA11	pTrcHis-hAOX1 A439E codon optimized	Amp
pFA12	pTrcHis-hAOX1 R1231H codon optimized	Amp
pFA13	pTrcHis-hAOX1 K1237N codon optimized	Amp
pFA14	pTrcHis-hAOX1 A437D codon optimized	Amp
pFA15	pTrcHis-hAOX1 N436D/A437D codon optimized	Amp
pFA16	pTrcHis-hAOX1 N436D/A437D/L438I codon optimized	Amp
pFA17	pTrcHis-hAOX1 N436D/A437D/L438I/I440K codon optimized	Amp
pFA18	pTrcHis-hAOX1 Q434R/N436D/A437D/L438I/I440K codon optimized	Amp
pFA19	pTrcHis-hAOX1 D1234H codon optimized	Amp
pFA20	pTrcHis-hAOX1 L438A codon optimized	Amp
pFA21	pTrcHis-hAOX1 L438F codon optimized	Amp
pFA22	pTrcHis-hAOX1 L438K codon optimized	Amp
pFA23	pTrcHis-hAOX1 L433F codon optimized	Amp

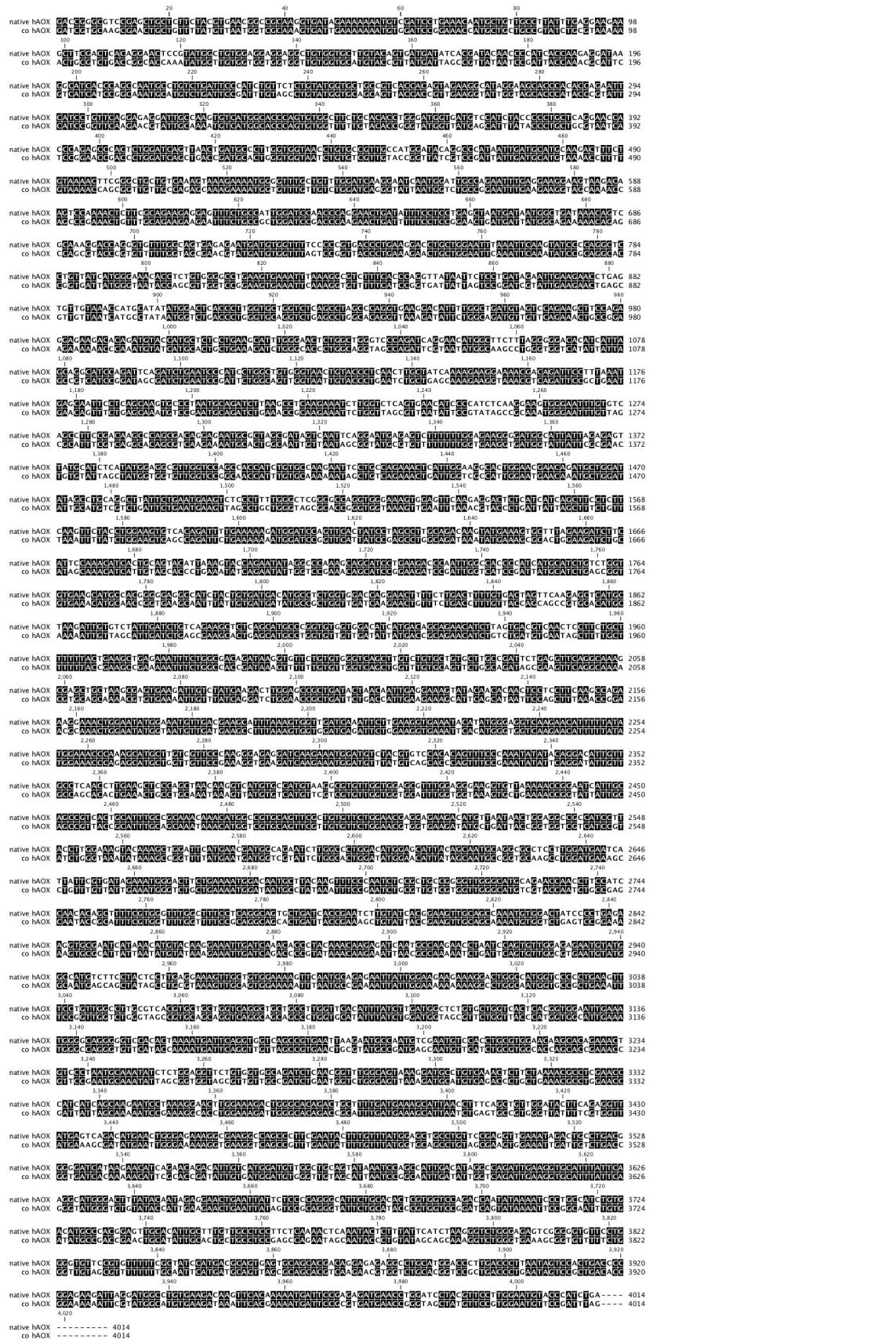


Figure A. 1. Sequence alignment of the DNA sequence of the native hAOX1 and a synthetic codon optimized sequence (co hAOX1). Identical bases in both sequences are boxed in black. Alignment produced by CLC Sequence Viewer - QIAGEN Bioinformatics.

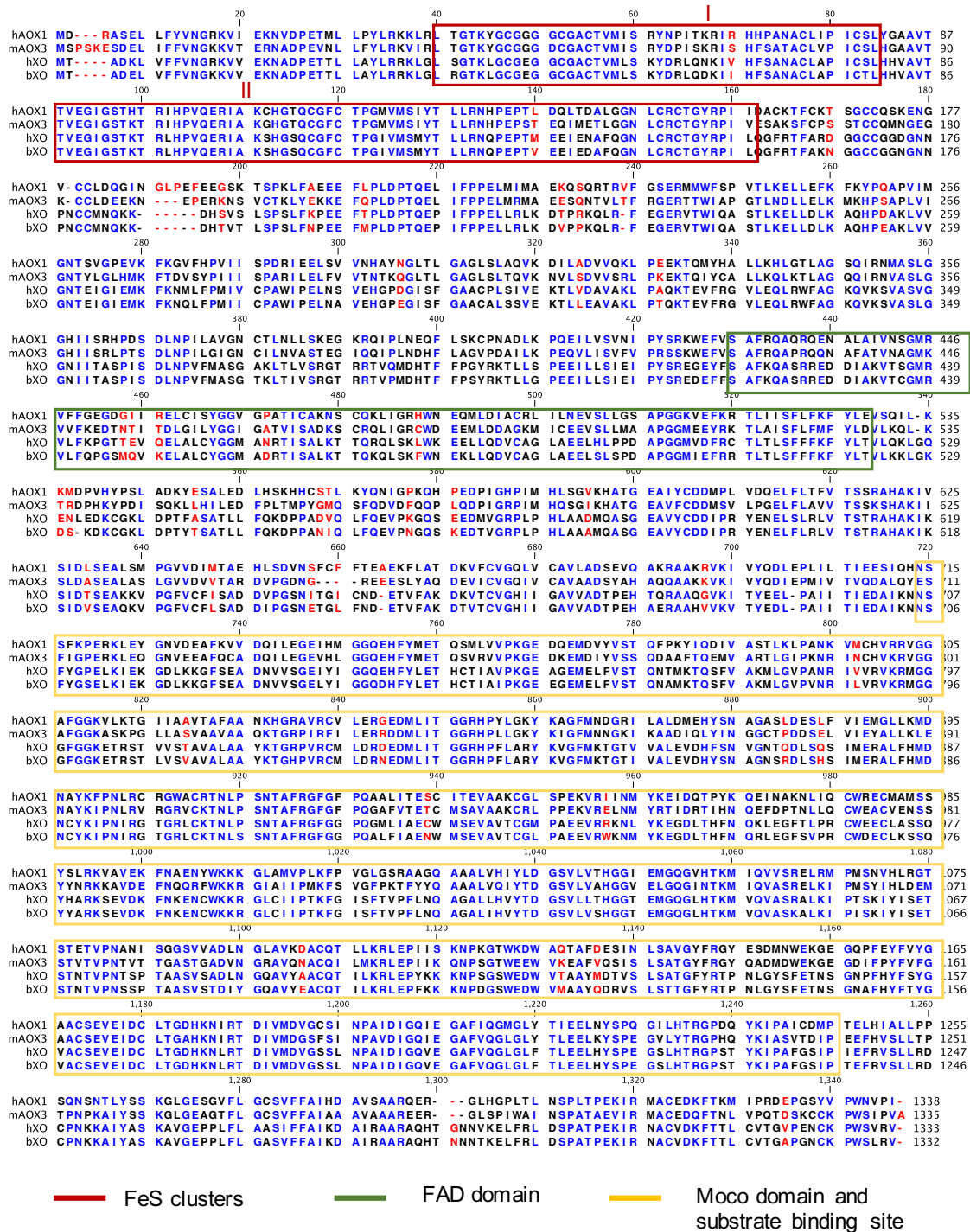


Figure A. 2. Amino acid sequence alignment of hAOX1, mAOX3, hXO and bXO. Highly conserved residues in blue; partially conserved residues in black; non-conserved residues in red. FeS clusters marked by red boxes, FAD domain marked by green box and Moco domain/substrate binding site marked in yellow. Alignment produced by CLC Sequence Viewer - QIAGEN Bioinformatics.

Acknowledgement

I would like to thank my supervisor Prof. Dr. Silke Leimkühler for the scientific and personal support during these years and also for the several opportunities for international cooperation and meetings.

Many thanks to the members of the crystallography group of the Departamento de Química Faculdade de Ciências e Tecnologia Universidade Nova de Lisboa, Lisbon, in particular Catarina Coelho, Teresa Santos-Silva and Maria João Romão for their structural studies and helpful discussions. I'm really thankful to Takeshi Nishino, Ken Okamoto and Yuko Yamaguchi from the Nippon Medical School of Tokyo for the great support they gave me for the redox titration experiments and also for the wonderful experience I had in Japan. Thanks also to Enrico Garattini and the other participants of the Moco conference in Budapest in 2015 for the useful suggestions regarding my project.

I would like to thank all the members of my working group Molecular Enzymology, in particular Mariam Esmaeeli, Gökhan Küçükgoze, Tobias Hartmann and Jan Dahl for their amazing support.

An enormous thanks to my family in Italy and my family in Berlin. Without you, nothing could be possible.